THERMAL HYDRAULICS OF SFR FUEL BUNDLE WITH INSERTS IN PERIPHERAL SUBCHANNELS

By

G PADMAKUMAR

(Enrolment Number: ENGG 02 2011 04 002)

Indira Gandhi Centre for Atomic Research, Kalpakkam

A thesis submitted to the Board of Studies in Engineering Sciences
In partial fulfillment of the requirements
For the Degree of

DOCTOR OF PHILOSOPHY

of

HOMI BHABHA NATIONAL INSTITUTE

January, 2019

THERMAL HYDRAULICS OF SFR FUEL BUNDLE WITH INSERTS IN PERIPHERAL SUBCHANNELS

By

G PADMAKUMAR

(Enrolment Number: ENGG 02 2011 04 002)

Indira Gandhi Centre for Atomic Research, Kalpakkam

A thesis submitted to the Board of Studies in Engineering Sciences
In partial fulfillment of the requirements
For the Degree of

DOCTOR OF PHILOSOPHY

of

HOMI BHABHA NATIONAL INSTITUTE

January, 2019

Homi Bhabha National Institute

Recommendation of the Viva Voce Board

As members of the Thesis Examining Committee, we certify that we have read the dissertation prepared by **Mr. Padmakumar G** entitled **"Thermal hydraulics of SFR fuel bundle with inserts in peripheral sub-channels"** and recommend that it may be accepted as fulfilling the dissertation requirement for the Degree of Doctor of Philosophy.

Chairman: Dr. K. Velusamy

Date: 12/2/2019

Guide / Convener: Prof. B.V.S.S.S Prasad

Date: 12.2.19

Member: Dr. B.P.C. Rao

Date: 12/2/2019

Member: Dr. Shaju K Albert

Date: 12/2/19

External examiner: Prof Amaresh Dalal

Date:

Final approval and acceptance of this dissertation is contingent upon the candidate's submission of the final copies of dissertation to HBNI.

I hereby certify that I have read this dissertation prepared under my direction and recommend that it may be accepted as fulfilling the dissertation requirement.

Date: 12.2.19
Place: IGCAR, Kalpakkam

Prof. B.V.S.S.S Prasad
(Guide)

STATEMENT BY AUTHOR

This dissertation has been submitted in partial fulfillment of requirements for an advanced degree at Homi Bhabha National Institute (HBNI) and is deposited in the library to be made available to borrowers under rules of the HBNI.

Brief quotations from this dissertation are allowable without special permission, provided that accurate acknowledgement of source is made. Requests for permission for extended quotation from or reproduction of this manuscript in whole or in part may be granted by the Competent Authority of HBNI when in his or her judgment the proposed use of the material is in the interests of scholarship. In all other instances, however, permission must be obtained from the author.
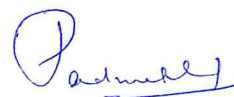
(G. Padmakumar)

Kalpakkam
January, 2019

ii

DECLARATION

I, hereby declare that the investigation presented in the thesis has been carried out by me. The work is original and has not been submitted earlier as a whole or in part for a degree / diploma at this or any other Institution/University.

(G. Padmakumar)

Kalpakkam
January, 2019

List of Publications arising from the thesis

International Journal Papers

1. G. Padmakumar; K. Velusamy; B.V.S.S.S. Prasad; K.K. Rajan; **Hydraulic characteristics of a fast reactor fuel subassembly: An experimental investigation**; *Annals of Nuclear Energy,* 102 (2017) 255–267.

2. G. Padmakumar; K. Velusamy; B.V.S.S.S. Prasad; P. Lijukrishnan; G.K. Pandey; P.Selvaraj; **Thermal-Hydraulic Effects of Inserts in Fast Reactor Fuel Bundle**, *Nuclear Engineering and Design,* 332 (2018) 226–237.

3. G. Padmakumar; K. Velusamy; B.V.S.S.S. Prasad; P. Lijukrishnan; P. Selvaraj; **Computational Fluid Dynamic Investigations on Effects of Inserts in Fast Reactor Fuel Bundle Hydraulics**, *Progress in Nuclear Energy,* 113 (2019) 84–94.

Conference Proceedings

1. G. Padmakumar; K. Velusamy; B.V.S.S.S. Prasad; P. Lijukrishnan; P. Selvaraj; "**Numerical Investigations on Complex Flow Pattern inside the Fuel Bundle of a LMFBR**", *flotek.g 2017- Innovative Solutions in Flow measurement and Control - Oil, Water and Gas*, August 28- 30, FCRI, Palakkad, Kerala, India.

2. G. Padmakumar; K. Velusamy; B.V.S.S.S. Prasad; P. Lijukrishnan; P.Selvaraj; **Computational Fluid Dynamic Investigations on Effects of Circular Rod Inserts in Fast Reactor Fuel Bundle**, *Proceedings of the 24th National and 2nd International ISHMT-ASTFE, Heat and Mass Transfer Conference* (IHMTC-2017), December 27-30, 2017, BITS Pilani, Hyderabad,India.

ACKNOWLEDGEMENTS

CONTENTS

SYNOPSIS

In Sodium cooled Fast Reactors (SFR) the core is very compact with large heat flux on clad surface. Understanding of the complex thermal hydraulics of the sodium flow through the core is vital for arriving at the design limits. In the case of a SFR the fuel subassembly, the fuel pins (clad tubes) are vertically held in the form of bundle within a hexagonal wrapper tube. The fuel pins are arranged in a triangular pitch and the gap between the fuel pins forms the sub-channels for coolant flow. The heat generation in fuel pin varies both in axial and radial directions because of the variation in neutron flux. The mass flow rate of coolant is not uniform in all the sub-channels surrounding the fuel pins. Hence, there are significant temperature variations around the fuel pins which give rise to local hot spots. The cooling efficiency of core definitely increases because of the presence of spacer wire. However, there still exists temperature non-uniformity across the cross section.

Reducing the bypass flow occurring in the peripheral sub channels would lead to a more uniform sub channel temperatures. This would also result in an optimized subassembly flow and eventually a high hot pool temperature.

Provisions of inserts in peripheral sub channels would reduce the flow area and in these sub channels thereby divert more flow towards the central sub channels. In this thesis, different types of inserts viz., circular, semi circular and triangular are studied. Both computations and experimental investigations have been performed to quantify the augmentation in Nusselt number, increase in friction factor and identify a shape that is optimum.

In open literature, investigations dealing with effect of non uniform sub-channel flow have been reported and some studies have focused on the feasibility of reducing the extent of non uniformity in coolant flow. However, not much information is available with respect to the type of devices to reduce this non-uniformity.

Various researchers have reported works on investigation of thermal hydraulics of SFR. subassemblies. Sub-channel approach to study the thermal hydraulics within the bundle has been conducted with the assumption that axial flow is dominant compared to transverse flow. However, literatures dealing with the modification in subassembly geometry to modify the

flow behavior have been sparse. The usages of inserts as an additional feature in the subassembly to improve the hydraulics and in turn heat transfer is also not reported widely.

Many options are possible for the inserts with each insert having different effect on Nusselt number, friction factor and hot spot factor. This knowledge is required for design of future fast reactors with optimized core flow. This is the main motivation for the present research where both CFD and experimental investigations have been carried out.

Computational Fluid Dynamics (CFD) investigation has been carried out to assess the efficacy of various types of inserts. Towards this a model of 7 pin fuel bundle with helical wire has been considered. The main focus of this thesis is increase in heat transfer coefficient and friction factor as a result of insert, improvement in clad circumferential temperature variation, reduction in clad hot spot factor, and arrives at optimum type of inserts. Toward validation of the CFD model, water experiments have been carried out on a model 7 pin bundle. Finally hydraulic experiments have been carried out on a 217 pin bundle of prototype SFR subassembly to quantify the pressure drop.

Computational analysis has been carried out for different Reynolds number values ranging from 4 x 104 to 2 x 105. Verification of hydraulic part of CFD model has been carried out by comparing computed values of frictional factor with correlations reported by various authors.

Thermal hydraulic simulations were carried out with a uniform heat flux of $2x10^6$ W/m^2 applied on the surface of fuel pins while the hexcan was treated to be adiabatic. The computational model was validated by comparing the computed Nusselt number with correlations proposed by various authors.

Towards the validation of the CFD model with inserts, two full scale experimental models with 7 pins were fabricated. They are (i) reference bundle without any inserts and (ii) bundle with circular inserts. The pin diameter, wire diameter, helical pitch, triangular pitch and dimensions of hexcan were same as that used in the CFD study. However, the fuel pin length was taken as 600 mm, corresponding to 3 helical pitch lengths. Water was used as simulant and the Reynolds number was varied from 5 x 10^3 to 1.3 x 10^4. The validation has been done by comparing velocity at the outlet, and also by comparing pressure drop in the bundle. Velocity has been measured by Particle Imaging Velocimetry (PIV).

The predicated velocity pattern and experimentally measured velocity patterns are in good agreement with each other. The measured pressure drop in the bundle is compared with the CFD predicted results

The modification of flow distribution among the sub-channels by the inserts also reduces the hot spots on the clad surfaces. The reduction of hot spots on the clad surface can be assessed by comparing the temperature profiles around the fuel pin for all the cases. Among the various inserts, it is seen that the circular inserts offer the lowest peak clad temperature.

Nusselt number for pin bundle of all cases are estimated for various flow regions ranging from Re=$5x10^4$ to Re=$1.7x10^5$ and compared for all the cases of inserts. Nu is seen to be proportional to Pe0.8 in the case of reference bundle without any inserts. Due to the addition of inserts, there is large increase in the Nu for all the cases. The increase is maximum in the case of circular inserts. The Nusselt number is nearly double with circular inserts.

The addition of inserts reduces the intensity of hot spot formation in the fuel bundle. The hot spot formation has been quantified using a non-dimensional term hot spot factor (ζ). From the comparison of mean clad temperature along the length, it is observed that, the circular inserts give the lowest peak clad temperature and lowest mean clad temperature among all the inserts. Nusslet number is high because the temperature difference between clad and coolant is small.

The inserts in pin bundle increase the heat transfer coefficient in the subassembly but with an additional pressure drop in the system. The selection criteria for the optimum geometry for the inserts are maximum heat transfer coefficient and minimum pressure drop. Both heat transfer and pressure drop can be quantitatively expressed in terms of Nusslet number and friction factor through a Performance Evaluation Criteria (PEC) . The computed values of PEC is maximum for circular inserts indicating that the circular inserts are optimum among the types of inserts studied. Further circular inserts are easy to manufacture and implemented in a prototype subassembly.

The results discussed in the earlier subsections were related to a 7 pin bundle. It is required to predict the performance of inserts in a prototype pin bundle also. As a first step an experimental loop was designed, fabricated and erected for conducting the hydraulic studies using water as the test medium. A 1:1 scale dummy fuel subassembly without inserts was fabricated and experiments have been conducted for various operating conditions of the

reactor and the results were transposed to the reactor condition using appropriate similarity laws. The data obtained from the experiments were transposed to the reactor condition by Euler number similitude. Bundle friction factor was calculated and compared with data available in literature and it is found that friction factor matches very well with the data reported in the literature. From the measured friction factor in a 217 pin reference bundle and computed friction factor in a 7 pin reference bundle , the friction factor for 217 pin prototype with circular inserts have been estimated.. The bundle pressure drop without insert is approximately 73% of the overall subassembly pressure drop and is equal to 375 kPa. This will increase to 437 kPa assuming the similar increase as found with 7 pin bundle (17%). The increase in overall pressure drop (480 kPa without insert) is13% more to with inserts (543 kPa) as it will not affect the pressure drop by other component of the subassembly like foot, bundle entry, exit etc.

This thesis elucidates the combined experimental and numerical study carried out to find the effect of addition of inserts on the sub-channel coolant flow pattern through the center and peripheral sub-channels, heat transfer coefficient and hot spot temperature.

LIST OF TABLES

LIST OF FIGURES

NOMENCLATURE

g	Acceleration due to gravity
D_h	Hydraulic diameter
K	Loss coefficient
fd	Doppler shift frequency
fo	Transmitting frequency
C	Speed of sound in liquid
k	Turbulence kinetic energy
G_k	Generation of turbulence kinetic energy
m	Mass flow rate
P	Pressure
S_{ij}	Strain tensor
u,v,w	Components of velocity vector
u	Time average velocity
$u_i{}'$	Fluctuating velocity
Fr	Froude number
We	Weber number
Re	Reynolds number
St	Strouhal number
t	Time

Greek Alphabets

ρ	Density
∇	Denotes gradient, derivative with respect to normal directions
∂	Partial differential operator
Δ	Denotes difference
μ	Dynamic viscosity of liquid
μ_{eff}	Effective coefficient of dynamic viscosity
μ_t	Turbulent viscosity coefficient
ε	Turbulence dissipation rate
θ	Angle
δ	Kronecker delta
υ	Kinematic viscosity
ω	Rate of dissipation per unit energy

CHAPTER 1

INTRODUCTION

1.0.   FOREWORD

Energy consumption is the key parameter for measuring the human development index of any nation. Energy production and consumption across the world has gone up multifold over the years and it is seen that the gap between the energy generation and demand is also widening. The countries all over the world utilize all the resources of energy to meet the demand. The total energy production in the world for the year 2016 is about 25000 TWh and the energy consumed is nearly 21000 TWh. In the Indian scenario for the same period it was 1423 TWh of electricity generated and 1065 TW of electricity consumed.

It is estimated that over a period of time the energy demand would be increasing and by the various forecasts it would certainly be a great challenge to meet the energy demand against supply by the year 2050. India is the world's third largest producer and third largest consumer of electricity. In India with its growing population the energy demand is very high and the per capita consumption which even though is lower as far as the other countries are concerned will increase. Of the 1.4 billion people in the world who have no access to electricity, India accounts for over 160 million, some 30 million homes. The International Energy Agency estimates India will add between 600 GW to 1,200 GW of additional new power generation capacity before 2050.

This necessitates that all the potential sources of energy available are to be harnessed to improve the national per capita consumption for a better standard of living for its people. India's electricity sector is dominated by fossil fuels, and in particular coal, which in 2017-18 produced about three fourths of all electricity. However, the government is pushing for an increased investment in renewable energy. Fossil fuel based power plants and

hydroelectric power contributes a substantial part of the energy generation. India with its sparse coal reserves will have to import the fuel for the thermal plants once these reserves get depleted. On the other hand hydroelectric power is subjected to the vagaries of the seasonal monsoons. This has certainly lead to a rethinking on the probable use of alternative sources of energy like solar, wind and nuclear. Nuclear energy is also envisioned in the country as a potential source of energy. Today nuclear energy contributes about 2.8 % of the electricity generation. The total installed capacity of by Nuclear power plants for the year 2016-2017 is ~ 6010 MWe.

1.1. INDIAN STRATEGY FOR NUCLEAR ENERGY

India has a 3 stage Nuclear Energy Program devised by Dr Homi Jehangir Bhaba in 1954. The nuclear power program was formulated to provide energy security to the country. The main objective was to capitalize on the availability of two naturally occurring elements namely Uranium and Thorium which have good potential as fuel for the nuclear power program. The estimated Natural Uranium deposits in India is approximately 70,000 tonnes and Thorium deposits accounts to about 3,60,000 tonnes. the uranium deposits account to only 1 % of the world reserves while the thorium deposits are one of the largest in the world. Therefore the 3 stage Indian nuclear power program has been formulated to utilize India's vast thorium reserves while accounting for its limited uranium reserves. The three stages are discussed below.

STAGE 1

Stage 1 consists of Natural uranium fuelled Pressurised Heavy Water Reactor (PHWR) using Natural UO_2 as fuel matrix and Heavy water as moderator and coolant. Natural U isotopic composition is 0.7 % fissile U-235 and the rest is U-238.

STAGE 2

Stage 2 consists of Fast Breeder Reactors (FBR) using plutonium based fuels. Liquid sodium is the coolant for FBR's. The second stage involves using Plutonium-239 obtained from stage 1 to produce mixed-oxide fuel, which would be used in fast breeder reactors. While Pu-239 forms the main fissile element in the FBR core, a blanket of U-238 surrounding the fuel core will undergo nuclear transmutation to produce fresh Pu-239 as more and more Pu-239 is consumed during the operation. A blanket of Th-232 around the FBR core also undergoes neutron capture reactions leading to the formation of U-233. U-233 is the nuclear reactor fuel for the third stage of India's Nuclear Power Programme.

STAGE 3

The third phase of India's nuclear power generation programme is, breeder reactors using a combination of U-233 and Th-232 fuel. U-233 is obtained from the nuclear transmutation of Th-232 used as a blanket in the second phase Pu-239 fuelled FBR. U-233 fuelled breeder reactors will also have a Th-232 blanket around the U-233 reactor core which will generate more U-233 as the reactor goes operational, thus resulting in the production of more and more U-233 fuel from the Th-232 blanket. The currently known Indian thorium reserves amount to 358,000 GWe-yr of electrical energy and can easily meet the energy requirements during the next century and beyond.

Currently there are 22 nuclear reactors operating in the first stage program of which 18 are PHWR's, 2 are Boiling Water Reactor (BWR) and 2 Water-Water Energetic Reactor VVER's. There are about eight other reactors which are under various stages of construction.

Fast breeder Test Reactor (FBTR) , the 40 MWth sodium cooled reactor based on the unique mixed plutonium uranium carbide fuel is in operation in the second stage program.

The 500 MWe Prototype Fast Breeder Reactor (PFBR) was designed, constructed and is being commissioned.

The U-233/Th-232 based breeder reactors which form the third stage are under development and would serve as the mainstay of the final thorium utilization stage of the Indian nuclear programme.

1.2.   LIQUID METAL COOLED FAST BREEDER REACTOR (LMFBR)

LMFBR's undergo fission with the capture of high energy neutrons. There is no moderator required to slow down the neutrons in fast breeders.
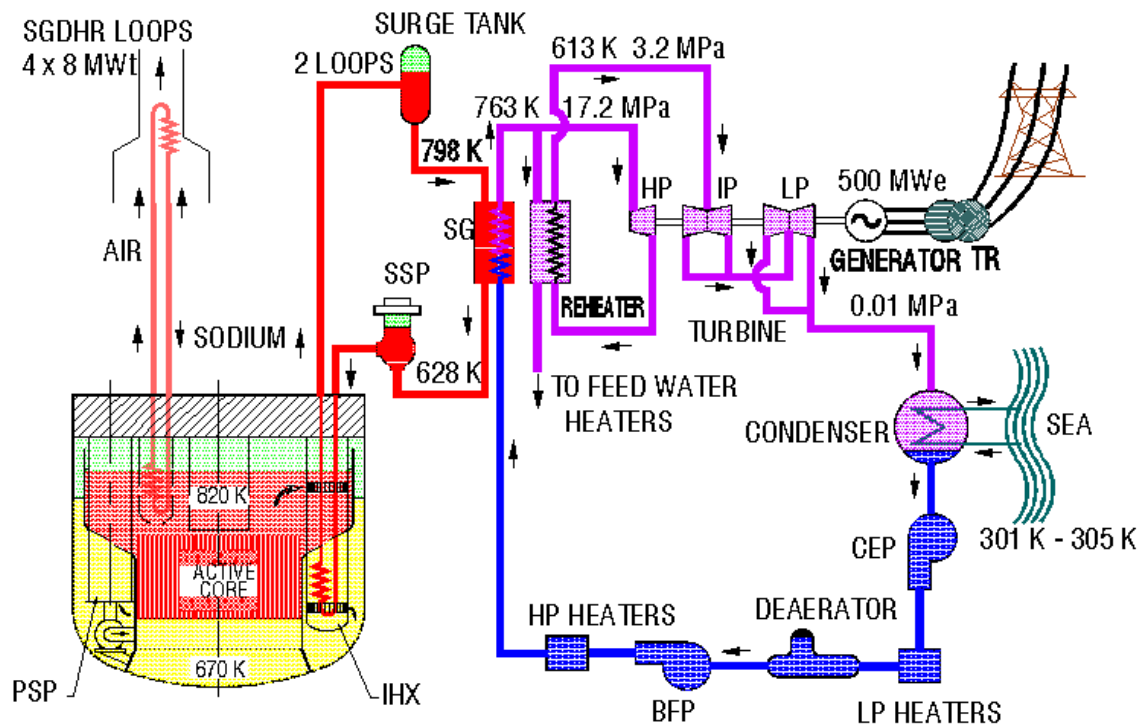
Fig. 1.1: Heat transport circuit of a LMFBR

LMFBR's derive it name as it uses liquid metal especially sodium as the coolant for transport of energy produced in the core to steam - water system. LMFBR's have been

5

constructed and operated for power production in France, Russia and Japan among other countries. The LMFBR's have a very high operating temperature of the order of 550 deg C and exhibit complex thermal hydraulic behavior in the core and in the heat exchange process.

LMFBRs are more efficient compared to thermal reactors. There are two types of FBR's viz: loop type and pool type. All the present designs of LMFBR's are pool type owing to its advantages on account of safety. The heat transport circuit of a typical LMFBR is shown in Figure 1.1.
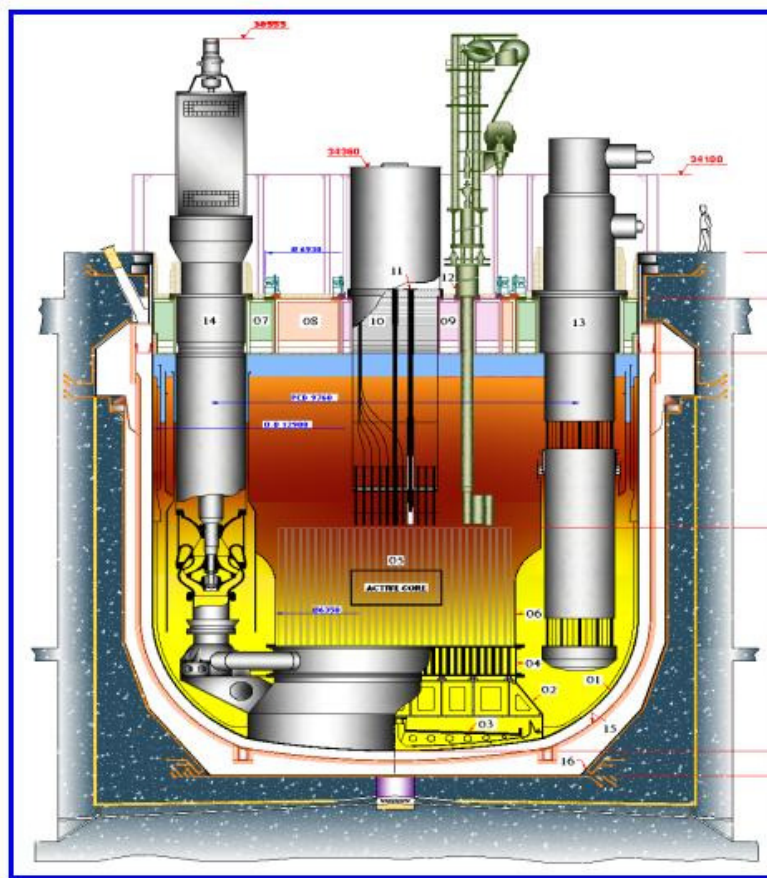
LEGEND

01. MAIN VESSEL
02. CORE SUPPORT STRUCURE
03. CORE CATCHER
04. GRID PLATE
05. CORE
06. INNER VESSEL
07. ROOF SLAB
08. LARGE ROTATABLE PLUG
09. SMALL ROTATABLE PLUG
10. CONTROL PLUG
11. CONTROL & SAFETY ROD MECHANISM
12. IN-VESSEL TRANSFER MACHINE
13. INTERMEDIATE HEAT EXCHANGER
14. PRIMARY SODIUM PUMP
15. SAFETY VESSEL
16. REACTOR VAULT

Fig. 1.2: Primary circuit of pool type LMFBR

A typical pool type LMFBR consists of three independent circuits to transfer the heat produced in the core of the reactor by the fission of uranium atoms to produce power in the turbo generator. There are two sodium circuits namely the primary and the secondary circuit. The third circuit is the steam water circuit. Among the two sodium circuits, the primary circuit is entirely inside the pool of the sodium. All the primary system components are housed inside the main vessel and the safety vessel. The primary circuit of the 500 MWe Prototype Fast Breeder Reactor (PFBR) is shown in Figure 1.2 (Chetal et. al., 2008).

The primary sodium pool of sodium is divided into two, a hot primary sodium pool (820 K) and cold primary pool (670 K) by an inner vessel. The other components immersed inside the pool of sodium are the primary sodium pumps, the Intermediate Heat Exchangers (IHX), control plug and the subassemblies housing the fuel, blanket and shielding material. The heat generated in the core is transferred to the primary circuit and this heat is then transferred to the secondary circuit in the IHX. The decay heat exchangers of the Safety grade decay heat removal system are used to remove the heat from the pool even during a station blackout condition.

The heat transferred to the secondary circuit is transported to the steam generator which has sodium in the shell side and steam/water in the tube side. The high temperature high pressure steam generated in the steam generator is fed to the turbine.

1.3. LMFBR FUEL ASSEMBLY AND ITS THERMAL HYDRAULIC BEHAVIOUR

The core of a typical medium sized LMFBR consists of subassemblies of various types. viz: fuel, blanket, storage and absorber rods. These subassemblies are held vertically in the grid plate. Each fuel subassembly consists of approximately 217 fuel pins. These fuel pins

7

are arranged in a tightly packed triangular pitch and are housed in a hexagonal sheath. The core of FBR is given in Figure 1.3.
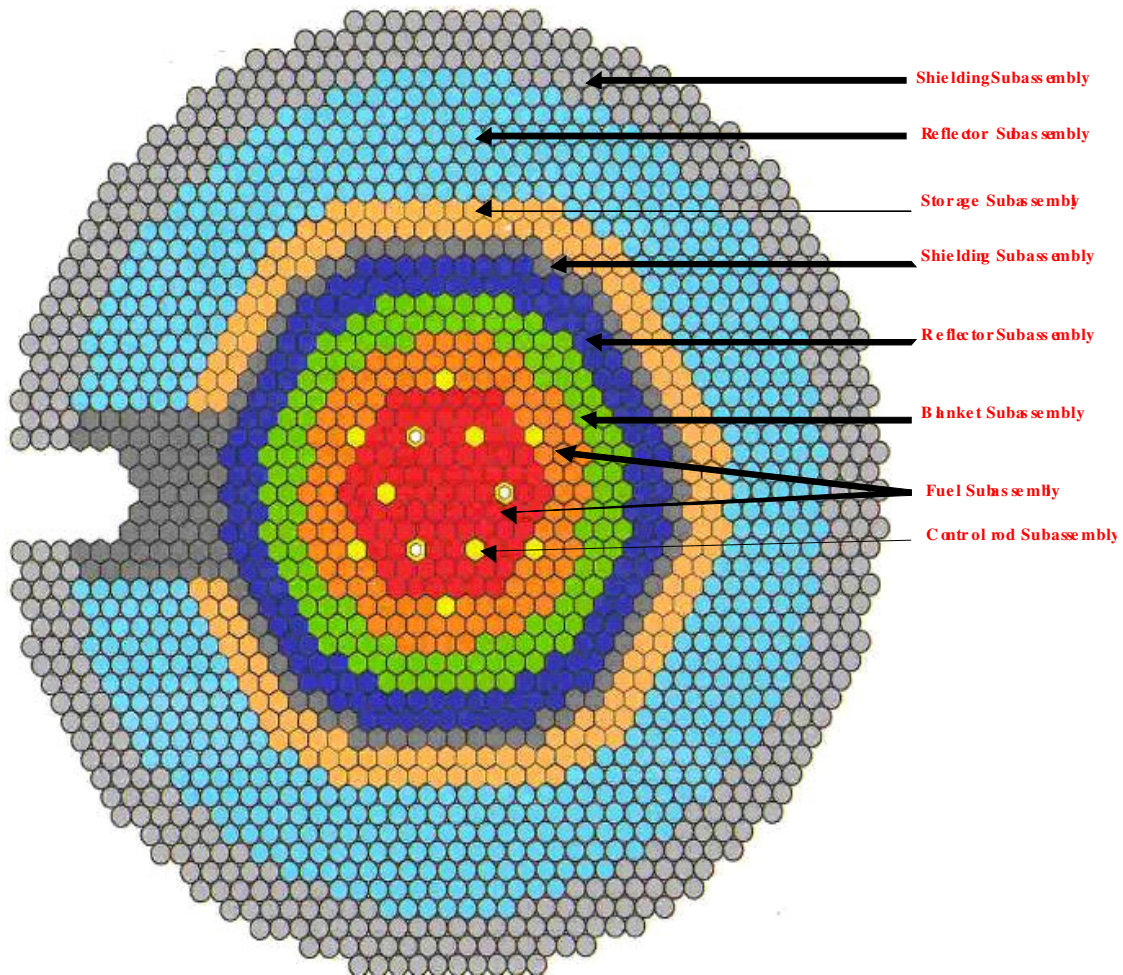
Fig. 1.3: Core plan of LMFBR

This compact core has a large power density with a heat flux in the order of 2MWt/m2. To extract this large heat flux with a small temperature difference between coolant and cad surface, the most appropriate candidate for coolant is liquid sodium. Liquid sodium with a melting point of 97 deg C and a boiling point of 883 deg C, becomes an ideal choice with a wide range for reactor operation. The thermal conductivity of Sodium (~70 W/m-K) results in high heat transfer coefficient. Space wires are wound helically over the

fuel pins. These spacer wires prevent collision between pins, provide lateral support, reduce the risk of flow induced vibration and aid in promoting turbulence. Typical spacer wire diameter is ~ 1.5 mm and the fuel pin diameter is ~ 6 mm. The pin length is about 2250 mm. The pins are arranged in a tight triangular lattice with a pitch of ~ 8 mm. The helical pitch of the spacer wire is ~ 150 to 200 mm. Sodium flows from the bottom of the fuel pins upwards. The presence of the helical wire results in significant heat transfer variation around the circumference of the fuel pin. There are various sub-channels in each sub assembly. The dimensions and thereby the flow area and hydraulic diameters of each of these sub-channels are different. The velocities of sodium through the sub-channels will also vary, leading to a non uniform flow distribution in the subassembly. The flow pattern and the thermal hydraulic characteristics of the fuel subassembly are quite complex. A clear understanding and knowledge of the thermal hydraulic behavior is essential for designing an efficient and safe core. The structure of a typical LMFBR sub assembly is detailed in Figure 1.4

Researchers have carried out studies using analytical techniques and validating with experimental results in arriving at flow and temperature distributions around the fuel pin. The advances in computational techniques have made it possible to carry out CFD analysis and 3 D simulations to predict this complex thermal hydraulic behavior.

It has been observed that the thermal hydraulics of the sub channels have been studied using porous body approach or by experiments. Fuel sub-assembly design by physical modeling and computational codes will not be able to determine the cross flow characteristics due to the wire wrap geometry and the development of the local thermal hydraulic couplings between the sub channels.

EXTERNAL VIEW OF HEAD

SPACER WIRE

FUEL PIN

Subassembly head

Graphite shielding

B4C shielding

Steel shielding

Axial top blanket

Bundle location

Axial bottom blanket

Fuel Bundle support rails

Subassembly Foot

Coolant Entry slots

Discriminator
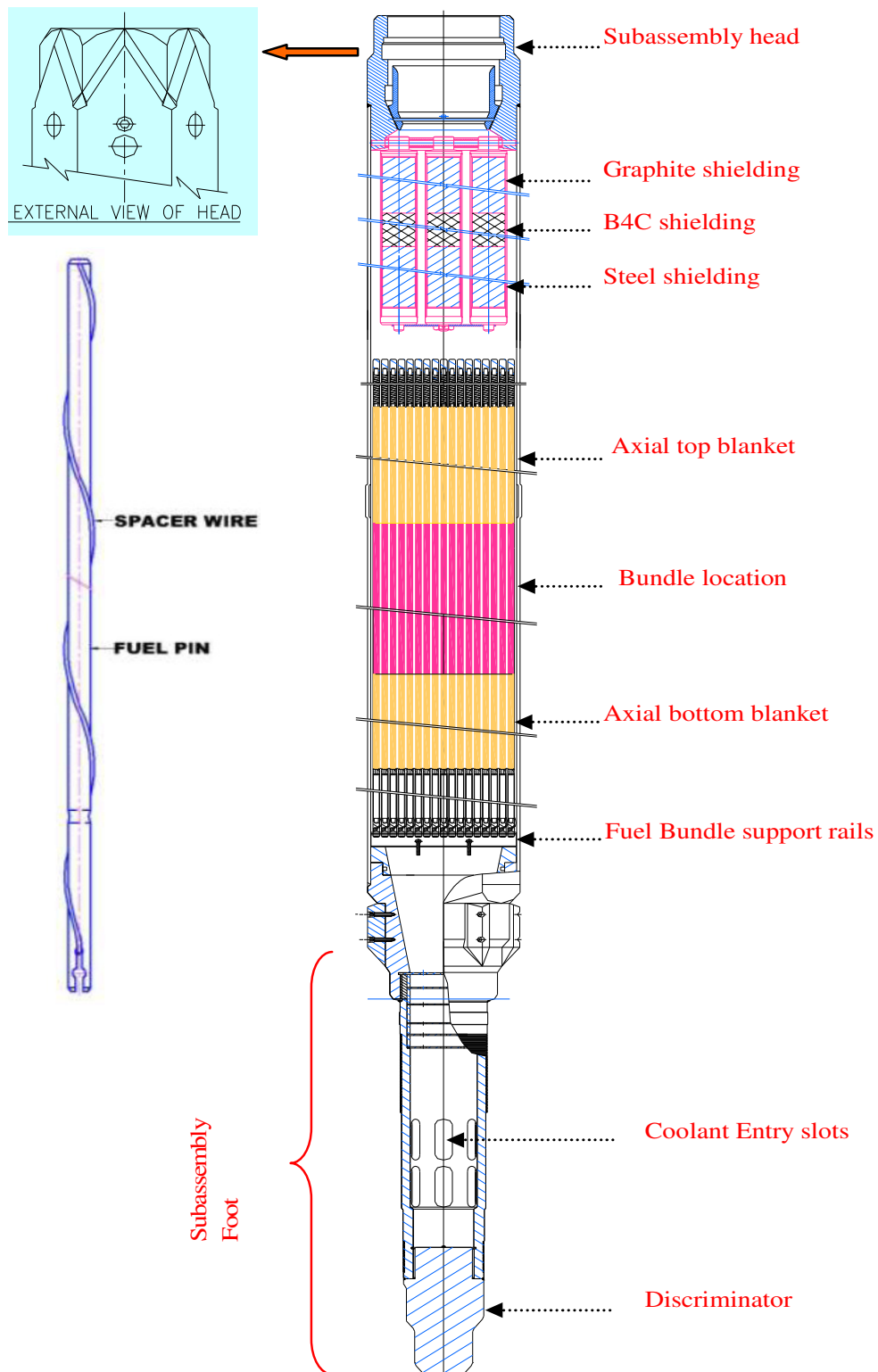
Fig. 1.4: Structure of a typical fuel subassembly in FBR

1.4. MOTIVATION FOR THE STUDY

Sustained and safe operation of LMFBR is characterized by the core configuration and the design limits of temperature for the various operating conditions. Understanding the complex thermal hydraulics of the sodium coolant flow through the core is vital for arriving at these design limits. A typical fuel subassembly has a large number of small diameter fuel pins arranged in a triangular pitch and with a positive gap between the fuel pins to allow flow of coolant. The cold sodium enters the subassembly and heat transfer from the fuel pin to sodium takes place when sodium flows through these sub-channels and hot sodium leaves at the top of the subassemblies. The heat generation in fuel pins varies both in axial and radial directions because of the variation in neutron flux. The mass flow rate of coolant is not uniform in all the sub-channels surrounding the fuel pins. Hence, there are significant temperature variations around the fuel pins which give rise to local hot spots. To minimize this issue, the fuel pins are separated by spacer wires helically wound around the pins which provide support for the fuel pins and also assist in mixing of coolant among the sub-channels. The heat transfer coefficient of the coolant also increases because of this transverse flow movement of sodium in the sub-channels. The coolability of core definitely increases because of the presence of spacer wire, however there still exists a temperature gradient across the cross section.

The central sub-channels are around the central fuel pins and the peripheral sub-channels are between the outer hexcan walls and outer row of fuel pins. The sub-channel flow areas around the central fuel pins are nearly the same. However, the edge / peripheral sub-channels have more flow areas than the central sub-channels and hence more sodium flow occurs through the peripheral sub-channels. On the other hand, the heat generation is relatively more in the central sub-channels and low in the peripheral sub-channels. This leads

11

to large variation in the sub-channel sodium temperature, characterized by low sodium temperature in the peripheral sub-channels and high sodium temperature in the central sub-channels. Higher sodium temperatures in the central sub-channels lead to large clad temperature in the central fuel pins. To respect the peak clad temperature limits, more sodium flow in to the subassembly is required.

There has been sparse information in literature about the studies conducted to minimize the flow bypassing through the peripheral sub-channels. Possible methods have also to be identified for introduction into the fuel subassemblies thereby bringing down the flow bypass. The temperature non uniformity across the cross section could be reduced and the mean temperature of sodium at the outlet of the core increased. The attempt to identify a suitable hydraulic device for this purpose forms the motivation for this study.

1.5. SCOPE OF WORK

It is important to reduce the non uniformity in the temperature distribution across the cross section of subassembly arising out of the non uniform coolant flow. The efforts towards reducing the bypass flow occurring in the peripheral sub channels would lead to a more uniform sub channel temperatures. This would also result in an optimized subassembly flow and eventually a high hot pool temperature.

Approach to reducing the peripheral sub channel flow area would be by the use of inserts which would reduce the flow areas and thereby divert more flow towards the central sub channels. Towards understanding the beneficial effect of these types of inserts, a 7 pin fuel bundle has been investigated. The study is mainly focused on uniformity of flow in all the sub-channels and thereby improving the heat transfer coefficient to achieve a lower clad hot spot temperature.

The improvement in the flow distribution among the central and peripheral sub-channels, reduction in mean clad temperature and the increase in Nusselt number as a result of inserts have been quantified. The investigation is based on 3 dimensional Computational Fluid Dynamic (CFD) simulations, where the model has been validated through experiments performed in water models. Also, the pressure drop in a 7 pin bundle with and without inserts has been measured using differential Pressure Transmitter. The pressure drop values in the bundle are then compared with the CFD predicted results. Clad temperature variation among the pins along the axial and circumferential directions, subchannel sodium temperature, Nusselt number, pressure drop and friction factor are studied in detail. The hot spot factor which is important for core design has been quantified and the Performance Enhancement Criterion (PEC) factor has been defined and compared for various cases. The pressure drop in a 1:1 subassembly have also been tested in water and then extrapolated to the reactor operating condition.

1.6. ORGANIZATION OF THE THESIS

The present thesis is divided into three parts. The first part comprises of three chapters with chapter 1 giving an introduction to the problem, chapter 2 critically reviews the literature and details of the computational modeling are given in chapter 3. The second part comprises of three chapters where chapter 4 details the hydraulic study conducted in the 7 pin bundle model and its experimental validation. The thermal analysis of the various insert geometries studied are detailed in chapter 5 and chapter 6 gives the simulation studies conducted in a 1:1 hydraulic sub assembly in water and its extrapolation to sodium at reactor operating condition. The third part, i.e., chapter 7 gives the conclusion and scope for future works.

CHAPTER 2

LITERATURE REVIEW

2.0. INTRODUCTION

Many numerical and experimental studies had been reported in the past to understand and identify the thermal hydraulic characteristics of the FBR core. Most of the experimental programs were carried out with a view to develop computer codes for easy prediction of the thermal behavior of the rod bundles of the core. During the initial development of FBR's the focus was towards developing sub channel analysis codes. Experiments with different number of fuel pins and different axial lengths have given valuable insight into the flow and temperature profiles of the wire wrapped rod bundle. With a view to understand the current level of understanding of the studies conducted in FBR rod bundle a detailed literature survey has been carried out and is presented below. The literature survey has been divided in to two portions, (i) Numerical studies and (ii) Experimental studies on FBR pin bundles.

The geometry of the fast reactor fuel subassembly is quite complex from thermal hydraulic considerations. The main complexity arises from the fact that the fuel bundle assembly consists of multiple fuel pins of cylindrical shape separated by helically wound spacer wires at suitable pitch. These heat generating fuel pins are tightly packed inside a hexagonal wrapper, which also forms the channel for coolant flow. The helical spacer wires provide support for fuel pin bundle and also assist in inter-subchannel coolant mixing.

2.1. NUMERICAL MODELING OF FBR PIN BUNDLES

Numerical studies on FBR pin bundles have been carried out by various researchers to characterize the hydraulics and observe thermal characteristics inside fuel pin bundle.

2.1.1. Numerical studies on hydraulics inside pin bundles

The spacer wire establishes positive gap around the fuel pins for coolant passage in addition to aiding in mixing. The flow ensuing from the slots provided in the foot of the subassembly reaches the bundle through a conical divergent section. The bundle section of the fuel subassembly is followed by bundle exit plenum and then subassembly exit. Estimation of the pressure drop contribution from each section of the subassembly is very important in understanding the subassembly hydraulics, although a major portion of the pressure drop is offered by the bundle region alone.

In order to estimate the friction factor, many researchers have proposed various correlations encompassing a wide range of geometrical parameters. Most of the correlations are geometry specific and their applicability over the entire spectrum of operating range has not yet been established.

3D computational fluid dynamic analysis of 7, 19, and 37 fuel bundles with helical wire wrap was carried out by Gajapathy et al. (2009) and the results were compared for sodium flow mixing and pressure drop against published correlations. Simultaneous development of flow and temperature fields in the entrance region of SFR fuel pin bundles with helical spacer wires has been investigated for its pressure drop characteristics by Govinda Rasu et al. (2014). The paper discusses the variation in parameters like Reynolds number, pitch of helical spacer wire and the number of pins in the bundle. The dimensions and the Reynolds number are chosen based on the conditions prevailing in a typical medium size fast reactor.

Coolant flow in a 19 pin bundle with wire wrap was studied numerically by Natesan et al. (2010) and the results were compared against reported correlations. Friction factor is observed to be a strong function of the helical pitch of the wire wrap, and a reduction in the

wire wrap pitch is found to enhance the cross flow velocity and turbulence intensity resulting in better thermal mixing for the coolant. However, a deviation of order of 20% is found when compared with the available experimental correlation signifying the need for experimental verification.

Jeffrey etal. (2008) carried out RANS based simulation on a 7 pin wire wrapped assembly of the Advanced Burner Test reactor to study mesh sensitivity, effect of boundary conditions in the flow domain and the choice of turbulence model in predicting the flow fields. It was observed that flow was generally insensitive to mesh resolution. The simple inflow/outflow conditions resulted in good convergence. The standard k-ε model was able to predict strong peak velocities while other models produced considerably more diffusive flow field.

Generalized distributed resistance models were proposed by Ninakota (1987) to replace the forced cross flow models used in sub channel analysis codes. The model specifically takes into account the effect of wire wrapped spacer and making it possible to be used in any lumped parameter thermal hydraulic codes. These models were plugged into the sub channel analysis codes and validated against the data from the ASFRE code. The model was found to be satisfactorily predicting the flow fields in the wire wrapped bundles.

Flow oscillations and anisotropy were studied by Chandra and Roelofs (2011) . It was observed that flow anisotropy increased with reduction in P/D ratio. Roelofs et al (2012) put forward the approach of low resolution CFD to aid in the prediction of medium scale flow features of fuel bundles.

The effect of the number of fuel pins on the flow features was insignificant when three dimensional simulation of flow and heat transfer in subassemblies were conducted by

Rolfoa et al. (2012). In the case of larger bundles of 217 pins the global swirl was predominant in the edge region.

2.1.2. Numerical thermal studies in pin bundles

Gajapathy et al. (2007) carried out CFD investigation of helical wire-wrapped 7 pin fuel bundle and assessed the effect of transverse flow in promoting flow and temperature uniformity. It is observed that due to the wire wrap, the difference in bulk sodium temperature between the peripheral and central sub-channels is reduced to by a factor of 4 when compared to that without spacer wire. Sreenivasulu et al. (2007) carried out detailed investigation on the effect of several parameters like pin to wire diameter ratio, the wire-pitch to diameter ratio etc. on the thermal hydraulic behavior of fluid flowing through a wire wrapped annulus. Wigeland and Hamman (2009) studied the efficacy of subassembly design changes to operate fast reactors with higher thermal efficiency. Simulations were carried out in a 19 pin fuel bundle. The studies showed that by varying the hexcan designs the average coolant temperatures could be increased by 14 deg C without increasing the peak temperatures.

Local flow and heat transfer characteristics in a seven tube bundle with helically wrapped wires of circular cross section were obtained computationally by Sreenivasulu et al (2011). Govinda Rasu et al., (2013), investigated entrance flow characteristics in a simultaneously developing flow for bundles with a maximum of 37 pins. They found that the flow is developed within an axial length of ~125 hydraulic diameters, but temperature development is achieved only when pin diameter is small or the number of pins is low. Govinda Rasu et al., (2014), investigated development of cross stream velocity as a function of helical pitch length and number of pins. They reported the existence of periodic spatial oscillations in friction factor and Nusselt number. Gajapathy et al., (2015) conducted a CFD

based computation on a 217 pin bundle and analyzed the effect of helical pitch on the flow and temperature distributions and the variation in friction factor and Nusselt number as a function of helical wire parameters.

Another study on calculations of coolant outlet temperature distribution of SFR test subassemblies by sub channel analysis method have been performed for 19, 37, 127 and 169 pin subassemblies by Syeilendra and Minoru (2013). The authors have concluded about usage of empirical correlations of pressure drop coefficient and have observed that inter-channel mixing significantly affects the prediction of coolant outlet temperature. It is also established that the correlations which consider three sub-channel types separately are capable of predicting the coolant temperature at bundle outlet.

Various researchers have reported work on investigation of thermal hydraulics of subassemblies. Wantland (1974), Basehore and Todreas (1980), Kim et al., (2002), Memmott et al., (2010), Wu et al., (2013), and Liu et al., (2015) have used sub-channel approach to study the thermal hydraulics within the bundle with assumption that axial flow is dominant compared to transverse flow. In the scheme of solution, the axial flow is rigorously treated by solving the governing equations, whereas the transverse flow is handled with a simplified model in the form of algebraic expressions. Computer codes namely SUPERENERGY, MANTRA-LMR, RELAP5-3D and COBRA-LM are some popular sub-channel codes used in SFR core design.

Numerical methods developed to determine temperature and pressure distributions in the pin bundle assemblies by the core designers employed the sub channel analysis approach. However a simplified porous body model for predicting the temperature distribution in wire wrapped fuel rod assemblies was developed by Khan et al. (1975). The rod array in the fuel assembly was divided into regions each being treated as a continuum by viewing the wire

wrapped bundle as a porous body. The results of this analysis matched with the available data with the same precision as that of the more complicated sub channel analysis. Correlations for the two empirical constants in the model were obtained as function of the geometrical parameters of the fuel assembly .

Peneguil et al. (2010) analyzed the thermal-hydraulics of wire wrapped fuel bundle with two different configurations of seven and nineteen pin fuel rods. The main finding was that the main flow features remain unchanged with the increase in number of pins. Two different turbulence models were tested finding good agreement with experimental correlations. On the other hand, the evaluation of the heat transfer requires more investigation. Experimental correlations for Nusselt number are quite scattered, making difficult the assessment of the CFD results. In this contest refined LES and DNS could play a big role providing a large and reliable amount of data for RANS modeling evaluation.

Razaet al. (2008) conducted three dimensional studies in 7 pin and 19 pin wire wrapped bundles. The studies indicated higher local axial velocities in the edge sub channels compared to the average axial velocity. The results were identical in both the models. The centre fuel pin and edge fuel pin temperatures were higher in 19 pin bundle assembly. It was concluded that computational results for the thermal field require further validation.

2.2. EXPERIMENTAL INVESTIGATIONS ON FBR PIN BUNDLES

2.2.1. Experimental studies on hydraulics inside pin bundles

Many researchers have reported experiments with SFR fuel subassembly for characterization of pressure drop in the subassembly. Lafay et al., (1975), conducted experiments in wire wrap 19 pin bundles, to study local pressure and peripheral flow distributions. Roychowdhury (1998) reported experimental data of pressure drop in a 217 pin

wire wrap bundle. Chen et al. (2013) presented correlations for friction factor for laminar, transition and turbulent flow regimes and calculation procedure to estimate hydraulic diameter with wire-wrapped pin bundle.

Other researchers who have offered suitable pressure drop correlations for wire wrapped rod bundles include the works of Novendstern (1972), Rehme (1973), Engel et al., (1979), Baxi et al., (1981), Cheng and Todreas (1986), Choi et al., (2003), Bubelis and Schikorr (2008) etc. Recently, Chen et al., (2014) made a detailed comparison of these correlations and evaluated their applicable ranges. Novendstern (1972) developed a semi empirical model to predict pressure losses in a hexagonal array of fuel pins utilizing a wire wrap spacer system. This model is able to predict pressure drop within ± 14% over a wide range of geometries in the turbulent regime. Following this, Rehme (1973) reported a simplified correlation for friction factor for a range of pitch to diameter ratio based on the investigation carried out on rod bundles having the number of pins ranging between 7 to 61. Engel (1979) performed studies to find friction factors for laminar, transition and turbulent flow wire wrapped hexagonal pin bundle. A correlation was also proposed by authors for all these flow regimes.

Parametric studies conducted illustrate the effect of various geometrical parameters over a range of Reynolds number. It is observed that among all the parameters, the triangular pitch to diameter ratio is the most sensitive parameter affecting friction factor. Hydrodynamic models for sub-channel friction factor and mixing parameters in wire wrapped rod bundles have been developed by Cheng and Todreas (1986). Correlations for flow split parameters as well as the friction factor have been proposed by them. These correlations were found to predict the bundle average friction factor data within ± 14% for turbulent flow ± 30% for laminar flow with 92% confidence level.

21

Moon and Kyong carried out water studies in a 19 pin helical wire wrapped bundle assembly with four different test sections with varying P/D and H/D ratios. The study compared five correlations to arrive at the best performing correlation in the sub channel pressure drop analysis. The study concludes that Novendstern (1972) correlation agrees well in the turbulent regime, Rheme (1972) under predicts the friction factor in all flow regions while Engels (1979) over predicts the friction factor in all flow regimes. It establishes the utility of Cheng and Todreas (1986) correlation for all flow regions.

Choi (2004) measured pressure drop data for a 271 pin fuel subassembly and confirmed the suitability of correlation proposed by Cheng and Todreas (1986) as the most suitable among the available correlations. Recent publication by Chen et al. (2014) have compared wide range of correlations and their applications for their relevant programs. The study emphasizes the application range for the Cheng and Todreas correlation in terms of P/D, while for H/D its range covers the lowest value of 4 to the second highest value of 52.

Bubelis and Schikorr (2008) brought out a comprehensive review and comparison of the empirical correlations for friction factor given by different authors for wire-wrapped fuel bundles based on a particular set of experimental data. These correlations usually are very good for the prediction of friction factors for wire-wrapped fuel bundle within the parameter range for which they were derived based on fluid and fuel bundle parameters. According to the authors, when one tries to apply these friction factor correlations to another fluid (coolant) or different fuel bundle parameters, one often obtains predictions of the friction factor that is not always possible to correlate with the experimental data.

Rehme, (1973, 1987) based on water experiments presented correlations to evaluate friction factor in a 7 pin bundle with helical spacer wire wrap. The authors recommended the usage of Rehme friction factor correlation in the thermal hydraulic evaluations in the

estimation of the pressure drops in wire-wrapped rod/fuel bundles for all reactor types, i.e. coolants.

Experimental studies in water to generate mixing data in a 91 pin bundle assembly were presented by Lorenz (1976). Isokinetic sampling techniques with electrolytic tracers were employed to generate data for code validation. The emphasis of the study was on peripheral sub channels. The velocity measurements revealed that pitch averaged edge and corner sub channel velocities were nearly equal to the bundle average velocities. The average swirl flows at the peripheral channels were 1.2 times greater than the predicted values. The average swirl velocity came down with increase in bundle size. Both swirl velocities and concentration profiles were insensitive to Reynolds number for the range of flows which was studied.

It is amply evident from the literature survey that even though the correlations available are useful in predicting the pressure drop in wire-wrapped bundles, an experimental investigation is useful in determining the exact characteristics and to establish the validity of applicable correlation. In this regard an experimental investigation is conducted on a 217 pin fuel subassembly and the results are compared with the correlations available in the literature.

2.2.2. Experimental thermal studies on pin bundles

Collingham et al. (1970) carried out an experimental study on an electrically heated 7 pin bundle of a typical FBR with sodium as coolant in order to analyze the effect of helical wire wrap on heat transfer mechanism in the bundle assembly. It is observed that the helical wire wrap causes a forced diversion of the coolant between inner and outer sub-channels and due to this sweeping mechanism, the bulk coolant temperature difference between the channels is reduced considerably compared to that without wire.

Lorentz and Ginseberg (1977) carried out experimental mixing studies in a 91 pin bundle water model to establish data base for validating thermal hydraulic codes. Fennech (1984) studied local heat transfer and hot spot factors for wire wrapped tube bundles. Heat transfer coefficients and hot-spot factors have been determined from measured local temperatures and calculated local mass flux in seven adjacent tubes and associated sub-channels of a 61 wire-wrap tube bundle of a gas cooled fast reactor.

Fenech (1985) investigated heat transfer coefficients and hot-spot factors from measured local temperatures and calculated local mass flux in seven adjacent tubes and associated sub-channels of a 61 pin wire-wrap tube bundle. The experiment used water at atmospheric pressure and temperature, as coolant. He presented dimensionless correlation for heat transfer coefficient which is applicable to gases and all non-metal fluids in single phase flow.

Experiments in water loops conducted for a 61 tube wire wrapped hexagonal bundle was used to determine the friction factor and heat transfer coefficients in laminar and turbulent regions by Arwikar (1979). Circumferential pressure and temperature profiles of tubes and the flow pattern produced by the injection of dye at the wall of the hexagonal bundle revealed the strong effect of wire wrap on local pressures, temperature and flow mixing. Change in Reynolds number had no impact on these profiles. Wire wrapping was found to increase the heat and momentum transfer much more in the laminar region compared to turbulent region.

Krauss (1998) conducted experimental investigations with turbulent air flow in a central channel of heated 37-rod bundles with triangular array at two different pitch-to-diameter ratios (1.12 and 1.06). A hot-wire probe with x-wires and an additional temperature wire was used to measure time mean velocities, time mean fluid temperatures, wall shear

stresses and wall temperatures, and various turbulent parameters in a central channel of the bundle. It was shown that with decreasing gap width the turbulence field in rod bundles deviates significantly from that in a circular tube. Also, data on the power spectral density functions of the velocity and temperature fluctuations showed the existence of large-scale periodic fluctuations of velocity and temperature in the gap.

Detailed survey of literature indicates that the literatures dealing with study of modification in subassembly geometry to modify the flow behavior have been sparse. In open literature, investigations have been reported dealing with effect of non uniform sub-channel flow and some studies have focused on the feasibility of reducing the extent of non-uniformity in coolant flow. However, not much information is available vis.a.vis the type of devices to reduce this non-uniformity. The usages of inserts as an additional feature in the subassembly to improve the hydraulics and in turn heat transfer is not reported widely. Many options are possible for the inserts with each inserts having different effect on Nusselt number, friction factor and hot spot factor. This knowledge is required for design of future fast reactors with optimized core flow. This is the main motivation for the present study where both CFD and experimental investigations have been carried out.

2.3. CLOSURE

The studies to assess the flow asymmetry and thereby the temperature distribution at the outlet do not find any mention in the literature. There has not been any effort on minimizing the flow bypass that occurs in the sub channels leading to a temperature gradient across the cross section with maximum at the centre and minimum at the periphery. The studies have been conducted in water mainly and sodium studies have also been conducted to investigate the profiles across the rod bundles. It is evident that detailed investigation in to the

effect of solid inserts to minimize the flow bypass in the peripheral sub-channels has not been carried out. Such inserts are expected to reduce the flow and temperature non-uniformities in FBR subassemblies. To respect a particular clad hot spot temperature, such inserts will lead to reduced coolant flow rate. However, these inserts can also increase the pressure drop in a subassembly. In the present thesis, both experimental and computational simulations have been carried out to understand the flow characteristics in a wire wrap bundle with inserts.

CHAPTER 3

COMPUTATIONAL MODELING

3.0.   INTRODUCTION

A computational model of 7 fuel pin bundle has been considered with sodium as the coolant. The diameter of fuel pin is 6.6 mm. The fuel pins are arranged in a triangular pitch of 8.28 mm and spacer wires of diameter 1.65 mm are helically wound over the pins. The helical pitch of the spacer wire is 200 mm and the pin bundle has been modeled for a single pitch length of spacer wire. The contact between fuel pin and spacer wire is a line contact. The difficulty in meshing due to the line contact between the pin and wire is overcome by providing a radial offset of 0.05 mm for the wire towards the center of the pins and thereby converting the line contact to surface contact. Various geometries of inserts are provided in the flow bypass gap between fuel pins and hexcan walls. Figure 3.1 shows the 3-dimentional view of the computational model developed for the 7 pin bundle.
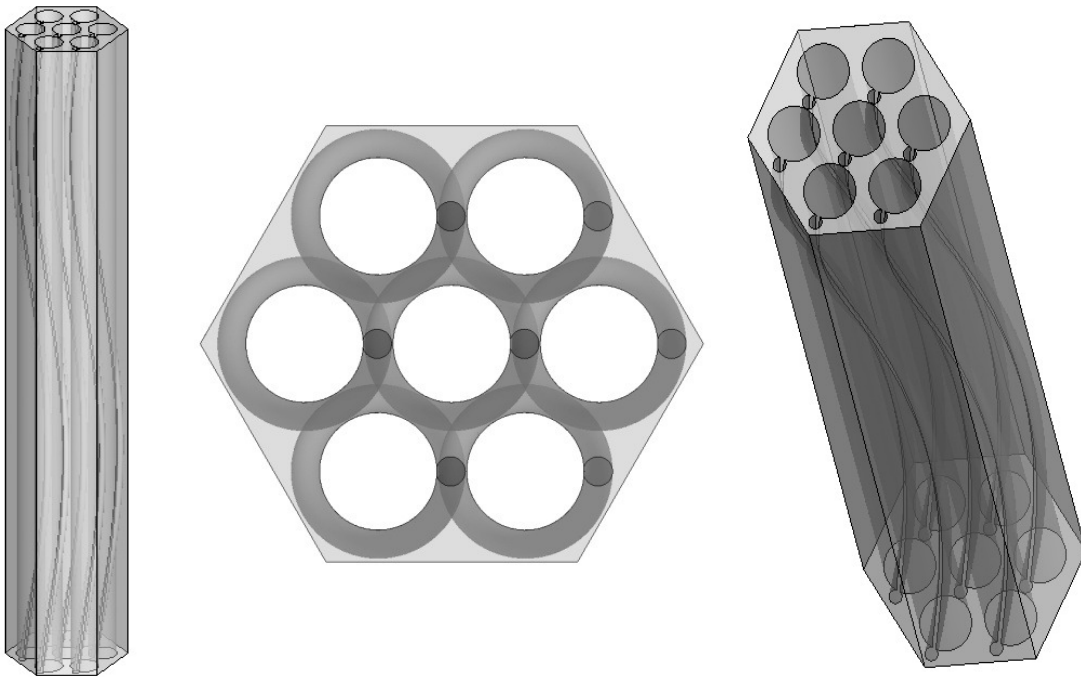
Fig. 3.1: Computational model of 7 pin fuel bundle without any inserts

Thermal hydraulic analysis has been carried out for various values of Reynolds number ranging from 4 x 10^4 to 2 x 10^5. Further, validation of the CFD model has been carried out by comparing the predicted results with measured velocity profiles and pressure drop values.

Figure 3.2 shows the geometrical details of inserts of the computational model developed for the 7 pin bundle. While choosing the dimensions of the inserts, the minimum distance between the peripheral fuel pins and the inserts is taken to be the same for all the types of inserts.

Semi-Circular insert	Triangular insert	Circular insert

	Isosceles triangle	
Diameter = 3.15 mm	a = 3.23 mm	Diameter = 1.87 mm
	b = 5.04 mm	
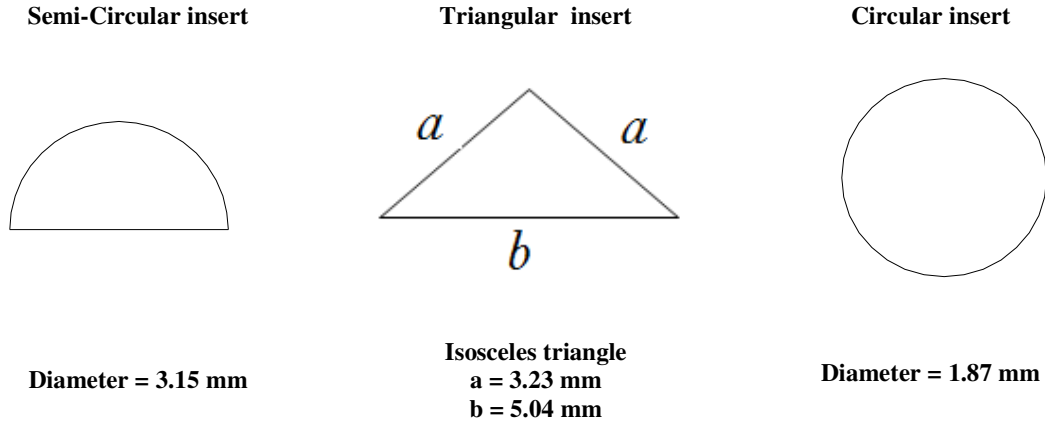
Fig. 3.2: Geometrical details of inserts

3.1. GOVERNING EQUATIONS

The steady state 3 dimensional form of incompressible Navier-Stokes equations and energy equations governs the coolant flow inside the fuel subassembly. To model the turbulence statistically, Reynolds-Averaged-Navier-Stokes (RANS) equations are used. The governing equations solved are :

3.1.1. Continuity equation

$$\frac{\partial U_i}{\partial x_i} = 0 \tag{1}$$

3.1.2. Momentum equation

The momentum equation with assumption of negligible viscous dissipation and surface tension effects is as follows

$$\rho U_i \frac{\partial U_j}{\partial x_i} = \frac{\partial}{\partial x_i}\left[\mu\left(\frac{\partial U_i}{\partial x_j} + \frac{\partial U_j}{\partial x_i}\right) - \rho\overline{u'_i u'_j}\right] - \frac{\partial P}{\partial x_j} + \rho g \delta_{j3} \tag{2}$$

$$\delta_{j3} = 0 \; (if \; j \neq 3)$$
$$\delta_{j3} = 1 \; (if \; j = 3)$$

3.1.3. Energy Equation

$$\rho c_\mu U_i \frac{\partial T}{\partial x_i} = -P \frac{\partial U_i}{\partial x_i} + \lambda \frac{\partial^2 T}{\partial x_i^2} - \tau_{ij} \frac{\partial U_j}{\partial x_i} \tag{3}$$

3.2.   BOUNDARY CONDITIONS

At the inlet to the pin bundle, specified sodium velocity has been provided as boundary condition. The inlet turbulence intensity and eddy viscosity ratio are 2% and 10 respectively. The outlet boundary condition is specified as pressure condition (atmospheric pressure). No slip condition is given to clad, hexcan as well as spacer wire walls. The heat flux in SFR fuel rod has an axial chopped cosine profile. In this analysis, an idealized model with 7 pins and uniform heat flux has been considered. The assumption of uniform heat flux does not affect the impact of inserts on the pressure drop, Nusselt number, flow uniformity and temperature uniformity in the pin bundle. A uniform heat flux of 2×10^6 W/m^2 is imposed

on the outer surface of the clad. The helical wire-wrap is considered to be adiabatic. The schematic of the 7 pin bundle with the boundary conditions is depicted in Figure 3.3. Since the fluid medium considered in the analysis is liquid sodium which is opaque for thermal radiation, thermal radiation is not considered in the analysis. The Richardson number (Ri) based on temperature difference and sodium velocity is <0.1 and this suggests that mixed convection effects are negligible. Hence, only forced convection is considered in the analysis.
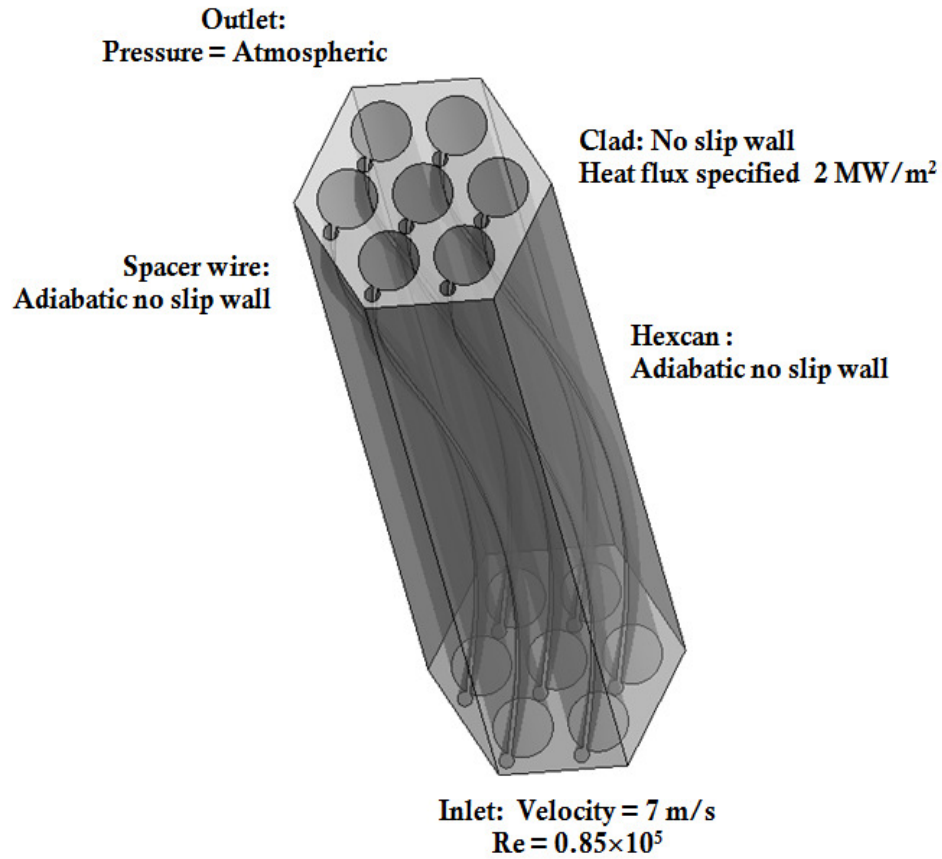
Fig. 3.3: Boundary conditions

3.3. GRID INDEPENDENCE STUDY

Tetrahedral mesh has been adopted due to the geometrical complexity, especially in the bundles with inserts. The minimum mesh size is 0.01 mm in all the pin bundles. Grid independence study for four different mesh patterns of the reference bundle without any

31

inserts has been carried out with different grid sizes ranging from very fine (9 million grids) to coarse (4 million grids). The number of points around the pin and the wire are varied from 20 to 40 and 5 to 15 respectively. It was found that reduction of grids from 9 million to 6 million doesn't cause change in solution and 6 million mesh is sufficient for the accurate solution and the solution is independent of the mesh size beyond this value. Hence, the number of mesh used in the reference bundle without any inserts is about 6 millions for one helical pitch length. The same, for pin bundles with inserts is about 8 millions. The mesh distribution at the inlet to the bundle is depicted in Figure 3 4 (a) for all the cases studied. The % change in coefficient of friction for each mesh is shown in Table 3.1.

Without any inserts

Semi circular inserts

Triangular inserts

Circular inserts
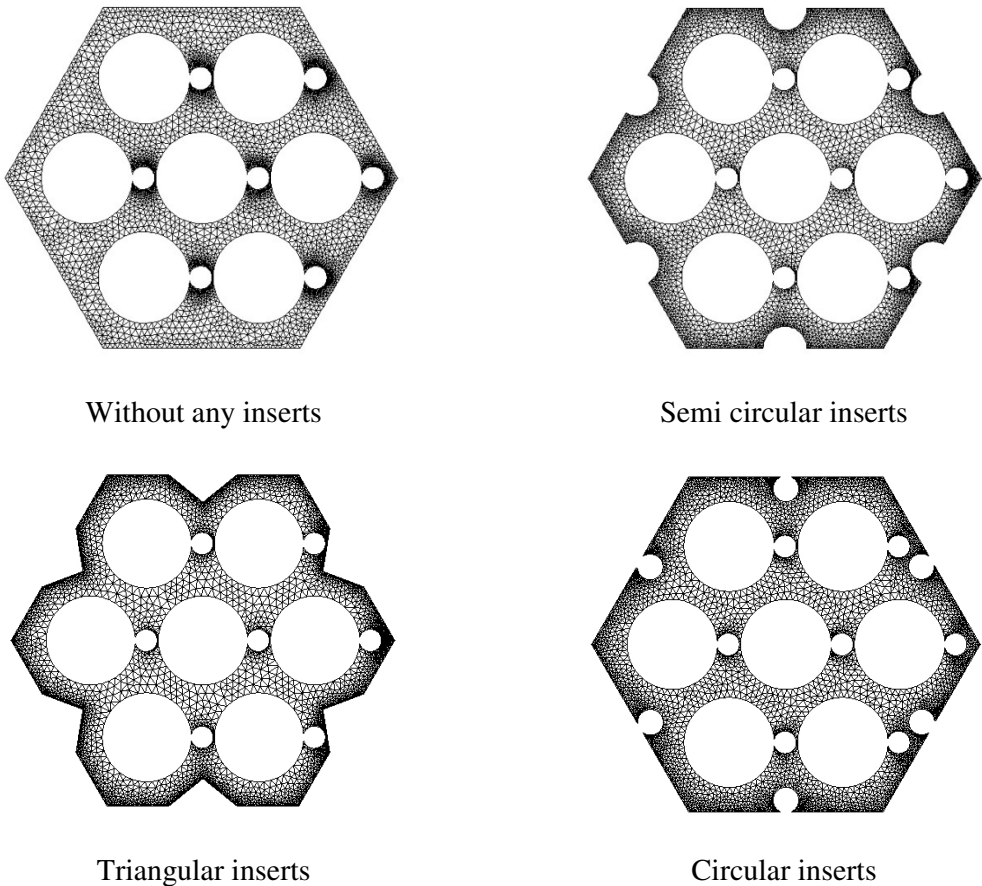
Fig. 3.4(a): CFD mesh pattern at the inlet plane

Table 3.1: The % change in coefficient of friction for various mesh sizes

Sl no.	No. of meshes (Million)	Friction factor	% in change friction factor
1	9	0.0196	-
2	6	0.0193	1.55
3	4	0.0185	5.94

3.4. TURBULENCE MODELS

The thermal and hydraulic predictions of various turbulence models (ANSYS FLUENT 13.0 User's Guide, 2010) are compared to identify a suitable turbulence model. The models considered are (i) Standard k-□ model, (ii) RNG k-□ model, (iii) Realizable k-□ model, (iv) Standard k-ω model and (v) SST k-ω model. Critical parameters at the exit of fuel pin bundle, viz., (i) cross stream velocity field, (ii) sodium temperature field, (iii) friction factor and (iv) Nusselt number, determined from various turbulence models have been compared. The governing equations are solved by a Finite Volume based CFD software – ANSYS fluent. Towards this, the case of reference pin bundle without any inserts at Re=0.85×10^5 has been considered. High-end workstations of 24 cores, with 32GB RAM and 2.2GHz speed have been used for the CFD simulations. It took about 3 days for one simulation to complete. Steady state solution method is used in this investigation and no time-marching is adopted.

The predicted cross stream velocity field and sodium temperature field at the pin bundle exit are compared in Figure 3.4 (b) and Figure 3.5. The distributions of cross-stream velocity and temperature are also nearly identical. The computed values of friction factor and Nusselt number are presented in Table 3.2. It can be seen that the maximum deviation in the predictions by various turbulence models is less than 0.05% in friction factor and 0.03% in

Nusselt number. It is evident that the distributions predicted by various turbulence models are nearly identical suggesting the usage of standard k-∈ model. It may be highlighted that standard wall function with a constant turbulent Prandtl number of 0.85 has been used in the standard k-☐ model.
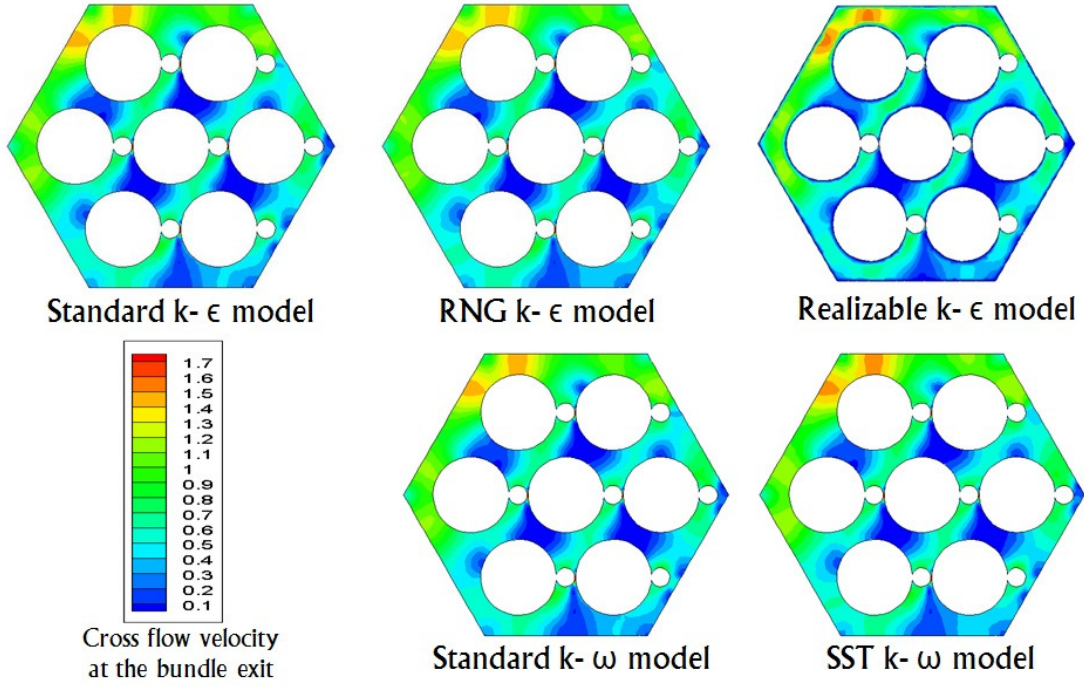
Fig. 3.4(b): Comparison of cross flow velocity (m/s) at bundle exit predicted by various turbulence models (Reference pin bundle without any inserts at Re=0.85×10^5)

Standard wall function approach has been adopted to capture the boundary layers adjacent to the walls. The y^+ values close to the pin surface are maintained in the range 30 – 80. The governing equations are solved by a Finite Volume based CFD code. The pressure velocity coupling has been resolved using the SIMPLE algorithm. For declaring convergence, the tolerances on the residual values for all the governing equations are set as

10^{-6}. Fully developed friction factor and Nusselt number predicted by various turbulence models at Re=0.85×10^{5} for reference pin bundle without any inserts is presented in Table 3.2.
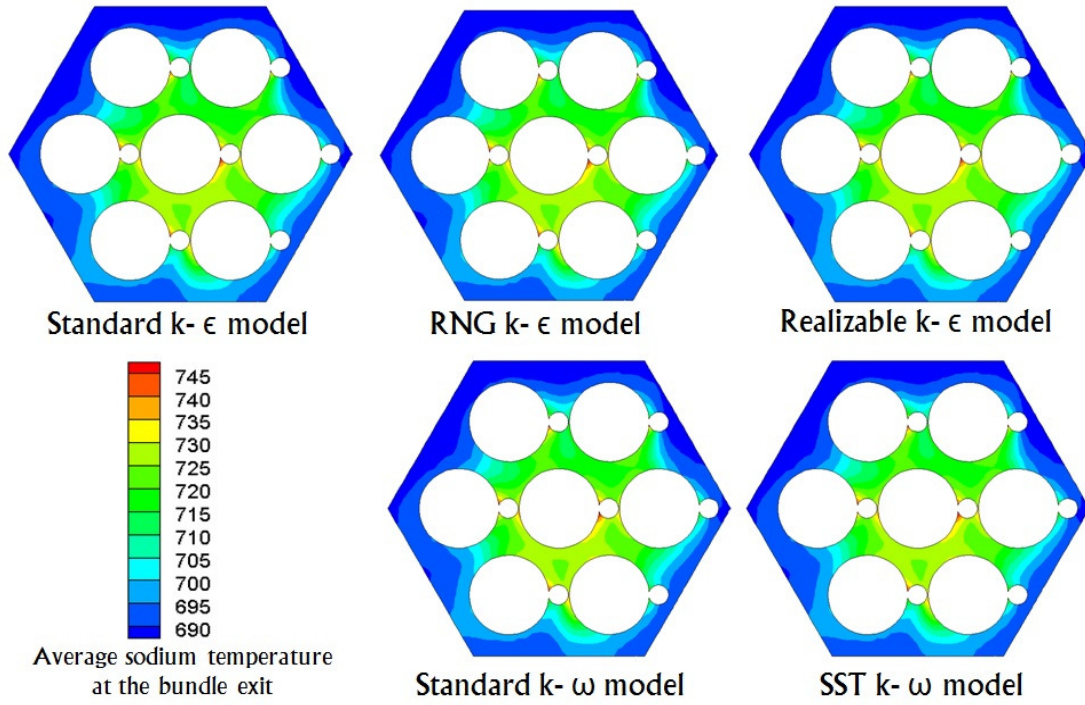
Fig. 3.5: Comparison of sodium temperature (K) at bundle exit predicted by various turbulence models (Reference pin bundle without any inserts at Re=0.85×10^{5})

Table 3.2: Fully developed friction factor and Nusselt number predicted by various turbulence models at Re=0.85×10^{5} for reference pin bundle without any inserts

Turbulence model	Friction factor	Nusselt number
Standard k-□ model	0.01931	6.371
RNG k-□ model	0.01932	6.373
Realizable k-□ model	0.01931	6.371
Standard k-ω model	0.01932	6.373
SST k-ω model	0.01932	6.373

3.5. SELECTION OF PITCH

In order to verify if an axial length of one pitch (i.e., 200 mm) is adequate to obtain fully developed flow and temperature fields, simulations were carried out for one and two axial pitch lengths. Figure 3.6 shows the 3-D views of 7 pin fuel bundle model with one pitch and two pitch lengths. The predicted values of friction factor (for Re = 0.85×10^5 in the reference bundle) at the end of 200 mm and 400 mm were 0.01931 and 0.01924 respectively, indicating a deviation of less than 0.4%. Similarly, the Nusselt numbers at 200 mm and 400 mm were compared and found to be 6.371 and 6.353 indicating a deviation of less than 0.3%.
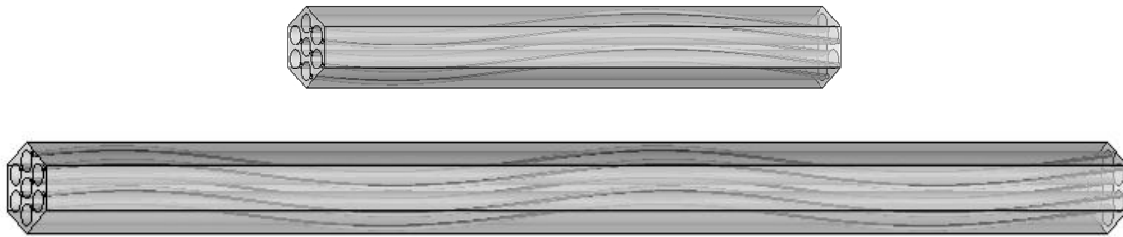
Fig. 3.6: 3-D views of 7 pin fuel bundle model with one pitch and two pitch lengths

The vertical (axial) velocity at the outlet of the pin bundle with one pitch length and two pitch lengths are shown in Figure 3.7. A comparison of cross flow velocity at the outlet for both the cases is presented in Figure 3.8. The variation of friction factors for both the cases is presented in Table 3.3. This exercise suggests that the simulation of one pitch length is adequate for the present objectives.

Table.3.3: Comparison of frication factors for one pitch and two pitch models

Axial length simulated	Friction factor
One pitch	0.019
Two pitch	0.019
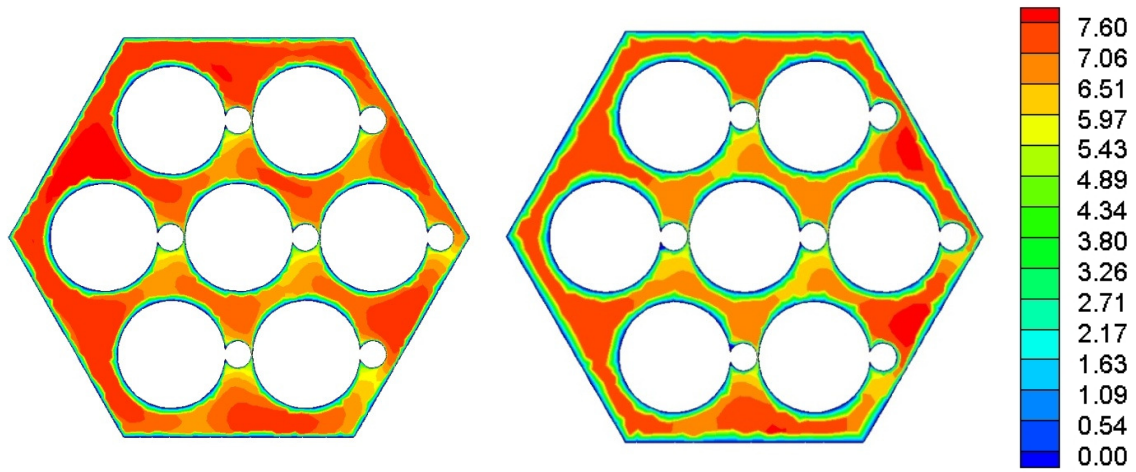
One pitch length model   Two pitch length model

Max V = 7.7 m/s   Max V = 7.63 m/s

Fig. 3.7: Comparison of vertical velocity (m/s) at the outlet (Re = 0.85×10^5)
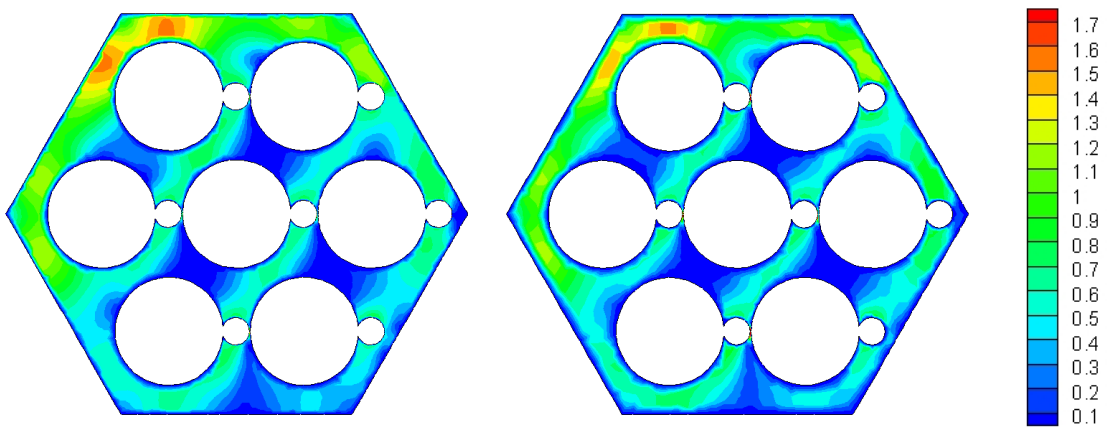
One pitch length model   Two pitch length model

Max V = 1.53 m/s   Max V = 1.52 m/s

Fig. 3.8: Comparison of cross flow velocity (m/s) at the outlet (Re = 0.85×10^5)

3.6.   SELECTION OF NUMBER OF PINS

The prototype fuel subassembly in the reactor contains 217 fuel pins. Complication in the modeling and carrying out numerical analysis of 217 pins with spacer wire and the limitations in the computational capabilities lead to the choice of 7 fuel pin bundle model as an ideal choice for detailed investigations. A 7 pin fuel bundle consists of a central pin and one row of peripheral pins. The peripheral row of pins with the helical spacer wire ensures the swirling motion of coolant inside the subassembly as in the case of subassembly with 217 pins and offer similar pressure drop characteristics. This point has been confirmed by comparing the friction factor of 7 pin bundle with a 19 pin bundle. The 19 pin bundle model includes the central pin surrounded by two rows of pins. A 3-D view of 19 pin bundle is shown in Figure 3.9.
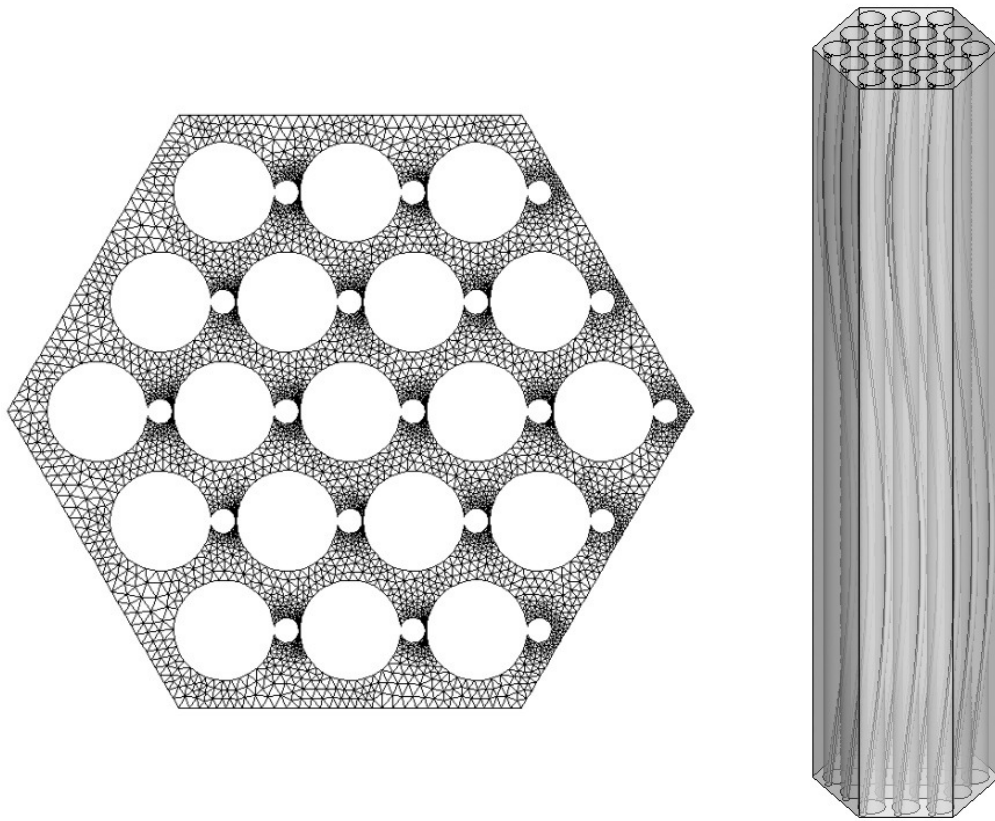
Fig. 3.9**:** 3-D views of 19 pin fuel bundle model

A comparison of sodium vertical velocity at the outlet and cross-flow velocity through the sub-channel area at the outlet for both the cases is presented in Figure 3.10 and Figure 3.11 respectively. It can be seen that the fully developed peak axial and cross flow velocity values are nearly similar for 7 pin and 19 pin bundles.

| 7 pin fuel bundle | 19 pin fuel bundle |
| Max: 7.70 m/s | Max: 7.77 m/s |
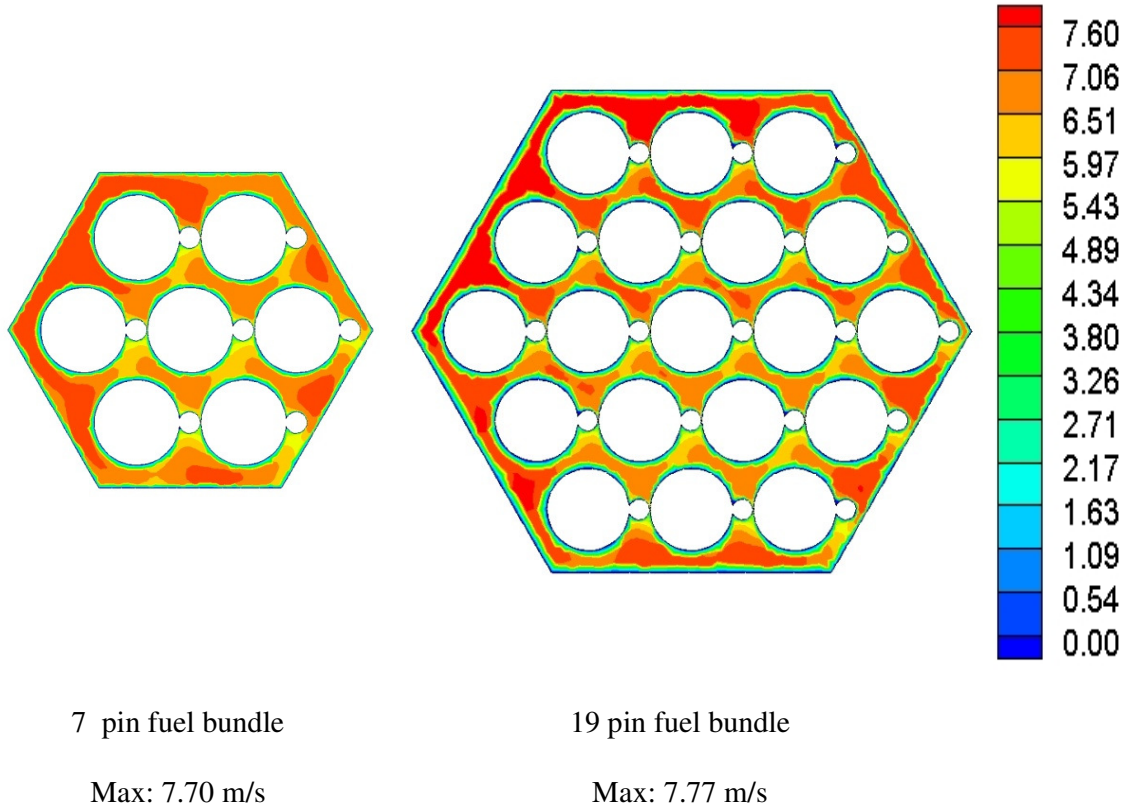
Fig. 3.10: The comparison of vertical velocity (m/s) at the outlet (Re = 0.85×10^5)

The maximum values of vertical velocity and cross flow velocity at the outlet are comparable for both 7 pin fuel bundle and 19 pin bundle models. Hence, a 7 pin bundle model is considered adequate to study the hydraulic characteristics of inserts.

7 pin fuel bundle
Max: 1.543 m/s

19 pin fuel bundle
Max: 1.524 m/s
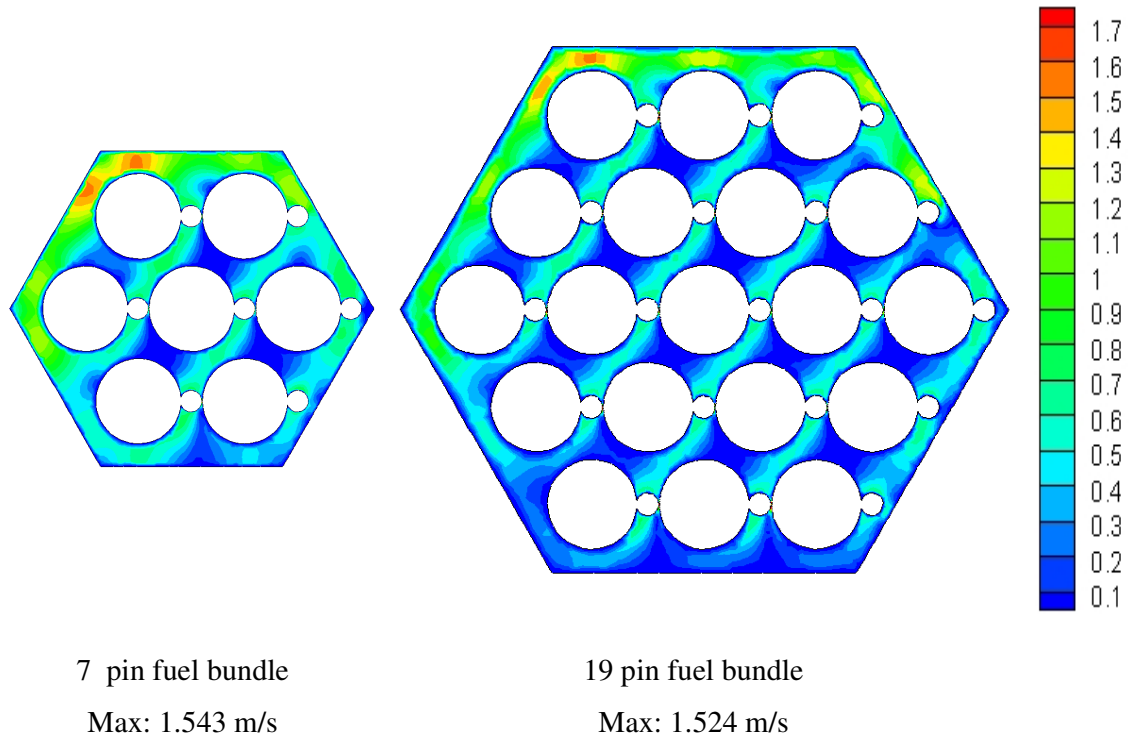
Fig. 3.11: The comparison of cross-flow velocity (m/s) at the outlet (Re = 0.85×10^5)

3.7. HYDRAULIC VALIDATION OF THE MODEL

Towards the validation of hydraulic aspects of the CFD model, two full scale experimental models with 7 pins were fabricated. They are (i) reference bundle without any inserts and (ii) bundle with circular insert. The pin diameter, wire diameter, helical pitch, triangular pitch and dimensions of hexcan were same as that used in the CFD model. However, the fuel pin length was 600 mm, corresponding to 3 helical pitch lengths. Water was used as simulant and the Reynolds number was varied from 5 x 10^3 to 1.3 x 10^4 in the experiments. The corresponding water flow rates are 1 m^3/h to 3 m^3/h respectively. The experimental assembly is depicted in Figure 3.12. The 7 fuel pins used in the experiments are depicted in Figure 3.13.

Fig. 3.12: Experimental model subassembly

Fig. 3.13: Pins used for the study

The experimental set up is shown in Figure 3.14. Since the experimental model was fabricated in stainless steel, it was difficult to get velocity pattern inside the pin bundle and hence velocity measurement is carried out at the exit of outlet plane. The pin bundle outlet has been connected to a rectangular perspex header of width 40 mm which is extended up to 230 mm in the downstream side. Velocity has been measured by Particle Imaging Velocimetry (PIV) and Ultra sonic Velocity Profiler (UVP). Velocities are measured along different planes and different axes. The pressure drop in the pin bundle has been measured at different flow rates.
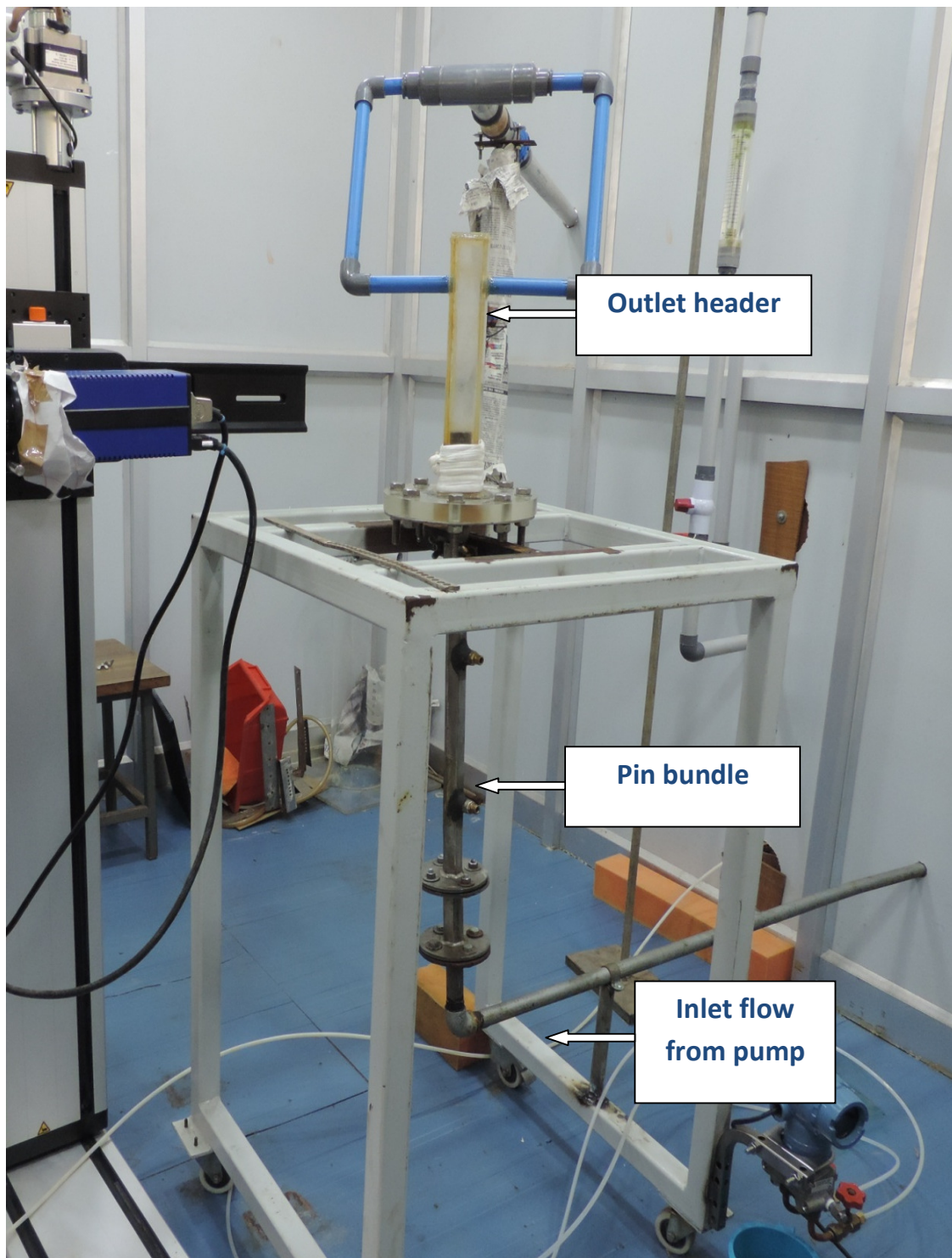
Fig. 3.14: Experimental set up for validation of CFD model.
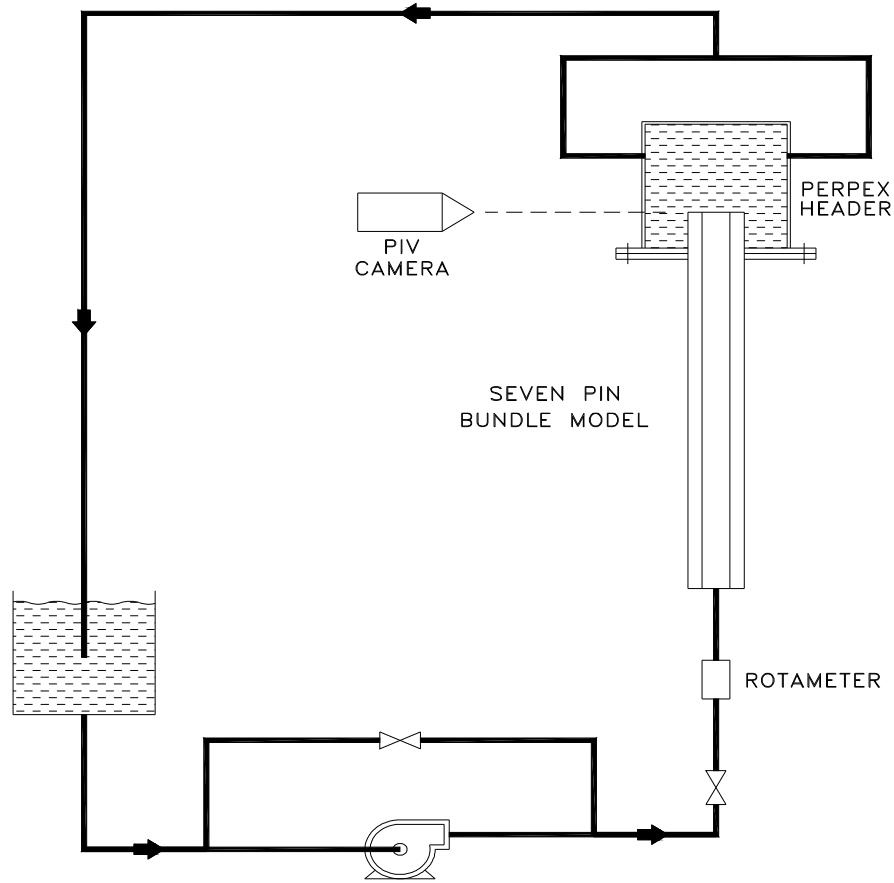
Fig. 3.15: Schematic of experimental set up

The schematic of experimental loop is shown in Fig. 3.15. A pump of 10 m^3/h capacity has been used to circulate water from a tank to the model through a rotameter. The required flow through the model is obtained with the help of valve at the discharge side of pump and the rotameter. The water from the outlet of the pin bundle is taken back to the tank through two pipe lines connected to a Perspex header. Pressure tapping points are provided at an elevation difference of 200 mm (one helical pitch length) in the hexcan walls for pressure measurements. These tapping points are connected to Differential Pressure Transmitter (DPT). The accuracy of the rotameter, which was calibrated before the experiment is ±1% and the accuracy of the DPT is ±0.4%.

3.7.1. Particle Image Velocimetry (PIV)

Particle Image Velocimetry (PIV) is a state of art non intrusive type velocity measurement device and it can be used for accurate velocity measurement of flow field. This is useful for qualitative and quantitative measurement of the velocity with good spatial and temporal resolution. This system offers wide velocity operation range hence can be used for low as well as high speed applications. Non intrusive nature of operation and higher accuracy of the device makes it very useful instrument. It consists of laser, camera, synchronization unit, traversing mechanism and system for analyzing the data. This is a sophisticated instruments needs careful handling, dust free environment and laser safe operation; hence it is required to set up in the enclosed room with necessary arrangements. This is mainly used for R&D pertaining to FBR components and systems.

This PIV system can be used for velocity mapping in the given planer field. Measurement of all three components of the velocity in given plane is carried out by stereoscopic PIV. Planer velocity component in the given plane is measured by 2D PIV. As this is optical based instrument, experimental model need to be transparent to light source hence mostly glass or perspex models are utilized for fabrication of the experimental set up.

The working principle of PIV is shown in Figure 3.16 and schematic arrangement for the PIV measurement with all the components is shown in Figure 3.17. Laser light beam is converted into light sheet using optics. This laser light is passed through fluid domain under investigation. Fluid domain need to be seeded with seeding particles to help laser light reflection in the flow field. This reflected laser light from flow field is captured by two cameras positioned inclined to the measurement plane. Two successive Laser light sheets are flashed in the measurement area with time gap and images are recorded with the help of camera. Images obtained by camera are analyzed with cross correlation technique and vector

filed is generated for given investigation area. PIV system needs to be calibrated with calibration plate in measurement plane before measurement. For 2D measurements similar arrangement and procedure is followed. However, only single camera, perpendicular to the measurement plane is used in this case.
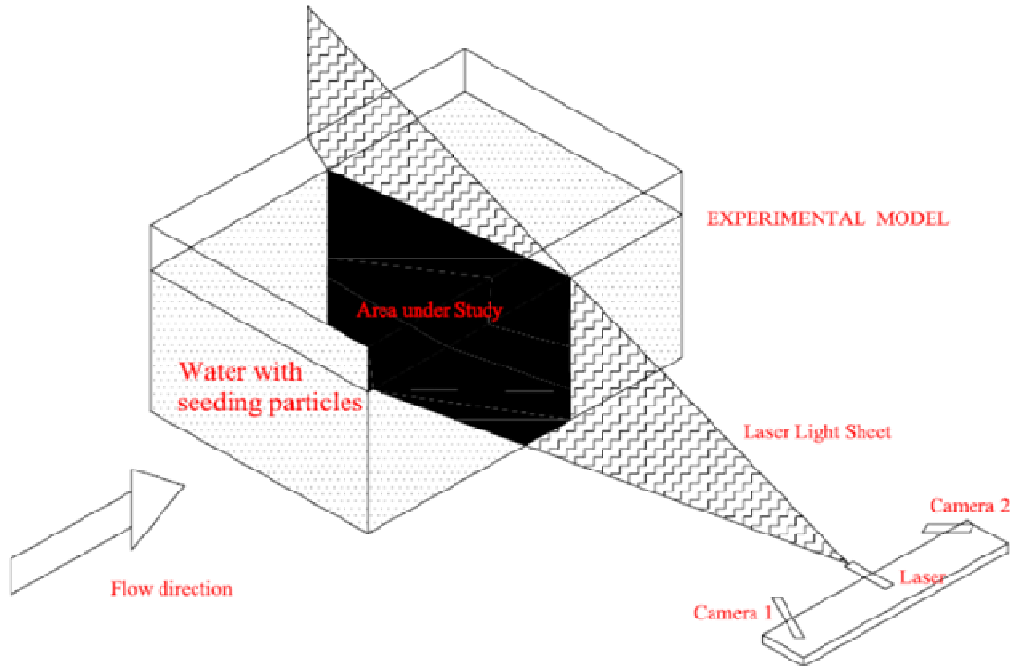
Fig. 3.16: The working principle of PIV
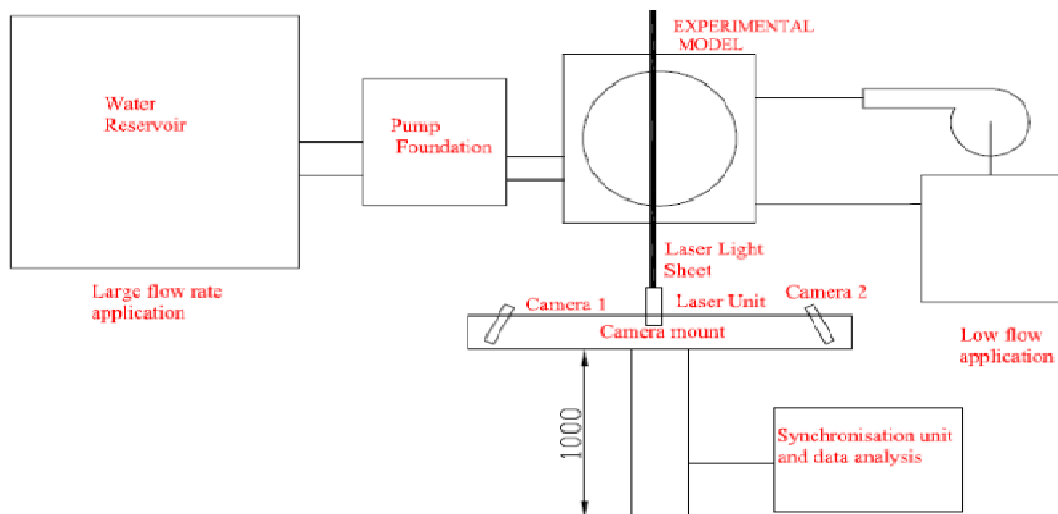
Fig. 3.17: Schematic of PIV set up with all the components

The actual experimental models in the lab with all the PIV system components are shown in Figure 3.18.
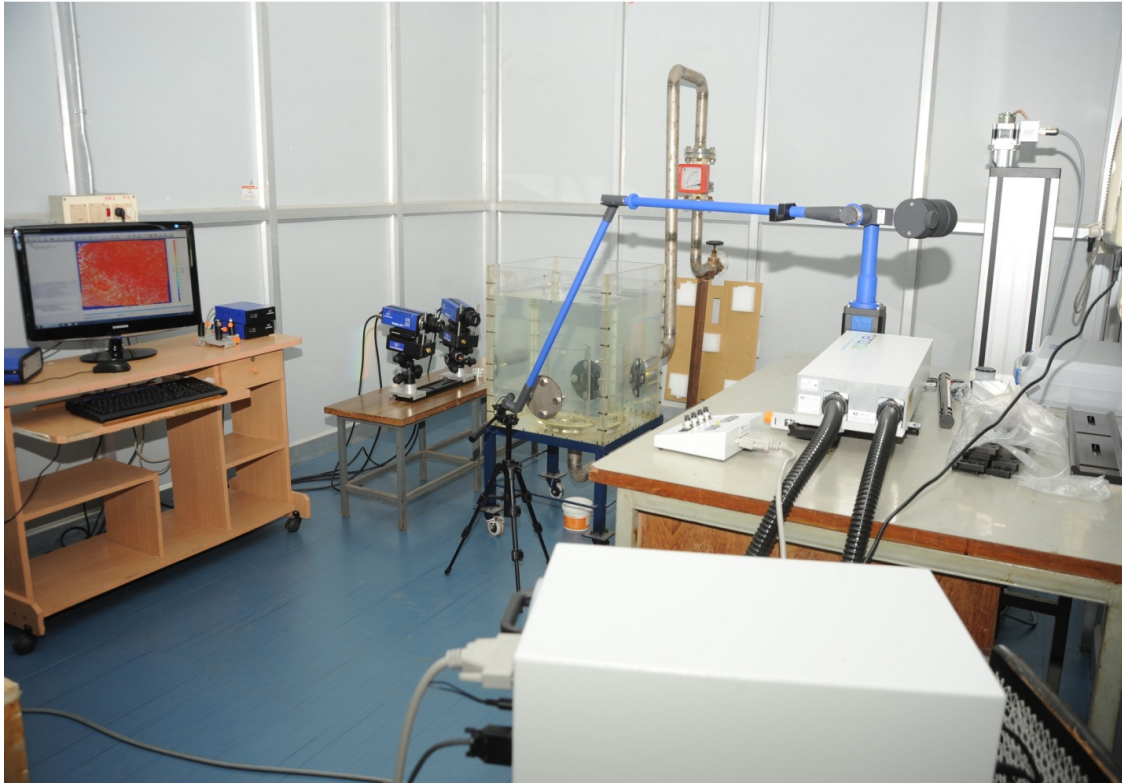
Fig. 3.18: Actual experimental set up in lab

3.7.2. Ultrasonic Velocity Profiler (UVP)

UVP is a non-intrusive technique which measures the velocity of micron-sized particles in the flow. To obtain velocity profile along the axis of the UVP probe, it is required to determine two parameters. One is the distance of the reflecting particle from the probe surface and the other is the velocity information.

The working principle of UVP is based on Doppler shift of ultrasonic pulse frequency which is depicted in Figure 3.19. An ultrasound pulse is emitted from a transducer into liquid, and the same transducer receives the echoes, which originate from tiny particles suspended in the fluid. The position information is given by the time duration between the pulse emission

and the instant of echo reception, thus recording the position from where the echo is reflected. The velocity information is derived from the instantaneous Doppler shift frequency at that instant.
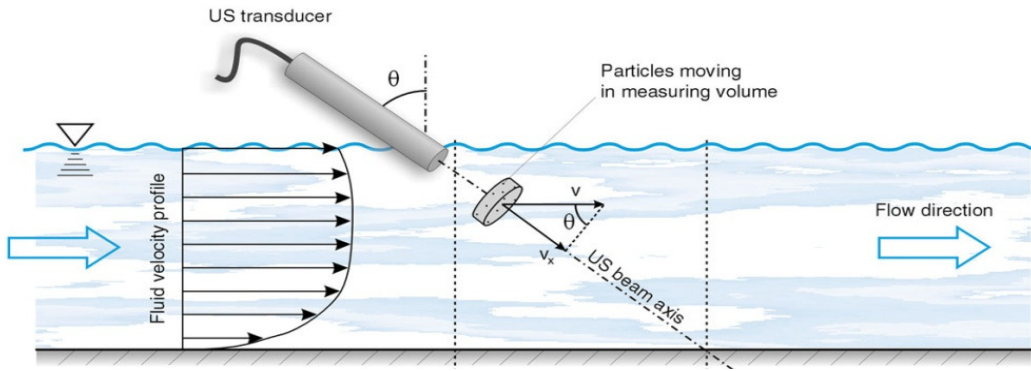
Fig. 3.19: The working principle of UVP

The distance of the particle is estimated from the following equation.

$$t = \frac{2x}{c} \tag{4}$$

Where, t = Time delay between transmitted and received signal (s)

      x = Distance of scattering particle from transducer (m)

      C = Speed of sound in the liquid (m/s)

The velocity can be estimated from the measured Doppler shift frequency using the following equation.

$$\frac{V}{C} = \frac{f_d}{2f_o} \tag{5}$$

Where, V = Velocity component into transducer axis (m/s)

      C = Speed of sound in liquid (m/s)

      f_d = Doppler shift frequency (Hz)

      f_0 = Transmitting frequency (Hz)

3.7.3. Experimental results and its comparison with CFD

Velocity along various lines at the outlet plane is measured by UVP and velocity mapping along the planes is carried out by PIV. Figure 3.20 shows the lines or axes at the outlet plane along which velocities are measured using UVP. Figure 3.20 also shows the vertical plane starting from the outlet plane along which PIV measurement of velocties are carried out. Comparison of measured velocity and numerically predicted velocity along the lines are shown in Figure 3.21. The comparison of experimentally measured velocity by PIV and numerically predicted velocity along X-X planes and Y-Y planes are presented in Figure 3.22 and Figure 3.23. The predicated velocity pattern and experimentally measured velocity patterns are in good agreement with each other.
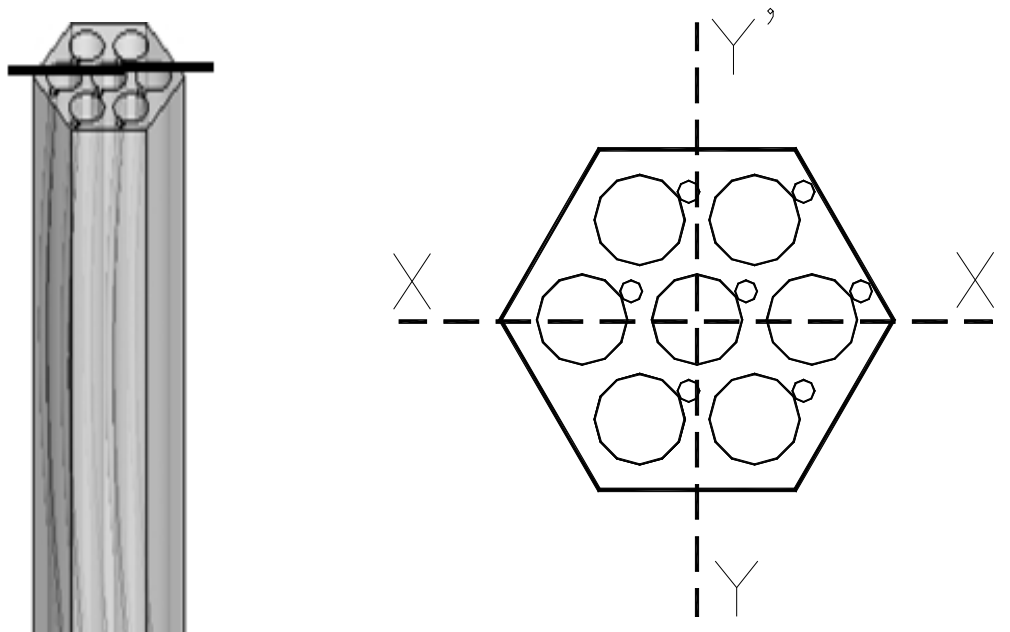
Fig. 3.20 : Lines at the outlet of the models along which velocities are measured using UVP / Planes starting from outlet plane along which measurements are carried out using PIV
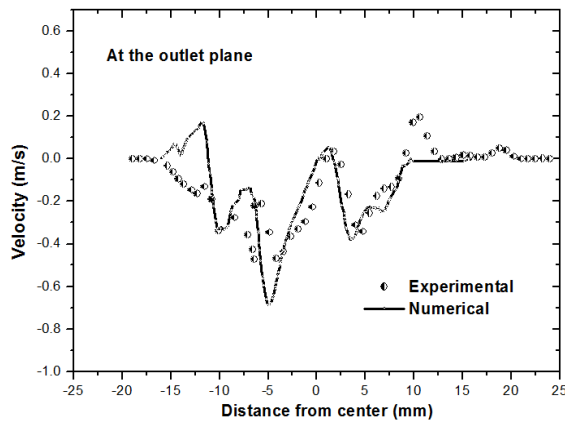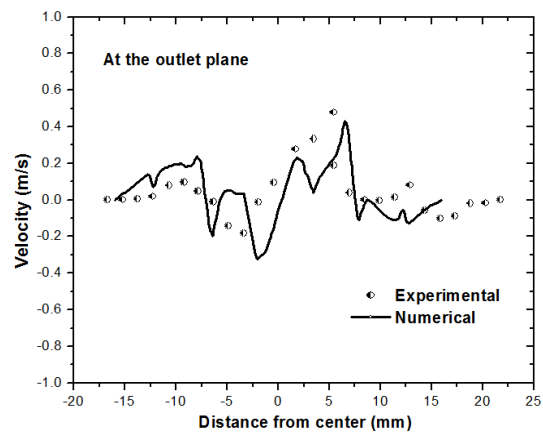
(a)   (b)

Fig. 3.21 :Comparison of velocity profile measured using UVP with CFD results

(a) along the corner to corner (XX') line
(b) along the flat to flat end (YY') line
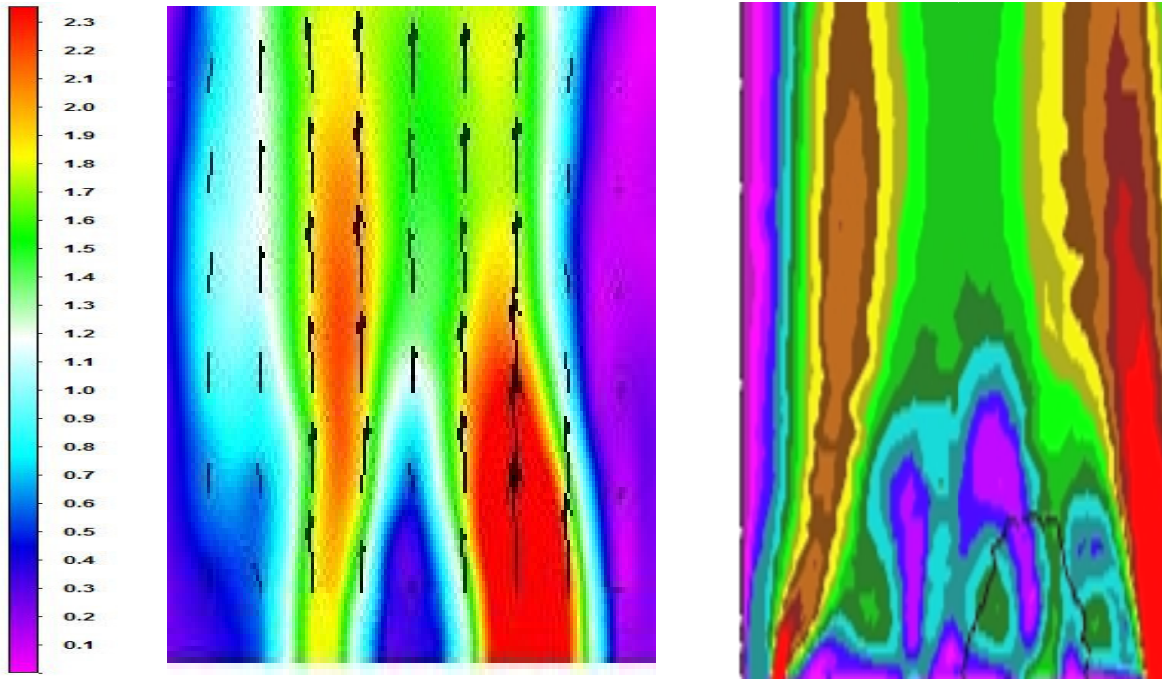
Experimental data   Numerical data

Fig. 3.22 : Comparison of experimental and numerical results of velocity magnitude (m/s) at the

X-X   (flat to flat) plane

<center>Experimental data   Numerical data</center>
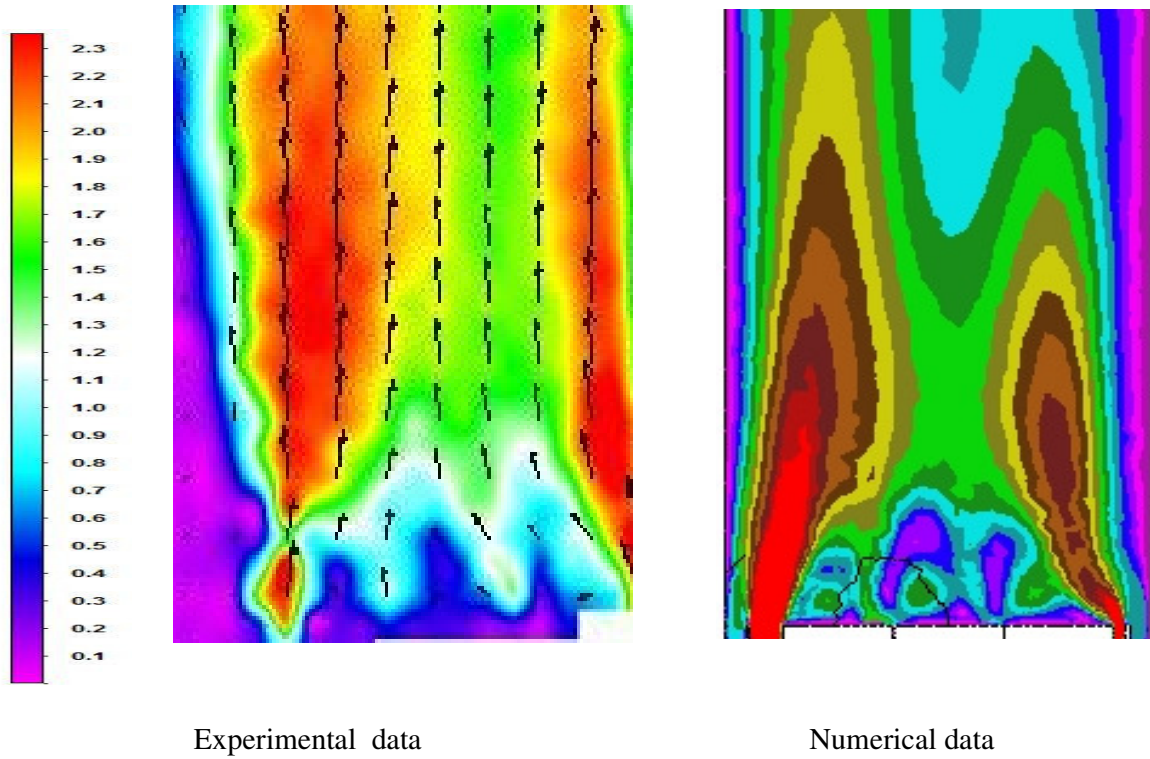
Fig. 3.23: Comparison of experimental and numerical results of velocity magnitude (m/s) at the

<center>Y-Y (corner to corner) plane</center>

With water flow rate as independent parameter, pressure drop in the bundle region was measured. The measured pressure drop in the bundle is compared with the CFD predicted results in Figure 3. 24 for reference pin bundle without any inserts. The pressure drop in the wire-wrap bundle is seen to follow the trend $\Delta P = \mathrm{Re}^{1.85}$ which is expected. Further, the measured pressure drop and CFD predictions are found to be very close. The validation of CFD model with inserts is also carried out by comparing predicted results with experimental results. The pressure drop in the pin bundle with circular inserts was measured in a Re range of $5\mathrm{x}10^3$ to $1.3\mathrm{x}10^4$. The comparison of measured pressure drop and numerically predicted pressure drop with circular inserts is presented in Figure 3. 25.

<center>50</center>
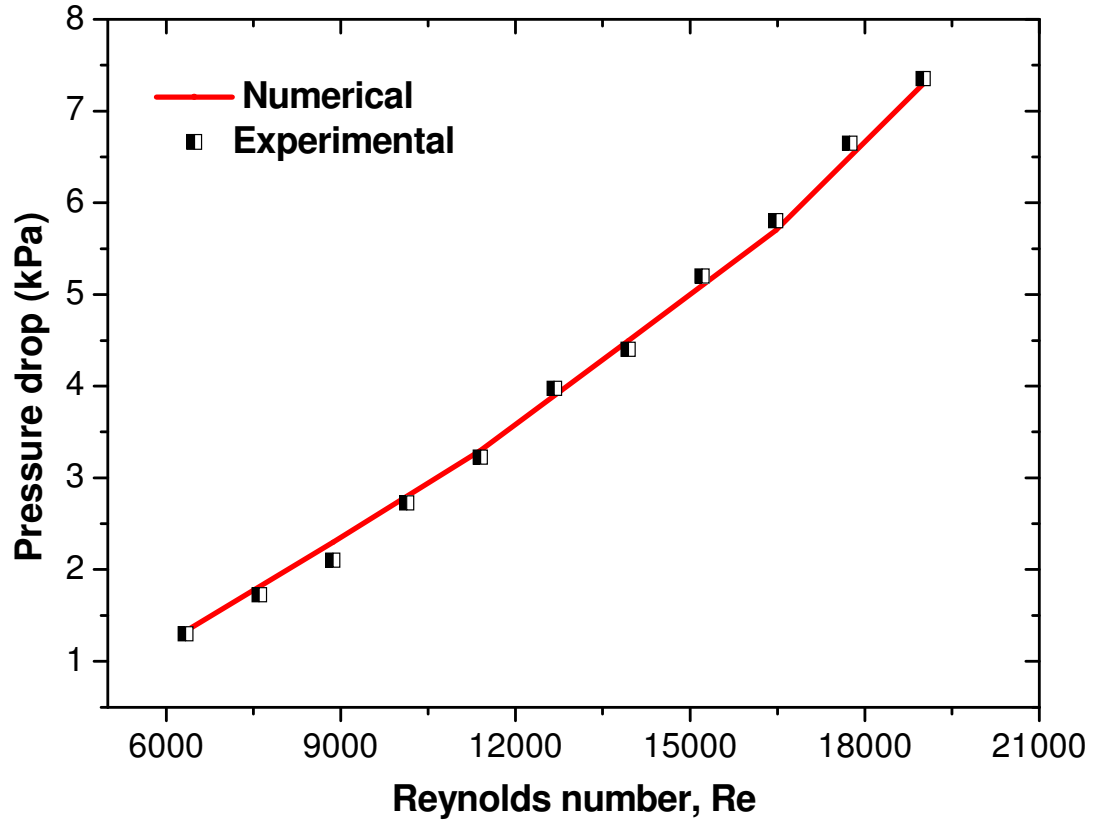
Fig. 3.24: Comparison of experimental and numerical results of pressure drop in the reference bundle without any inserts

The CFD predicated value of pressure drop and measured pressure drop value are in good agreement in low flow rates. It is seen that at higher flows CFD model marginally under predicts the pressure drop. The degree of under-prediction at the highest flow rate in the present experiments is ~14%. This is attributed to the possible lack of straightness in the cylindrical inserts when they are inserted from the top of the pin bundle.
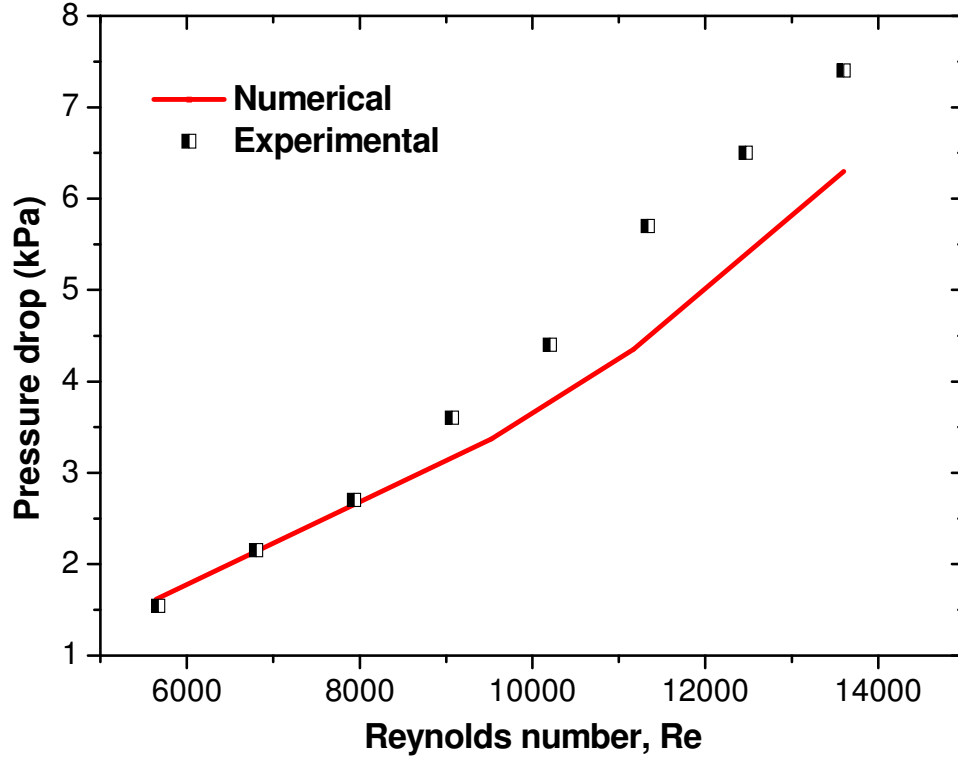
Fig. 3.25: Comparison of experimental and numerical results of pressure drop in the bundle
with circular inserts

3.8. CLOSURE

For investigating the efficacy of inserts in the peripheral sub channels of a model fast
reactor pin bundle with helical spacer wire, a 3 dimensional computational fluid dynamic
model of 7 pin fuel bundle have been developed. Grid independence studies, studies on effect
of various turbulence models, studies on selection of proper number of number of pitches of
spacer and selection of number of fuel pins for CFD analysis etc. are carried out. The CFD
model has been validated by comparing the predicted velocity profiles and pressure drop
against measured velocity and pressure drop for water flow, through bundle with / without
inserts.

CHAPTER 4

HYDRAULIC ANALYSIS OF MODEL PIN BUNDLE ASSEMBLY

4.0   INTRODUCTION

In this chapter the effects of all three different types of inserts, viz., triangular, semicircular and circular inserts on hydraulics of pin bundle have been compared and studied along with a bundle without any insert. The model of 7 pin fuel assembly bundle without any insert has been verified by comparing computed values of frictional factor with correlations proposed by various authors. The variations of axial velocity and cross flow velocity, friction factor and mass flow fraction in the central sub-channels for the reference design and all cases of inserts are compared with pin bundles with different inserts for same inlet velocity.

4.1.   MOTIVATION AND METHODOLOGY OF REDUCING BYPASS

Even though spacer wires promote mixing of sodium flow inside the subassembly, temperature profile is still not uniform within the fuel subassembly since the sub-channel flow areas are not uniform all over the cross section of fuel subassembly. The sub-channels flow areas around the central fuel pins are same. However, the edge / peripheral sub-channels have more flow areas than the central sub-channels and more sodium flow occurs through the peripheral sub-channels. The various flow channel areas in a representative 7 pin fuel bundle are presented in Figure 4.1. For the purpose of present investigations, the fuel pin diameter, spacer wire diameter, fuel pin pitch, gap between fuel pin and hexcan are 6.6 mm, 1.65 mm, 8.28 mm and 1.78 mm respectively. These are the values used in typical oxide fueled power reactors.
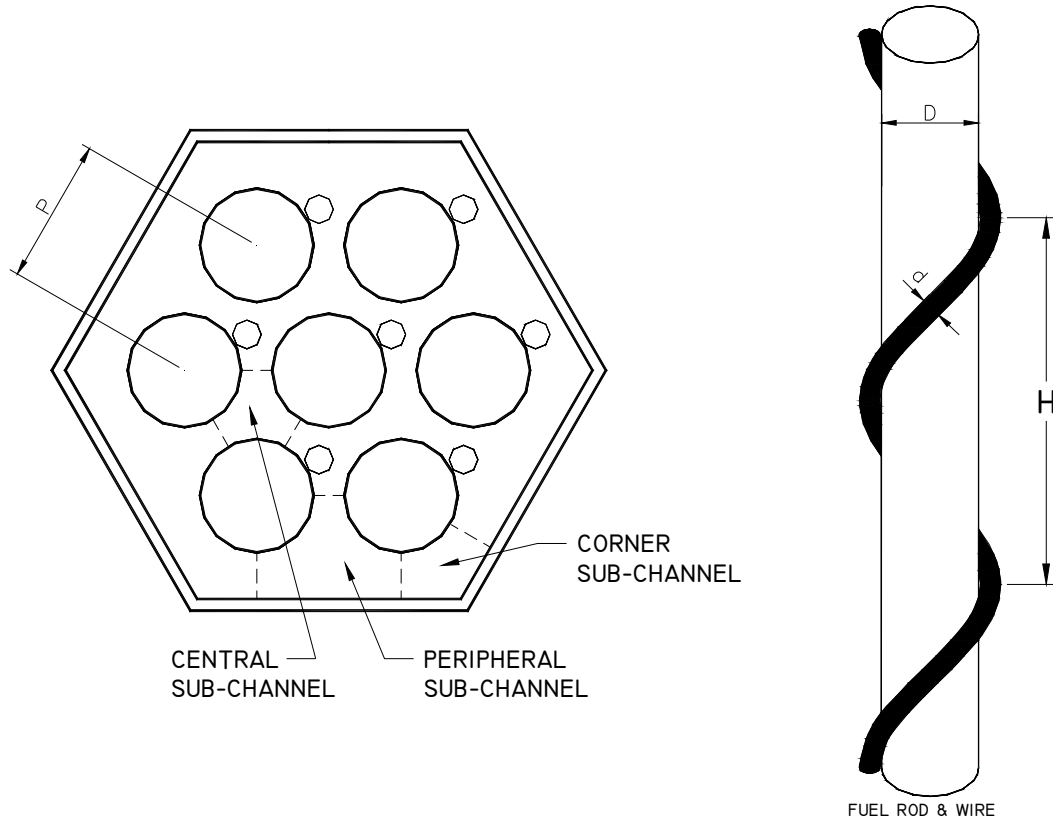
Fig. 4.1: Various types of sub-channels in a representative 7 pin fuel subassembly

The central sub-channels are around the central fuel pins and the peripheral sub-channels are between the outer hexcan walls and outer row of fuel pins. Hence, the heat generation is relatively more at the central sub-channels and low at the peripheral sub-channels. However peripheral sub-channels have more coolant flow area than the central sub-channels. This discrepancy in heat generation and coolant flow between the central and peripheral sub-channels can be quantified with the P/A ratio, where A is the flow area in the sub-channel and P is the total perimeter of fuel pins in the sub-channel. The P/A ratio in the central sub-channels has been calculated as 0.824 mm^{-1} and for the peripheral sub-channels the value is only 0.414 mm^{-1}. The "P/A ratio" at the center is ~ 2 times of the peripheral sub-

channel. The ratio of P/A ratios can be defined as a ratio factor 'S' whose preferred value is 1 for uniform sodium outlet temperature (Table 4.1). The increased coolant flow near the lower heat generated peripheral sub-channels and lower coolant flow at the central sub-channels results in temperature variations around the fuel pins leading to local hot spots. An over-cooled sodium flow at the periphery and hot sodium flow in the centre create non-uniform outlet temperature in the subassembly. A proper balanced sub-channel flow can enhance the heat transfer between fuel pins and sodium so as to get uniform sodium outlet temperature and lower hot spot temperature.

Table 4.1: Details of P/A ratio at various sub-channels

Sl no.	Sub-channel type	Flow area (A) mm^2	Fuel pin perimeter (P) mm	P/A Ratio mm^{-1}	S factor
1	Central sub-channels	12.58	10.367	0.824	1.98
2	Peripheral sub-channels	24.99	10.367	0.414	

The P/A ratios of sub-channels near the hexcan boundary and at the fuel bundle center can be made uniform by insertion of solid devices in the gap between fuel pins and hexcan walls. This insert reduces the flow area near hexcan boundaries and gives better P/A ratio at the periphery too. The geometry of the insert is also very important because of its effect on friction factor and heat transfer. The addition of inserts offer an additional pressure drop to the sodium flow and it varies with the geometry of the inserts. The optimum geometry of the insert gives lower S factor, lower friction drop, better heat transfer, uniform coolant outlet temperature and lower hot spots. This is the objective for the present chapter, where a numerical analysis has been carried out to understand the efficiency of circular, semi-circular wire-type and triangular rod type inserts in obtaining better P/A ratio, uniform outlet velocity

with lower frictional drop. Figure 4.2 shows the schematic of various insert geometries in 7 pin fuel bundle. Velocity profiles and friction factor in a 7 pin wire wrapped bundle with and without inserts have been analyzed. Out of the three different geometries, selection of optimum geometrical profile for the insert has been done. This chapter describes the effects of inserts on 7 pin bundle hydraulics, improvement in S factor and additional pressure drop for each inserts.

| Semi circular | Triangular | Circular |
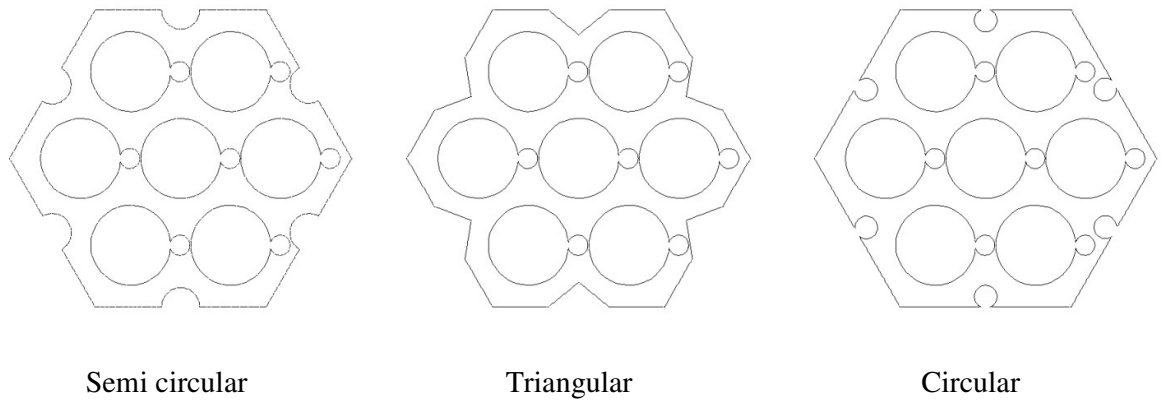
Fig. 4.2: Various insert geometries studied

4.2.   HYDRAULICS WITHOUT INSERTS

Hydraulic analysis has been carried out for different Reynolds number values ranging from 4×10^4 to 2×10^5. Computed values of frictional factor were compared with correlations proposed by various authors. The friction factor has been compared with correlations by Baxi and Dalle-Donne (1981), Rehme (1973), Modified Engel (1979) and Govinda rasu (2013).

Friction factor for different regimes are calculated for the sodium flow through the bundle. Hydraulic diameter has been calculated as 3.99 mm for the 7 pin bundle assembly in the hexcan with 6.6 mm pin diameter and 1.65 mm spacer diameter. Darcy frictional factor has been calculated from the pressure drop in the fuel pin bundle from the CFD study.

Hydraulic diameter, D_h = 4 * (Area / Wetted perimeter)

$$= 3.992 \text{ mm}$$

Reynolds number, $$Re = \frac{\rho V D_h}{\mu}$$

Darcy formula, Friction factor, $$f = \frac{2\Delta P\, D_h}{l\rho\, v^2}$$

A comparison of friction factor with correlations proposed by various studies is shown in Figure 4.3 and it is seen that the present results are in good agreement with the published correlations.
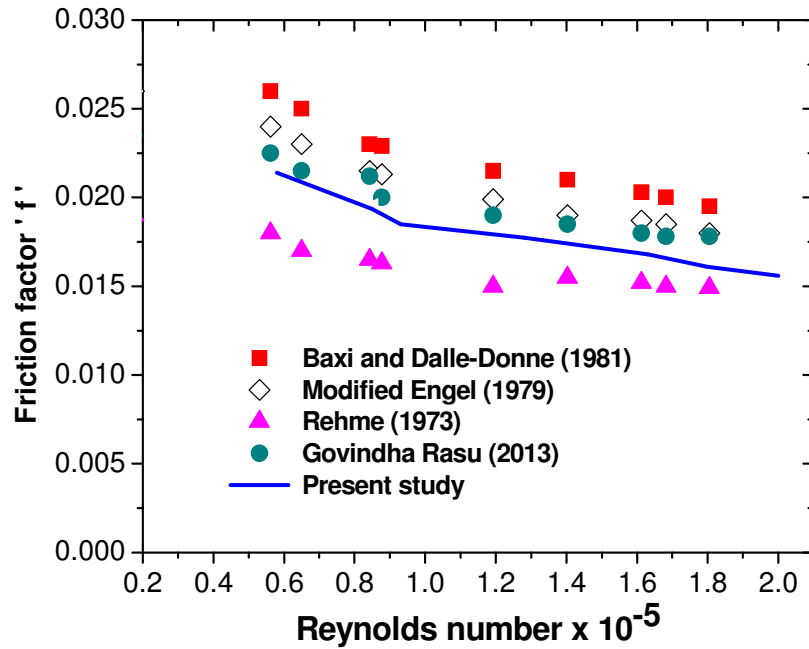
Fig. 4.3: The comparison of friction factor with correlations proposed by various studies

4.2.1. Cross flow development

The cross flow development in the 7 pin fuel bundle from the inlet plane to outlet plane is shown in Figure 4.4. It is seen that the flow gets developed within 86 mm from the inlet of the bundle after which the changes in the flow is marginal. This sodium swirl flow occurring at the peripheral sub-channels is found to be periodic and is found to be a function of wire position. From the figure it can be seen that, from the inlet plan to outlet plane in the

axial direction, the locus of spacer wire moves in anti-clockwise and as a consequence of this, the sub-channel sodium flow is developed anti-clock wise direction. This circumferential flow developed due to the helical wire is very important from the thermal hydraulics point of view, as it enhances mixing of the coolant between the sub-channels which enhances the heat transfer and helps to attain uniform coolant temperature at the outlet of the subassembly. It can also be seen that the circumferential velocity is maximum in the peripheral sub-channels which are diametrically opposite to the channels where a spacer wire blocks the sub-channel. There is a local maximum value of 1.54 m/s for the cross flow velocity at the outlet. In order to get uniform outlet temperature, the mass flow rate of sodium in the peripheral sub-channels should be same.
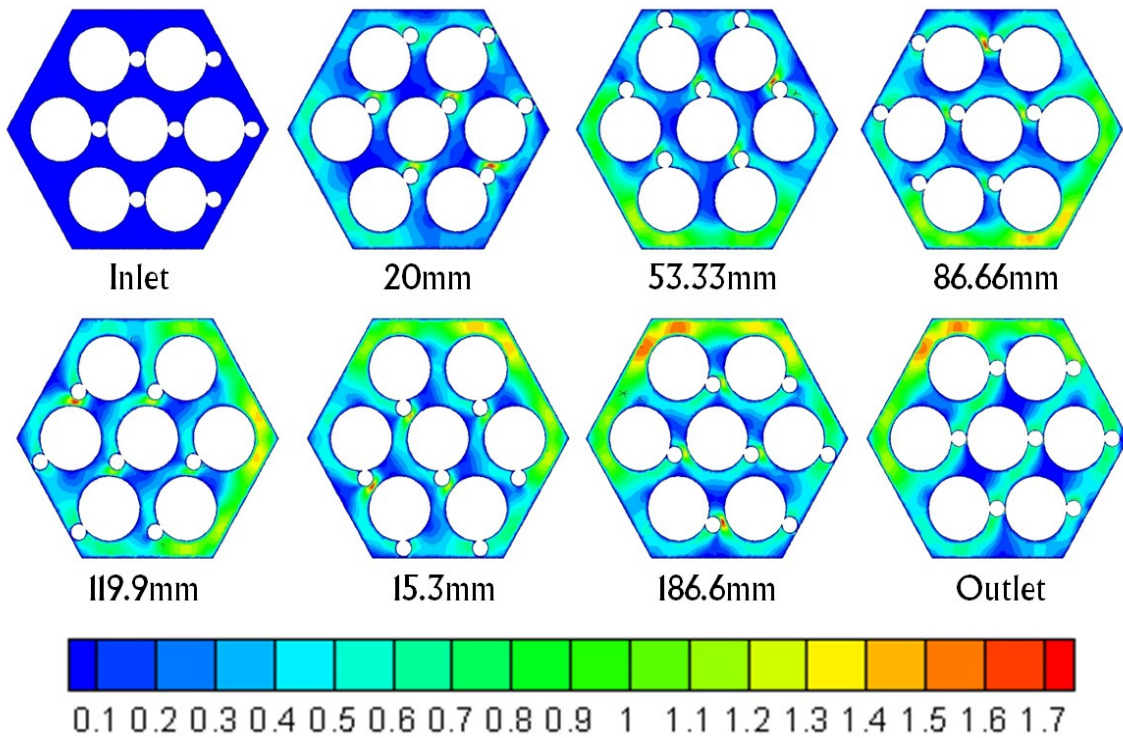
Fig. 4.4: The cross flow velocity development (m/s) in the 7 pin fuel bundle form inlet to outlet plane

4.3. HYDRAULIC ANALYSIS WITH INSERTS

Addition of resistance to the sodium flow at the less resistance flow paths (peripheral sub-channels) helps to attain uniform flow and hence uniform temperature field. The resistance can be added by inserting rods of various geometries. The comparison of cross stream velocity at outlet planes is presented in Figure 4.5. Table 4.2 shows the maximum cross flow velocity at the outlet for 7 pin bundle for all the cases of inserts.

7 Pin fuel bundle – No inserts   Semi- circular inserts

Triangular inserts   circular inserts
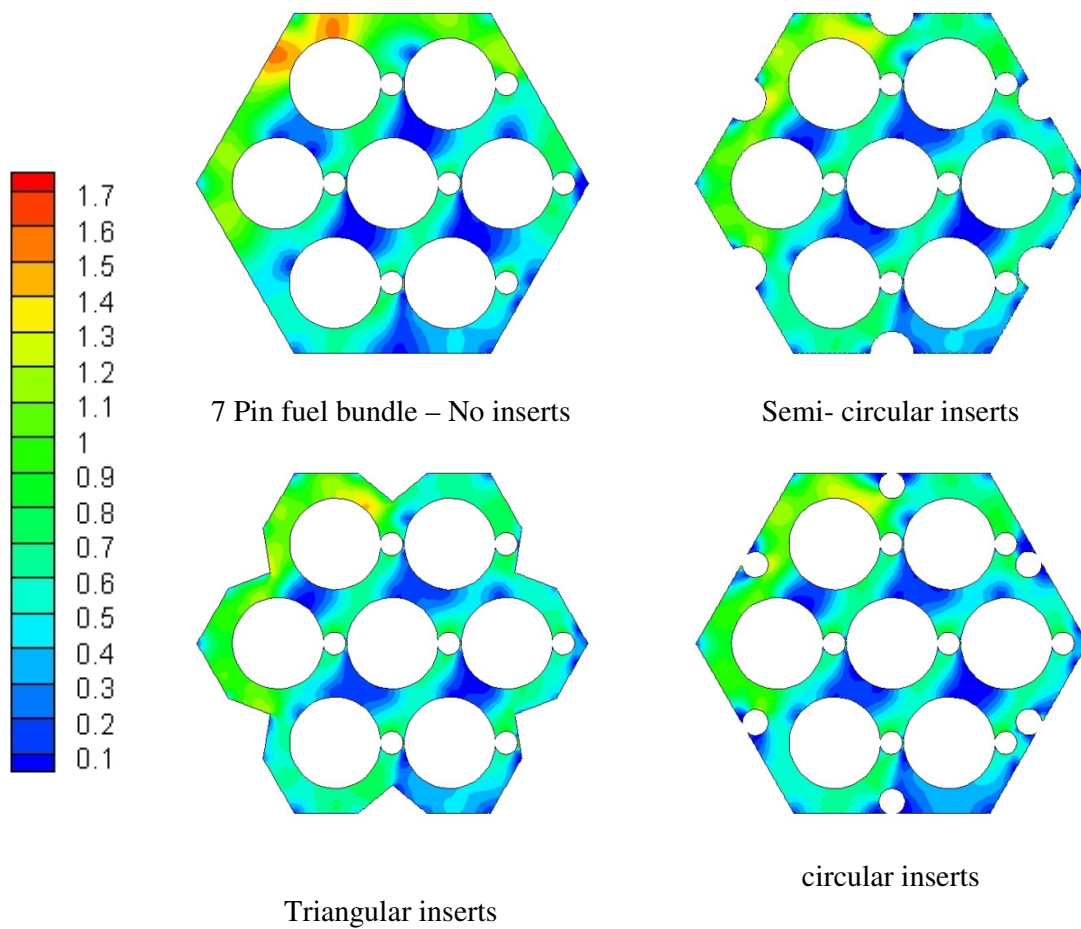
Fig. 4.5 : Cross flow velocity (m/s) at the outlet of 7 pin bundle for different inserts

Table 4.2: Maximum value of cross flow velocity at the outlet

Type of inserts	Cross flow velocity (m/s)
No inserts	1.54
Semi-circular	1.33
Circular	1.31
triangular	1.41

7 Pin fuel bundle – No inserts   Semi- circular inserts

Triangular inserts   circular inserts
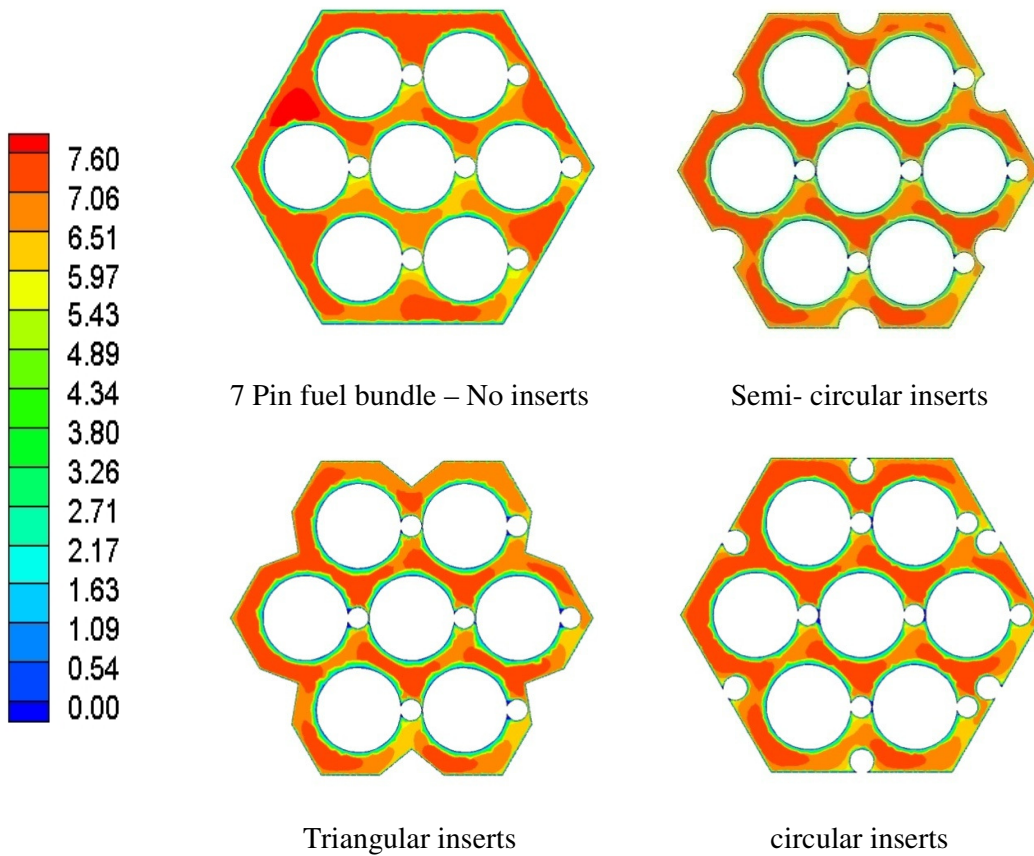
Fig. 4.6: Vertical velocity (m/s) at the outlet of 7 pin bundle for different inserts

The computed vertical velocity profile at the outlet plane of the pin bundle without and with inserts is shown in Figure 4.6. It can be observed that, without any inserts the maximum vertical velocity is at the peripheral sub-channels. The addition of inserts has

increased the vertical velocity through the central sub-channels surrounding the central fuel pin. This increased flow at the central sub-channels gives better uniformity of coolant temperature at the outlet.

4.4.   COEFFICIENT OF FRICTION

An important parameter relevant in the hydraulic analysis is the friction factor. The addition of inserts causes resistance to the coolant flow through the peripheral sub-channels and increases the friction pressure drop. The variation of friction factor with Re ranging from 0.5×10^5 to 1.7×10^5 has been compared for all the cases of inserts and is shown in Figure 4.7. Comparison of friction factor without inserts and with various inserts for Reynolds number 0.85×10^5 (reactor full power condition) is presented in Table 4.3. The friction factor in the pin bundle without any inserts has been estimated as 0.0193. Among the inserts, the maximum value of friction factor occurs for circular inserts and its value is 0.0226. The increase of friction factor due to the addition of circular inserts is 17.0 %. The increase in friction factor for semi circular and triangular inserts is 11.9 % and 9.8 % respectively. Thus, it can be seen that triangular inserts have the advantages of lower frictional factor compared to the rest of the inserts.

Table 4.3: The effect of inserts on friction factor (Re = 0.85×10^5)

Type of inserts	Friction factor 'f'	% Change in f
No inserts	0.0193	-
Semi circular	0.0216	11.9
Triangular	0.0212	9.8
Circular	0.0226	17.0
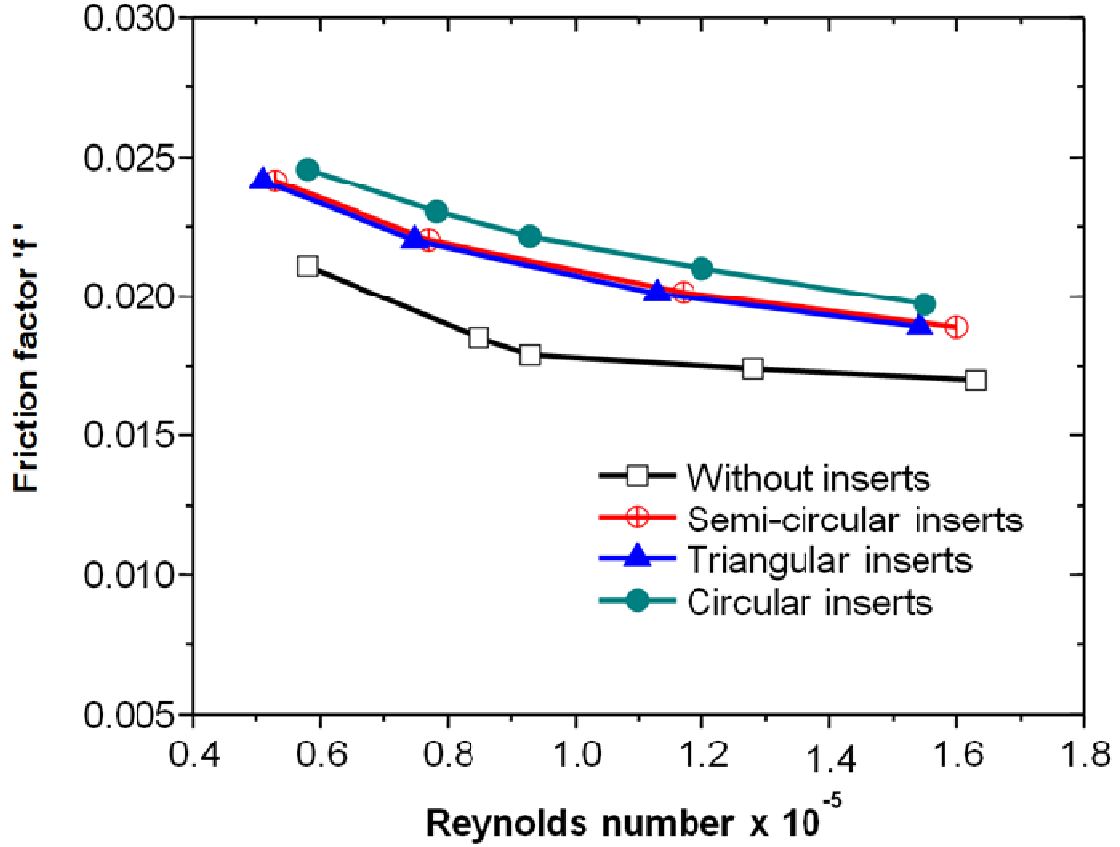
Fig. 4.7: Comparison of friction factor for different inserts
(For flow range : Re=0.5×10^5 - 1.7×10^5)

4.5. AXIAL VELOCITY FRACTION

The axial velocity fraction (i.e., the ratio of mean axial velocity in the sub-channel outlet to the uniform axial velocity in the sub-channel in the inlet) in the various central, peripheral and corner sub-channels numbered from 1 to 18 is shown in Tables 4.4, 4.5 and 4.6 respectively. The position of various sub-channels is numbered in Figure 4.8. It is observed that the addition of inserts in the pin bundle has increased the coolant velocity through the central sub-channels. At the same time, the inserts have reduced the velocity in the peripheral sub-channels.
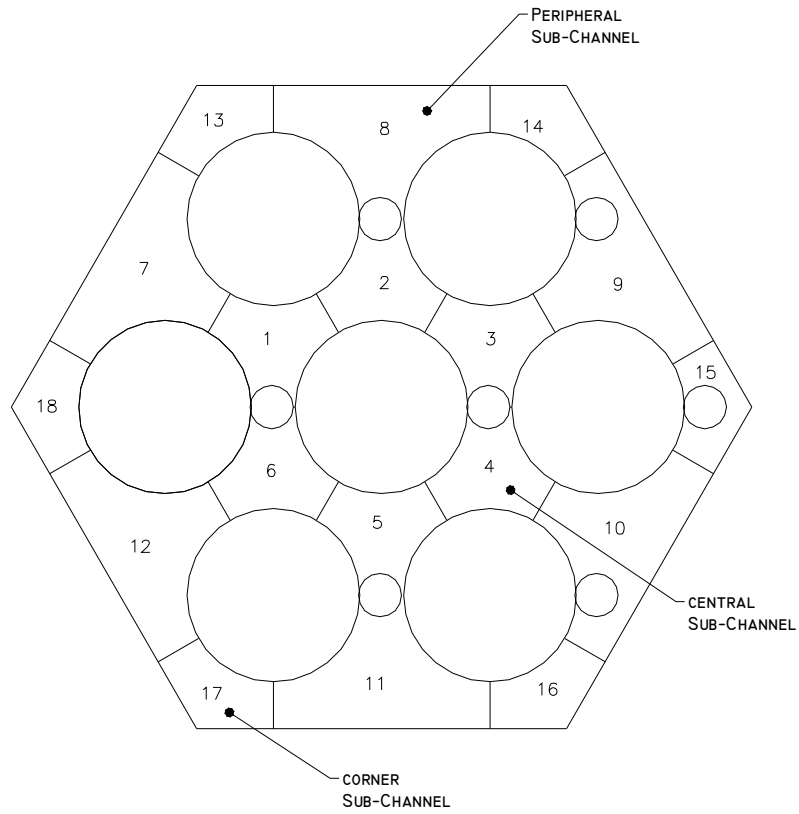
Fig. 4.8: The numbering of all sub-channels in 7 pin bundle

Table 4.4: Axial velocity fraction in the central sub-channels (Re = 0.85×10^5 for ref. case)

Sub-channels	Axial velocity fraction in central sub-channels			
	Without inserts	Semi-circular	Triangular	circular
1	1.000	1.034	1.042	1.037
2	0.952	0.996	1.004	0.999
3	0.993	1.030	1.037	1.035
4	0.918	0.978	0.985	0.977
5	0.966	1.025	1.032	0.984
6	0.932	0.981	0.988	0.982
Average	0.960	1.007	1.015	1.002

Table 4.5: Axial velocity fraction in the peripheral sub-channels (Re = 0.85×10^5 for ref. case)

Sub-channels	Axial velocity fraction in peripheral sub-channels			
	Without inserts	Semi-circular	Triangular	circular
7	1.073	1.037	1.036	1.037
8	1.035	0.999	0.992	0.999
9	0.992	0.978	0.973	1.035
10	0.993	0.987	0.985	0.977
11	0.981	0.969	0.963	0.984
12	1.031	1.017	1.016	0.982

Table 4.6: Axial velocity fraction in the corner sub-channels (Re = 0.85×10^5 for ref. case)

Sub-channels	Axial velocity fraction in corner sub-channels			
	Without inserts	Semi-circular	Triangular	circular
13	1.044	1.011	1.007	1.030
14	1.014	0.991	0.984	0.997
15	0.931	0.940	0.936	0.937
16	0.956	0.965	0.966	0.965
17	1.009	1.022	1.024	1.019
18	1.053	1.029	1.028	1.029

4.6. CLOSURE

A combined experimental and numerical study has been carried out to find the effect of addition of inserts on the sub-channel coolant flow pattern through the center and peripheral sub-channels. A model with 7 pin fuel assembly has been considered for the computation and the hydraulics has been validated with experiments. From the hydraulic analysis it is observed that the addition of inserts in the hexcan enhances the axial velocity fraction of coolant in the central sub-channels with an additional pressure drop. It is observed that with insert, the axial velocity fraction is improved in all central sub-channels. The triangular inserts have the lower frictional drop compared to all other insert geometries. There is an increase of 9.8 % in friction factor for triangular inserts and 11.9 % rise in semi-circular inserts. Circular inserts have the maximum pressure drop (17%) and hence the highest friction factor.

CHAPTER 5

THERMAL ANALYSIS OF MODEL PIN BUNDLE ASSEMBLY

5.0. INTRODUCTION

After establishing a satisfactory validation of the hydraulic aspects of CFD model against in-house water experiments, the thermal aspects of CFD model is verified against published data for sodium flow and detailed parametric studies have been carried out for sodium coolant flows. The parameters varied include Reynolds number and type of inserts. Three types of inserts - circular, triangular and semi-circular, have been considered in the thermal investigation also. Sub-channel sodium temperature, axial and circumferential temperature distributions of clad among the pins and Nusselt number are the parameters targeted for the investigation. To find the optimum insert type, a Performance Enhancement Criterion (PEC) factor has been defined.

5.1. THERMAL HYDRAULIC VERIFICATION OF CFD MODEL

Towards further validating the prediction capability of the CFD model for thermal aspects, thermal hydraulic simulations were carried out for Reynolds number values ranging from 4×10^4 to 2×10^5. A uniform heat flux of 2×10^6 W/m^2 was applied on the surface of fuel pins while the hexcan was treated to be adiabatic with sodium as the coolant. Verification of the CFD model has been carried out by comparing computed values of Nusselt number with correlations proposed by various authors. Estimated Nusselt number has been compared with correlations by Subbotin et al. (1965), Borishanskii et al. (1969), Kazimi and Carelli (1976) and Govindha Rasu (2013) in Figure 5.1. It is seen that the present results are in good agreement with the published correlations. The trend of the present result is very close to that of Borinshanski et al (1969) and Govindha Rasu (2013). It may be highlighted

that the experimental results of Borinshanski et al. (1969) and Kazimi and Carelli (1976) are without any spacer wires. On the other hand, the results of Govindha Rasu (2013) are from 3-D CFD calculations with wire-wrap. The results from these literature suggest that the 'Nusselt number vs. Peclet number' curve exhibits a steeper rise with wire-wrap. Further, the slope of the present curve compares better with that of Govindha Rasu (2013). Moreover, the uncertainties in the reported experimental Nusselt number data are relatively large (Mikityuk, 2009). Considering these facts, it is judged that the present calculations are reasonably accurate. The maximum deviation in the predicted Nusselt number is ~15% at the highest Peclet number.
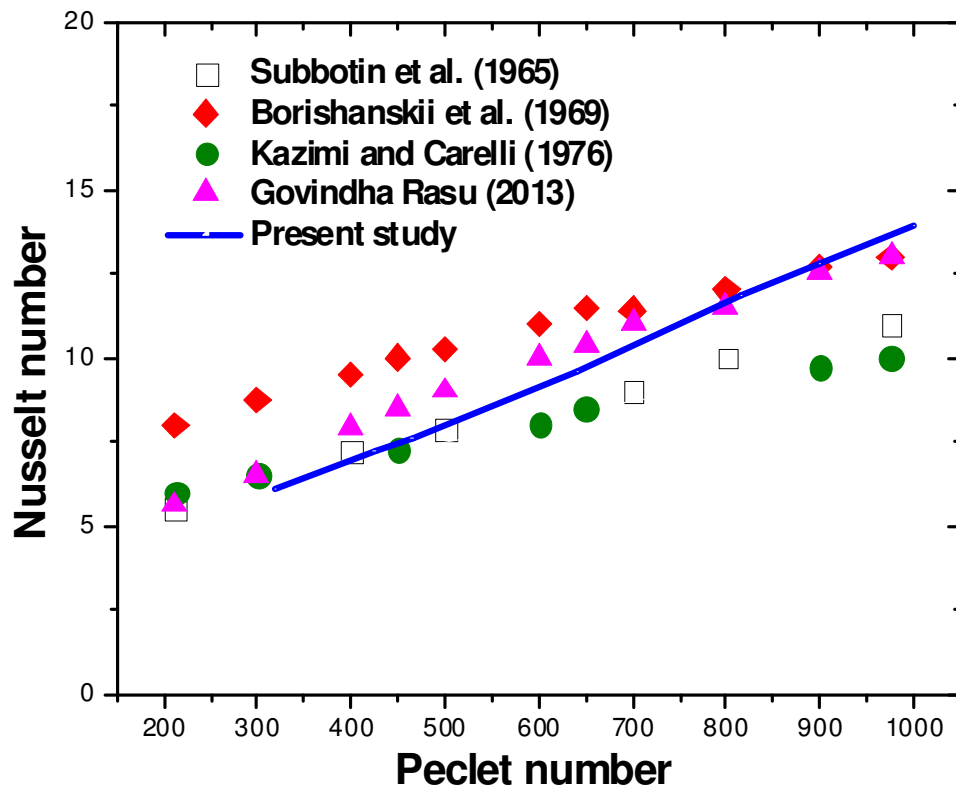
Fig. 5.1: Comparison of predicted Nusselt number with correlations proposed by various studies (Pr = 0.00506)

5.2. TEMPERATURE PROFILE IN PIN BUNDLE WITHOUT INSERTS

The variation of sodium temperature development from inlet plane to outlet plane in the 7 pin fuel bundle without any insert is shown in Figure 5.2. It can be seen that the sodium temperature is maximum in the central sub-channels compared to peripheral sub-channels. Also the temperature is maximum in the central sub-channels where a spacer wire blocks the sub-channel. The coolant flow rate in the peripheral sub-channels needs to be reduced and flow rate in the central sub-channels needs to be increased to obtain a more uniform temperature in all sub-channels at the outlet.
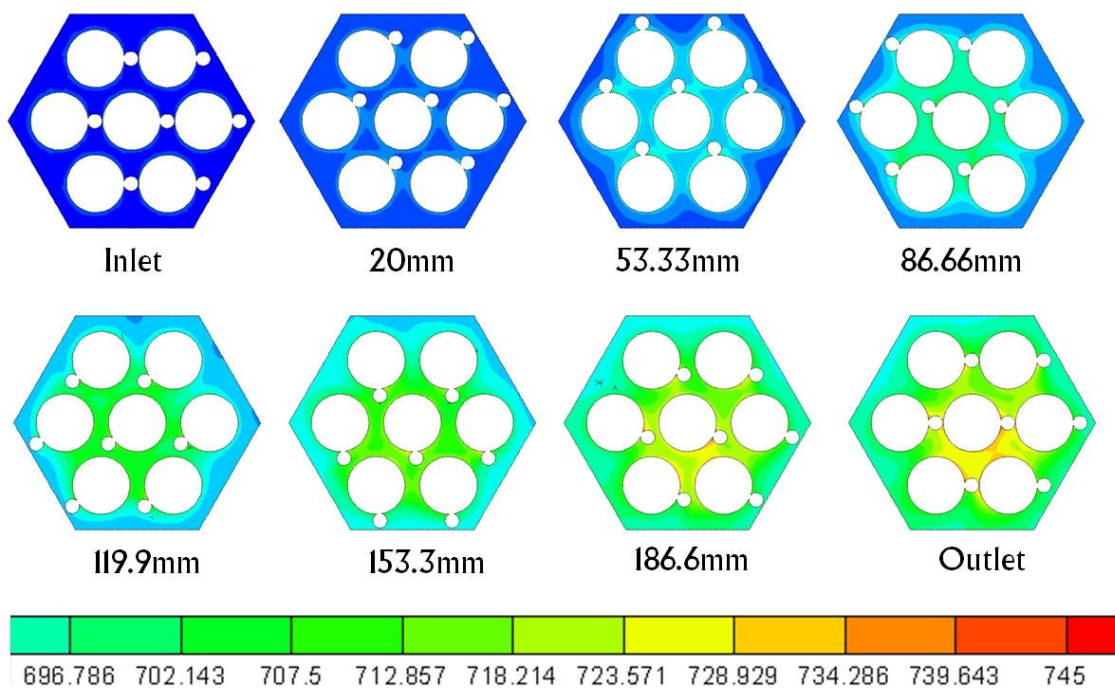
Fig. 5.2: Variation of Sodium Temperature (K)
from inlet to outlet

5.3. TEMPERATURE PROFILE IN PIN BUNDLE WITH INSERTS

The variation of sodium temperature development from inlet to outlet along the length of the 7 pin fuel bundle for all cases of inserts are shown in Figure 5.3. to Figure 5.6. It can be seen that as flow enters from inlet of fuel pin bundle, it gradually picks up the heat and the temperature rises across the length. The maximum sodium temperature in the central sub-channel reduces from 741 K to 737 K, 735 K and 731 K due to addition of the semi circular, circular and triangular inserts respectively, there by resulting in more uniform temperature at the outlet.

| 7.41e+02 |
| 7.38e+02 |
| 7.34e+02 |
| 7.31e+02 |
| 7.27e+02 |
| 7.24e+02 |
| 7.20e+02 |
| 7.16e+02 |
| 7.13e+02 |
| 7.09e+02 |
| 7.06e+02 |
| 7.02e+02 |
| 6.99e+02 |
| 6.95e+02 |
| 6.91e+02 |
| 6.88e+02 |
| 6.84e+02 |
| 6.81e+02 |
| 6.77e+02 |
| 6.74e+02 |
| 6.70e+02 |

| 7.37e+02 |
| 7.34e+02 |
| 7.30e+02 |
| 7.27e+02 |
| 7.24e+02 |
| 7.20e+02 |
| 7.17e+02 |
| 7.14e+02 |
| 7.10e+02 |
| 7.07e+02 |
| 7.04e+02 |
| 7.00e+02 |
| 6.97e+02 |
| 6.93e+02 |
| 6.90e+02 |
| 6.87e+02 |
| 6.83e+02 |
| 6.80e+02 |
| 6.77e+02 |
| 6.73e+02 |
| 6.70e+02 |
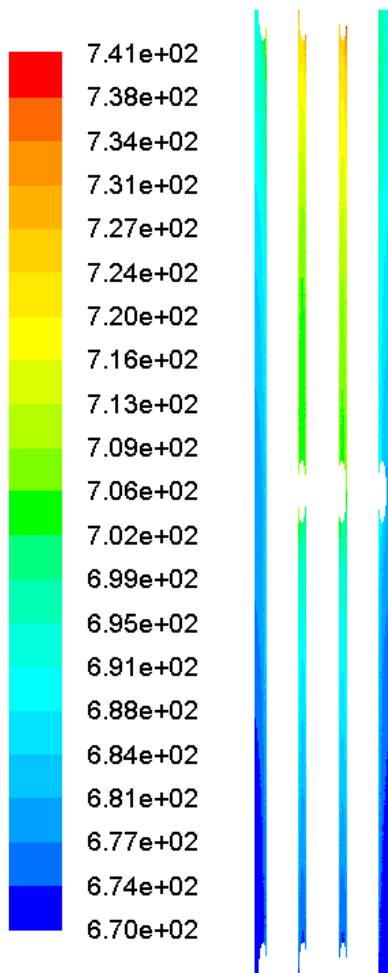
Fig. 5.3: Variation of sodium temperature (K) from inlet to outlet for no inset case
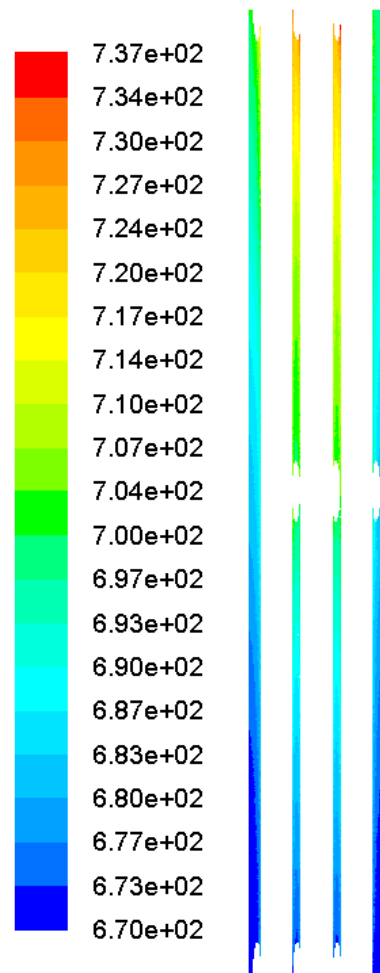
Fig. 5.4: Variation of sodium temperature (K) from inlet to outlet for semi circular inset case
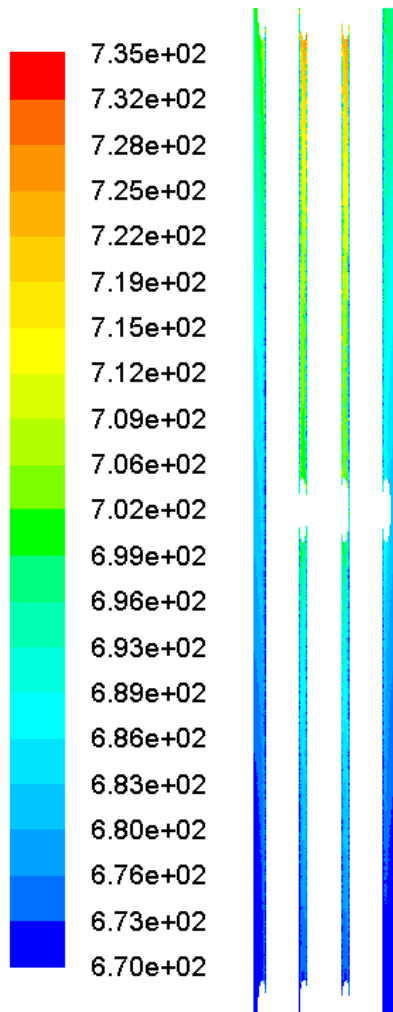
Fig. 5.5: Variation of sodium temperature (K) from inlet to outlet for circular inset case
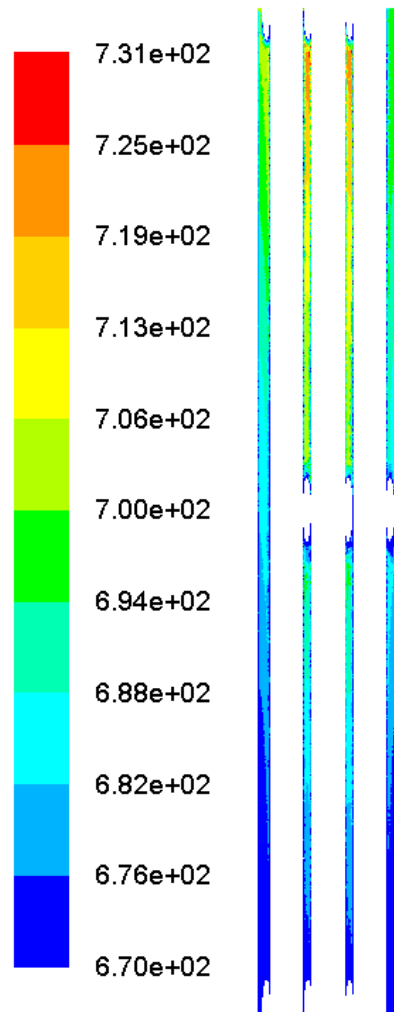
Fig. 5.6: variation of sodium Temperature (K) from inlet to outlet for triangular inset case

5.4. MEAN CLAD TEMPERATURE ALONG PIN BUNDLE

The fuel pin numbering adopted for the present discussion is depicted in Figure 5.7. It may be re-iterated that for the thermal analysis, a uniform heat flux of 2 x 10^6 W/m^2 was imposed on all the pins. The coolant flow rate was 1.6 kg/s for all the cases. Sodium temperature at the inlet to the bundle was 670 K. Based on heat balance, the bulk sodium outlet temperature from the bundle is 704.4 K. The improvisation of flow distribution among sub-channels by the use of inserts for the same heat generation reduces the clad temperature.

To understand this, a comparison of mean clad temperature along the length of each pin for all the cases of inserts are shown in Figure 5.8 to Figure 5.14 and the effectiveness of inserts in reducing the mean clad temperature can be observed with the help of these figures. It can be seen that the clad temperature increases along the flow direction, as the sodium temperature increases. In the case of central pin, the temperature increases more or less linearly in all the cases. This is due to the fact that the bulk temperature of sub channel sodium around the central fuel pin increases nearly linearly due to thermal symmetry. However in the case of peripheral pins, such uniform increase is not seen. This is due to the development of circumferential flow in the peripheral sub channels and the associated thermal asymmetry. As a consequence of this, the temperature rate is steep in some axial segment and is not so steep in some other segment. Among the four cases, the clad temperature is seen to be the minimum in the case of circular inserts for all the 7 pins. Further, the clad temperature is the maximum for the reference bundle without any inserts.
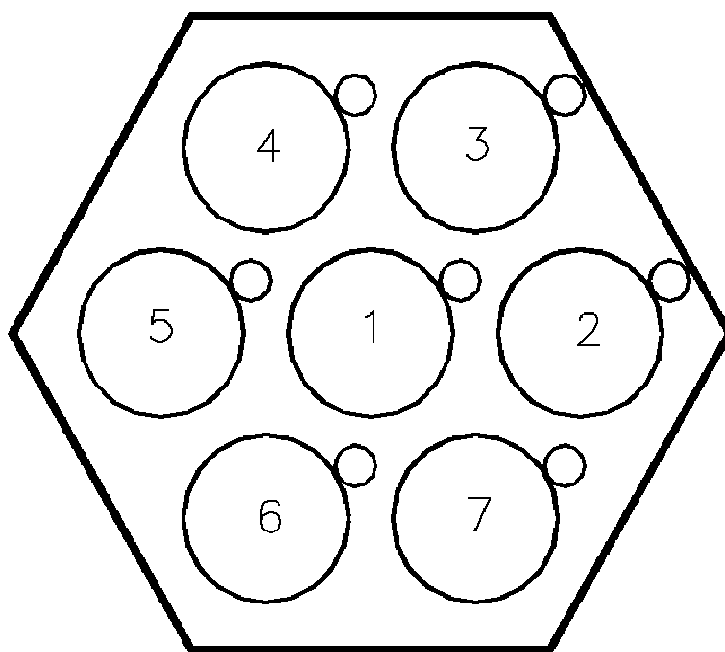
Fig. 5.7: Fuel pin numbering
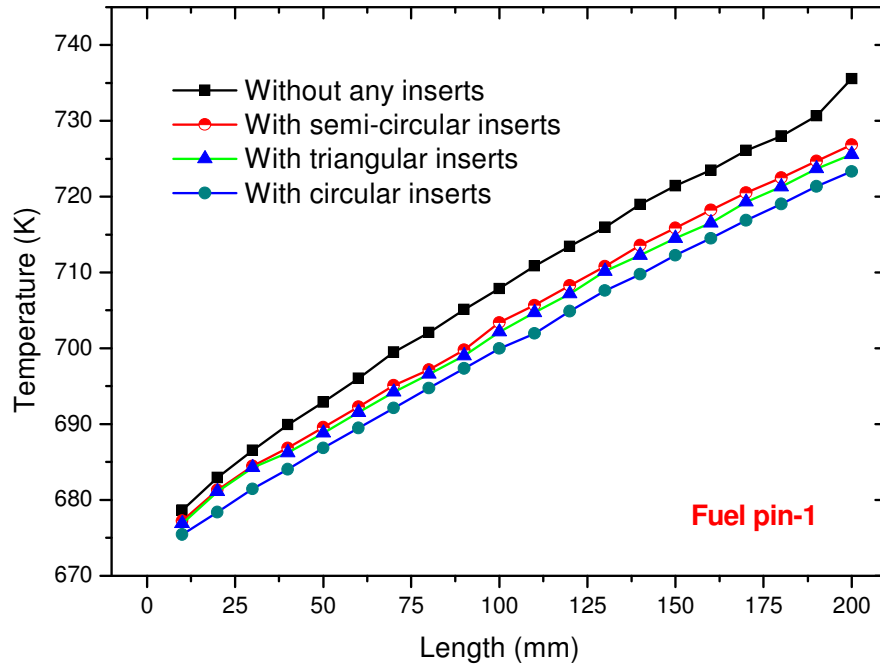
Fig. 5.8: Comparison of mean clad temperature along the length for fuel pin no. 1

(Central pin)
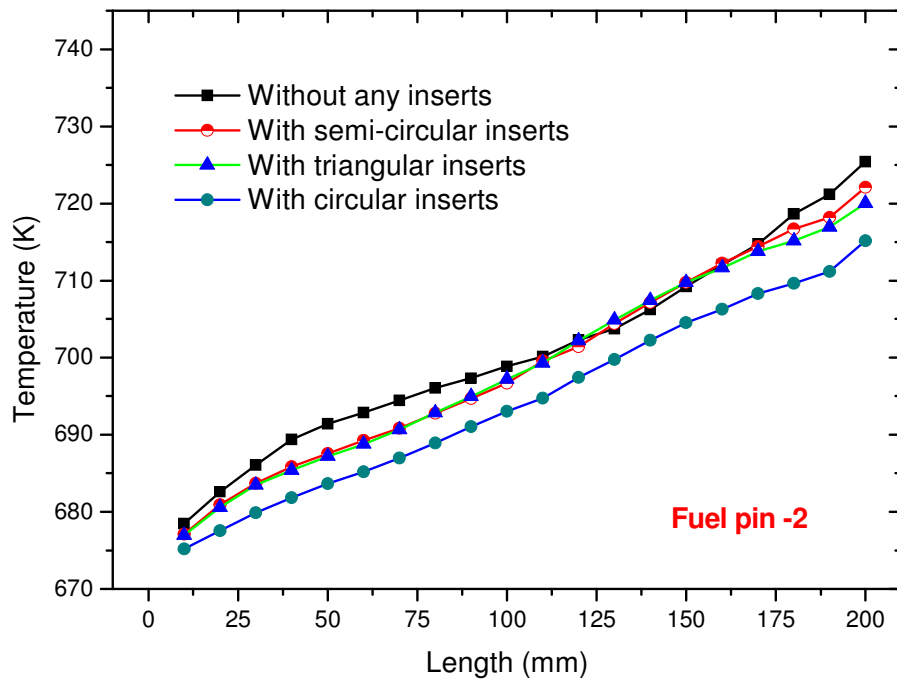
.5.9: Comparison of mean clad temperature along the length for fuel pin no. 2

Fig. 5.10: Comparison of mean clad temperature along the length for fuel pin no. 3

Fig. 5.11: Comparison of mean clad temperature along the length for fuel pin no. 4

Fig. 5.12: Comparison of mean clad temperature along the length for fuel pin no. 5

Fig. 5.13: Comparison of mean clad temperature along the length for fuel pin no. 6
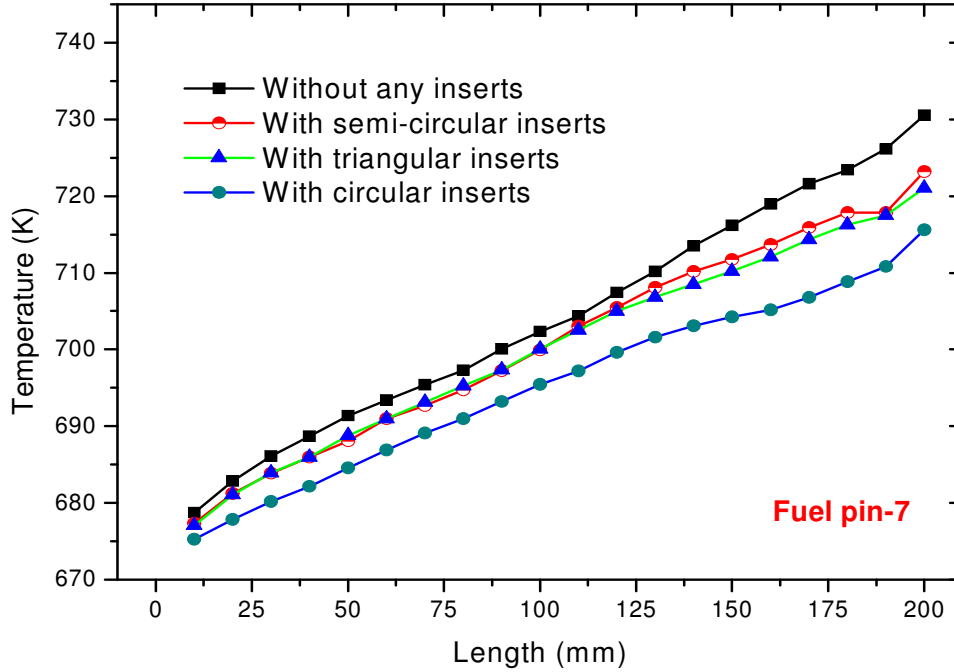
Fig. 5.14: Comparison of mean clad temperature along the length for fuel pin no. 7

5.5. CLAD TEMPERATURE ALONG THE CIRCUMFERENCE OF PIN

The modification of flow distribution among the sub-channels by the inserts also reduces the hot spots on the clad surfaces. The reduction of hot spots on the clad surface can be assessed by comparing the temperature profiles around the fuel pin for all the cases. The nomenclature adopted for circumferential angle and the position of spacer wire at the elevation of 100 mm are depicted in Figure 5.15. The variation of clad temperature for all pins along the circumference of various fuel pins in a plane 100 mm from the inlet are shown in Figure 5.16 to Figure 5.22. It can be seen that the clad circumferential temperature difference is the minimum (~30K) for the central pin as expected. For example, it is 45K in the case of Pin-2. In all the cases, the peak clad temperature occurs near the junction between the clad and the spacer wire, where the flow is less. Provision of an insert drastically reduces the peak clad temperature. Among the various inserts, it is seen that the circular inserts offer the lowest peak clad temperature.

77
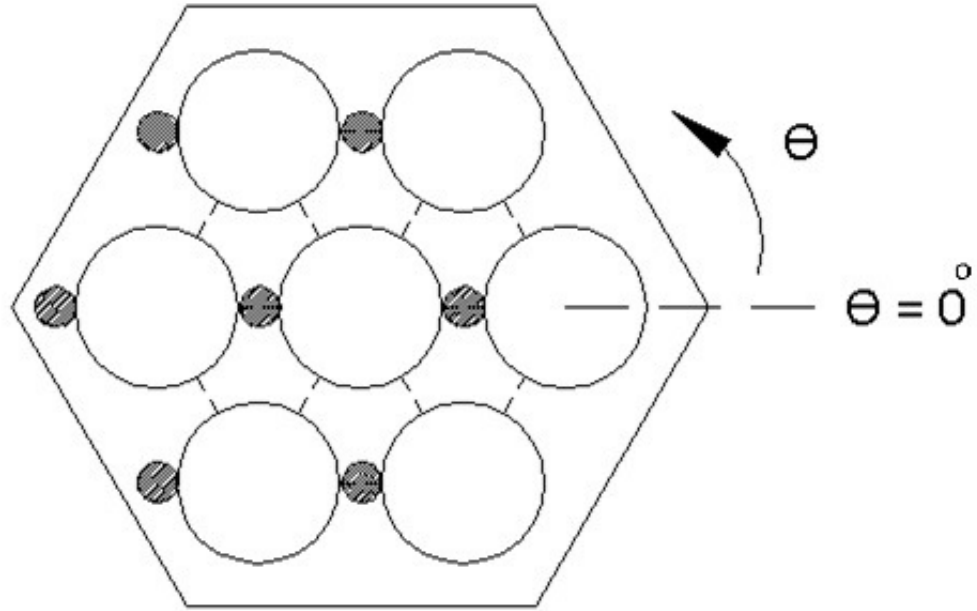
Fig. 5.15: The nomenclature adopted for circumferential angle and the position of spacer wire at the elevation of 100 mm
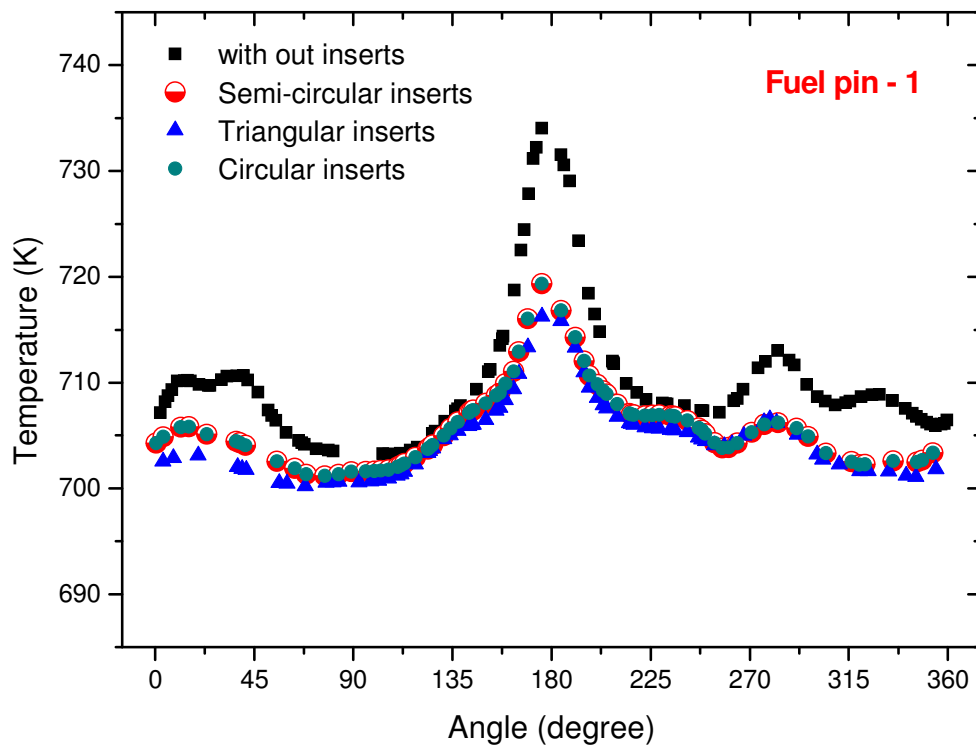
Fig. 5.16: Comparison of clad temperature along the circumference for fuel pin no. 1(Central pin)
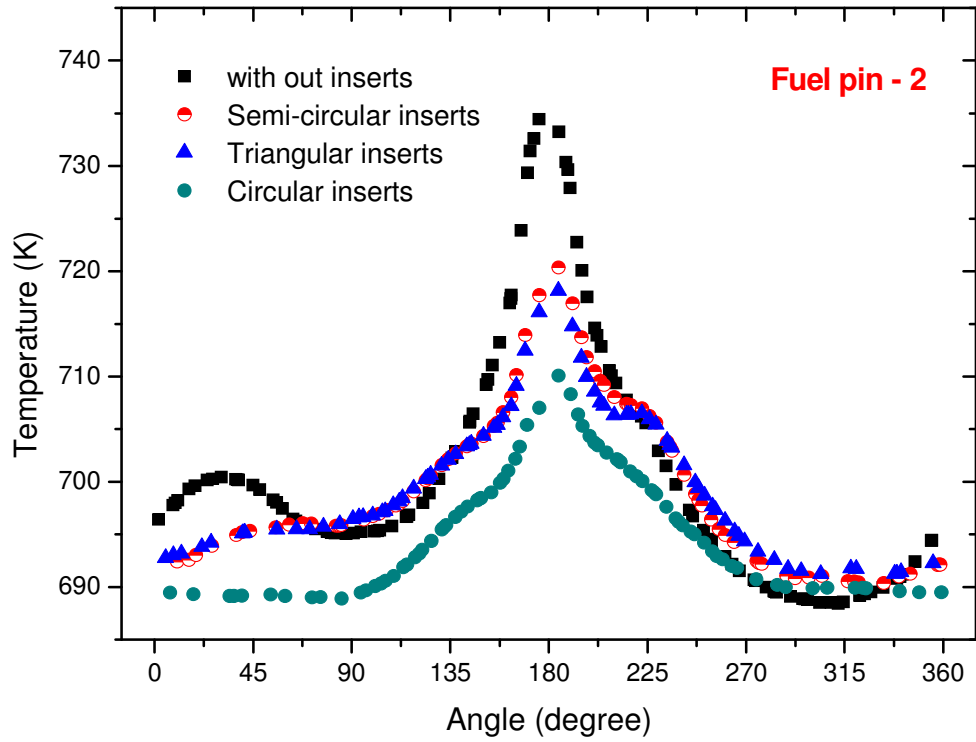
Fig. 5.17: Comparison of clad temperature along the circumference for fuel pin no. 2
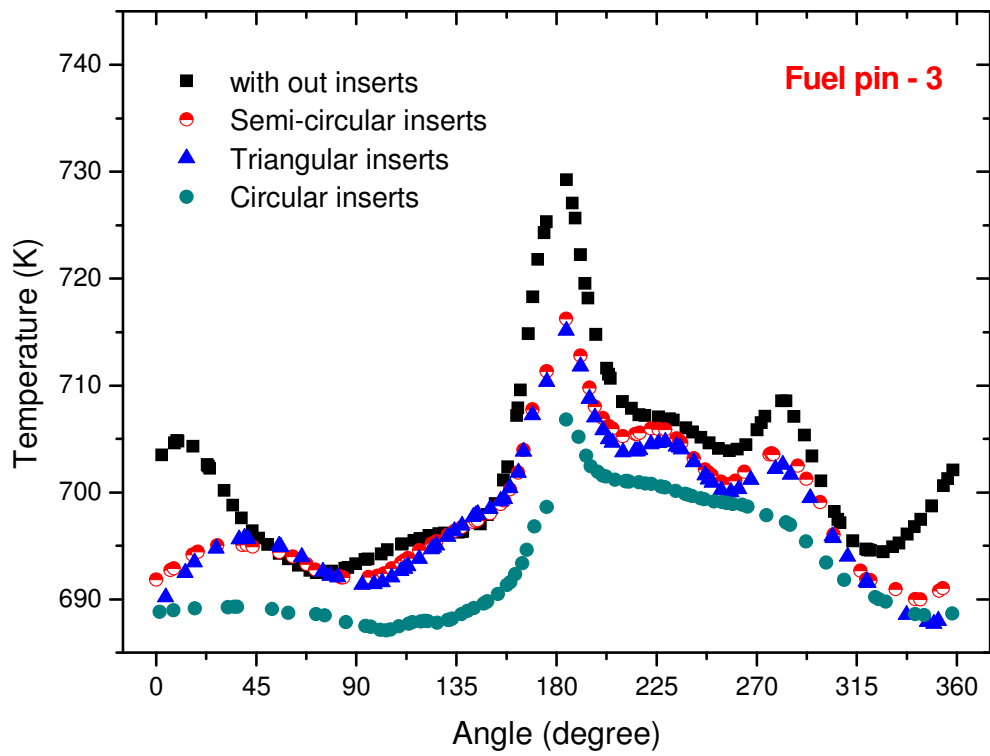
Fig. 5.18: Comparison of clad temperature along the circumference for fuel pin no. 3
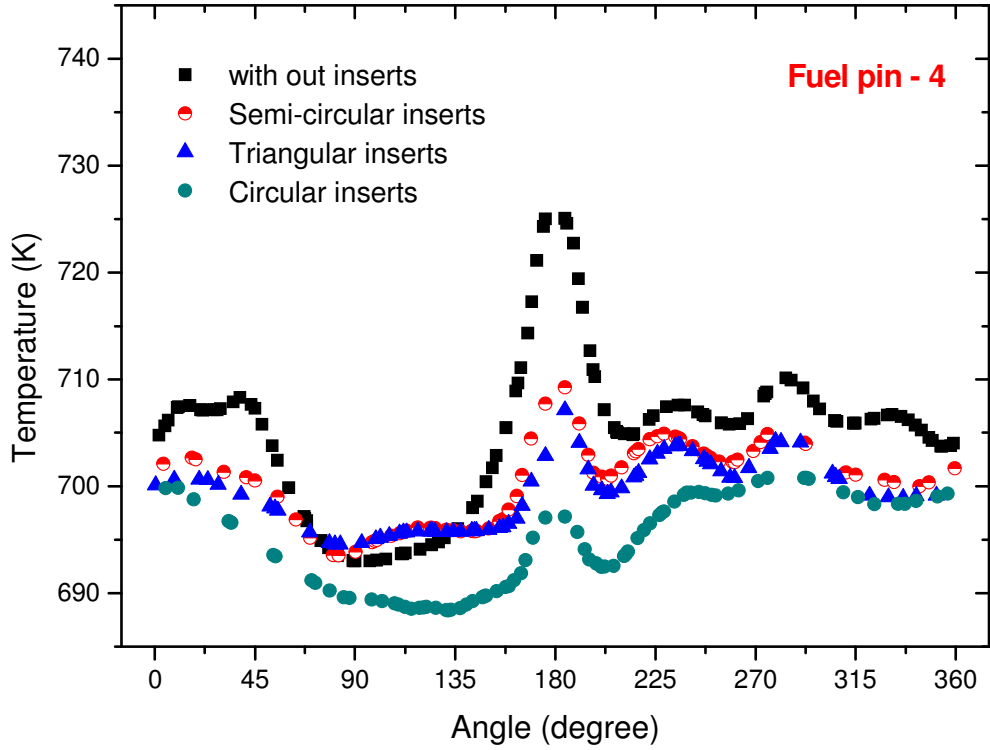
Fig. 5.19: Comparison of clad temperature along the circumference for fuel pin no. 4
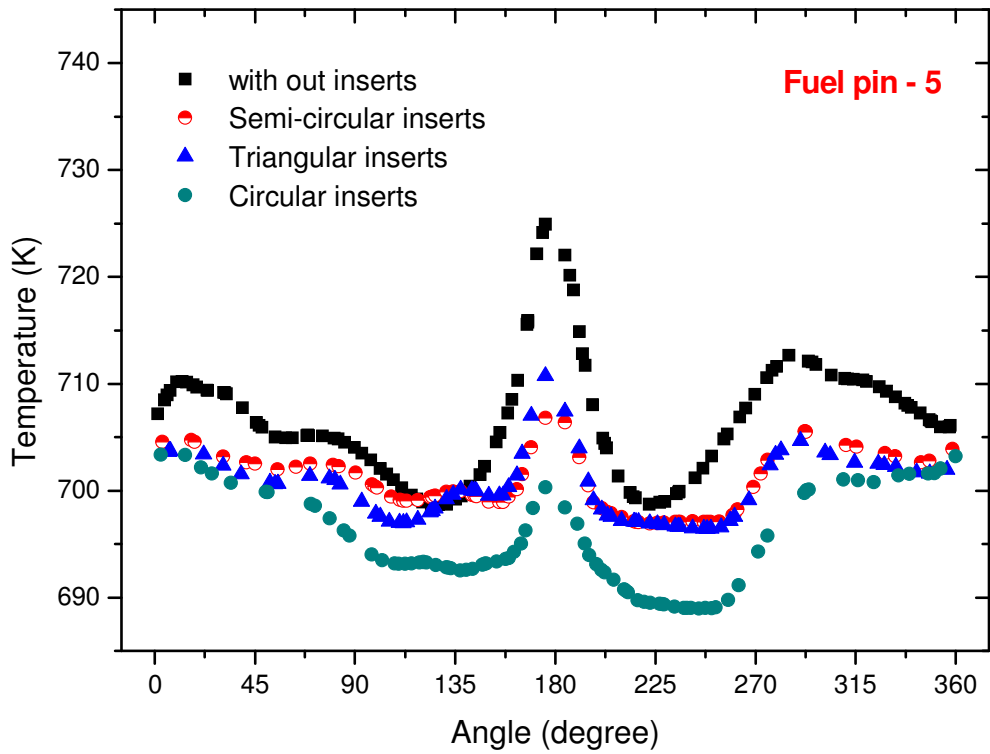
Fig. 5.20: Comparison of clad temperature along the circumference for fuel pin no. 5
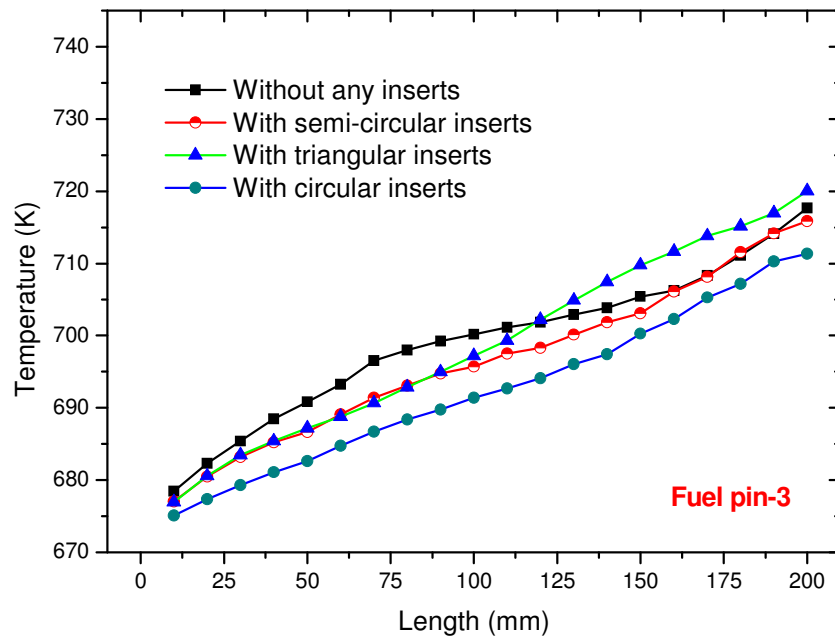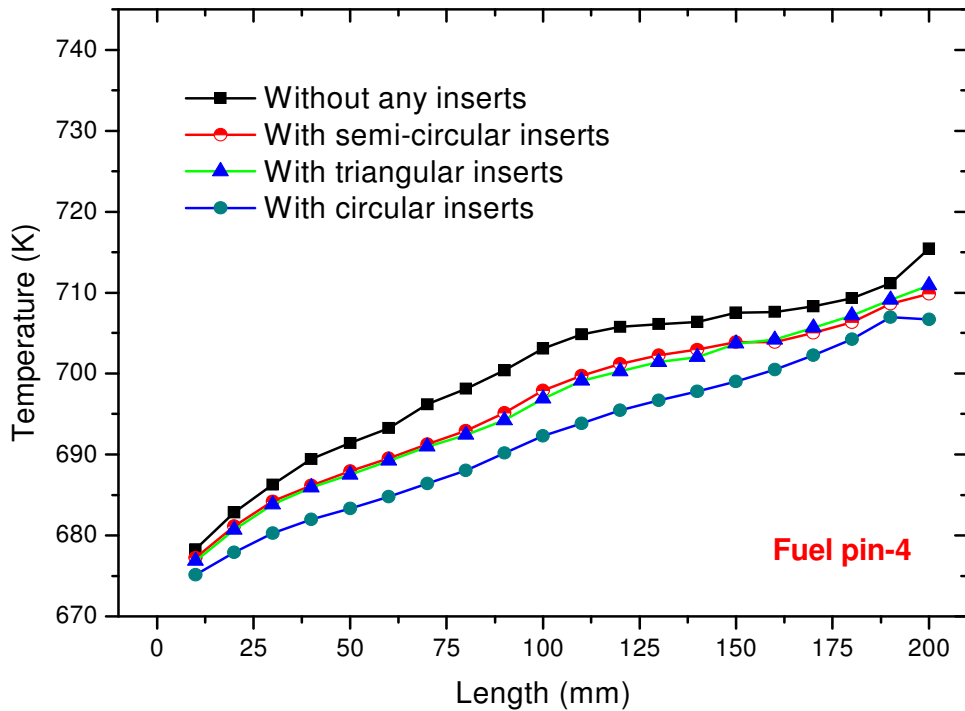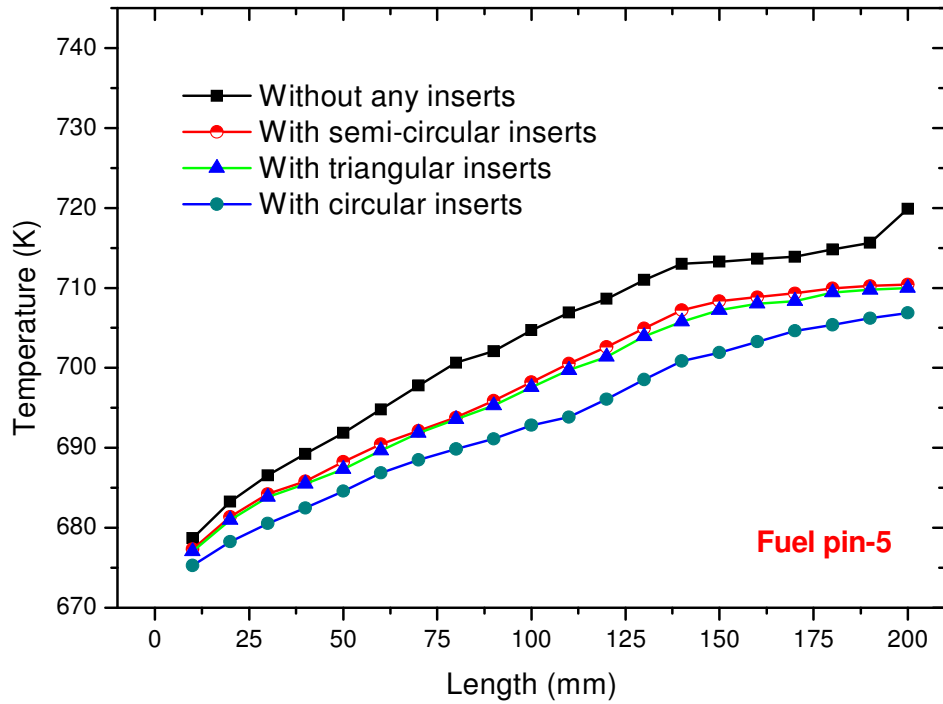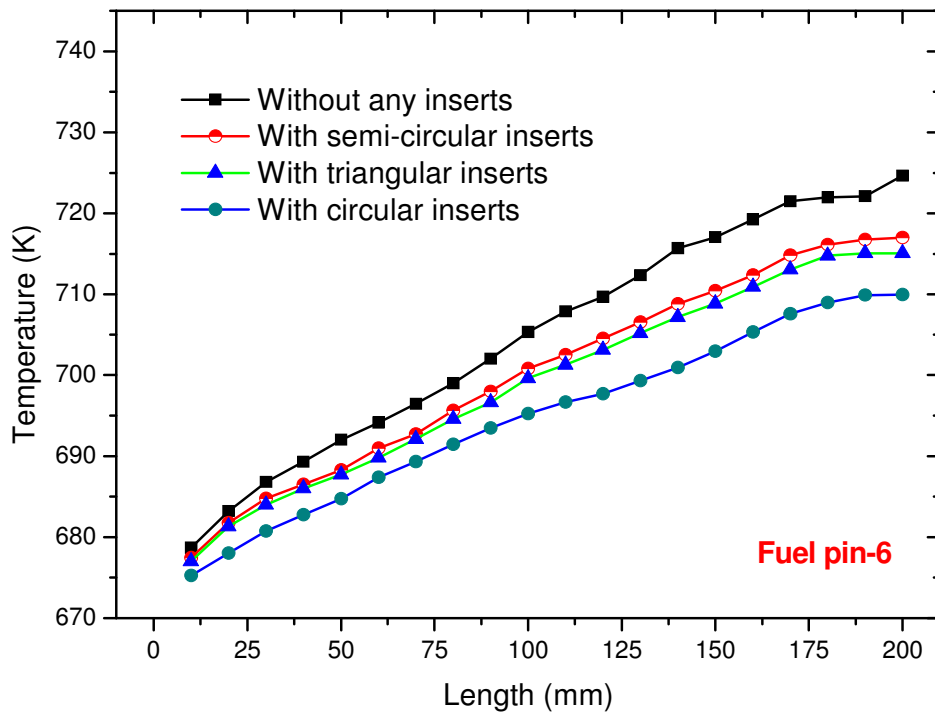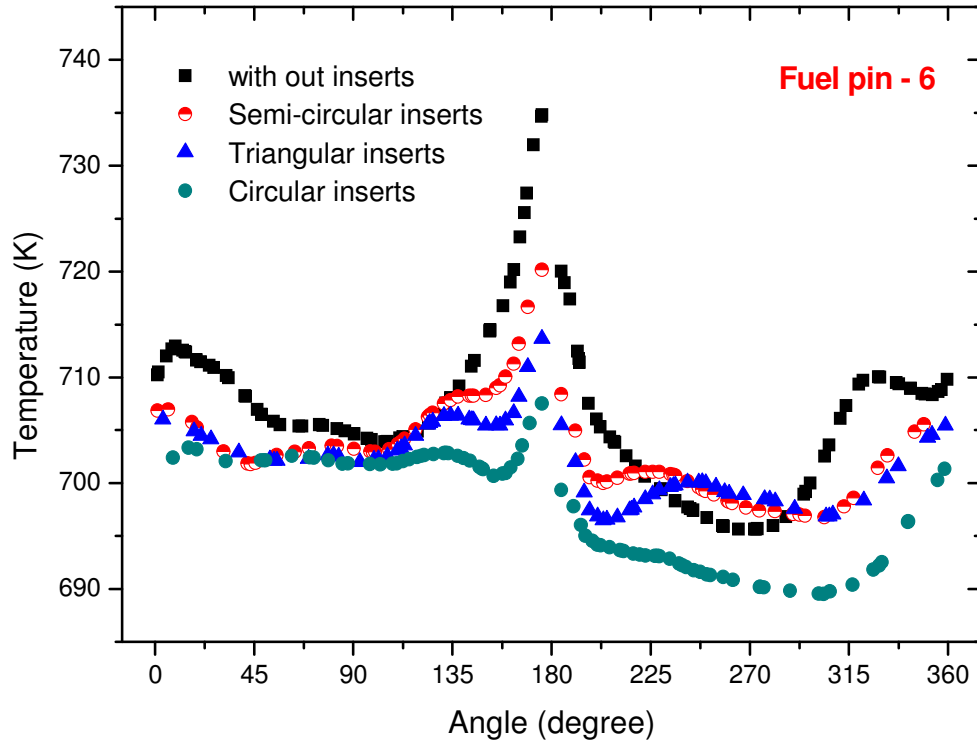
Fig. 5.21: Comparison of clad temperature along the circumference for fuel pin no. 6
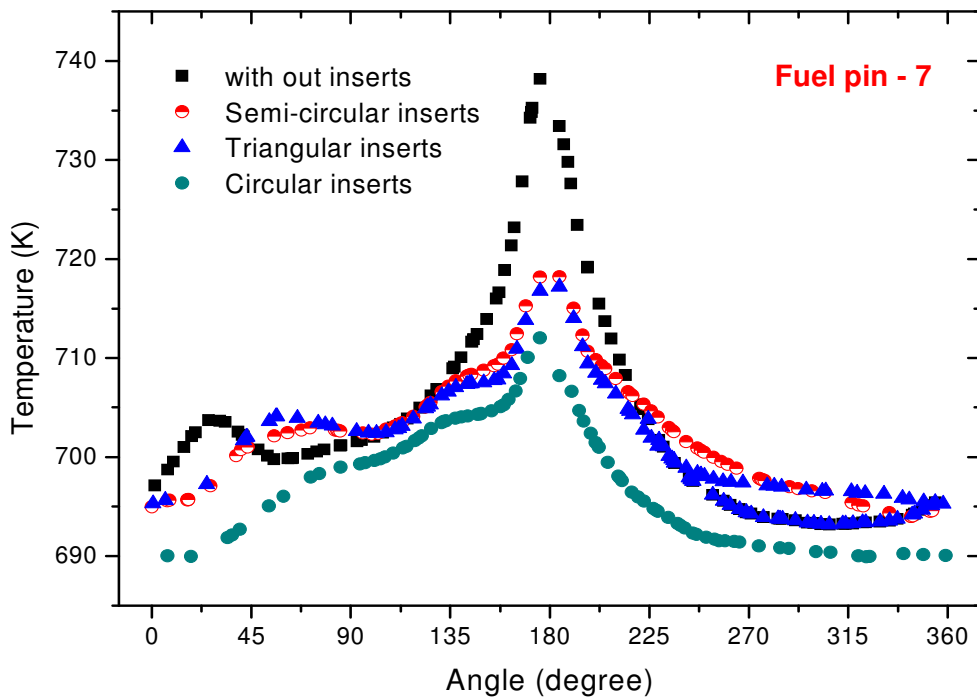
Fig. 5.22: Comparison of clad temperature along the circumference for fuel pin no. 7

5.6.   SUB-CHANNEL SODIUM TEMPERATURE AT BUNDLE EXIT

In the fuel pin bundle, the central fuel pin has a lower coolant flow around the pin and hence the coolant temperature is higher in the central sub-channels. Addition of inserts offers resistance in the peripheral sub-channel flow and hence there is an increase in flow through the central sub-channels correspondingly. As a result of this central sub-channel sodium temperature reduces with addition of inserts. Due to the flow diversion as well as reduction in sub-channel cross section area, the peripheral sub-channel sodium temperature increases. Hence the difference in temperature of sodium between peripheral and central sub-channel also reduces. The computed mean sub-channel sodium temperatures around the central pin for all the cases are compared in Table 5.1. The nomenclature for sub-channel numbering is depicted in Figure 5.23. It can be seen that the mean temperature at the sub-channel sodium in the reference case without any insert is the maximum. With the introduction of inserts, there is significant reduction in the sub-channel sodium temperature.
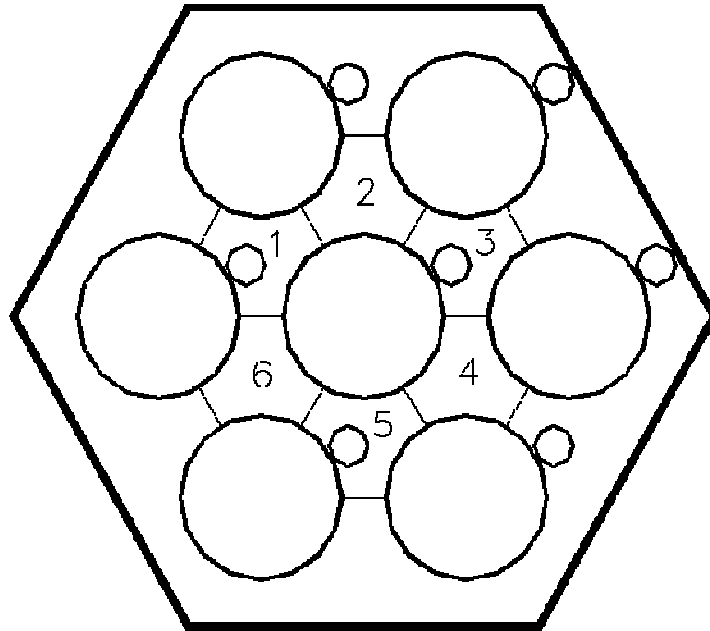
Fig. 5.23: The nomenclature for sub-channel numbering (section at bundle exit)

Table 5.1: The mean sub-channel sodium temperatures around the central pin for all the cases at bundle exit

Sub-channel	Mean central sub-channel sodium temperature at pin bundle exit (K)			
	No inserts	Semi-circular	Triangular	Circular
1	709.29	706.17	706.98	707.25
2	716.58	713.79	714.39	715.33
3	719.45	716.31	715.48	715.80
4	723.71	719.11	717.01	717.39
5	725.79	720.30	719.17	721.25
6	715.16	707.95	707.64	708.81
Mean	718	714	713	714

Mean bundle exit temperature for all the cases = 704 K

Figure 5.24 shows the sodium temperature at the bundle outlet for all the cases. The temperature has become more uniform due to addition of inserts. For example, the peak to peak temperature variation in the reference case, viz. 55K has reduced to ~35K with the addition of inserts.
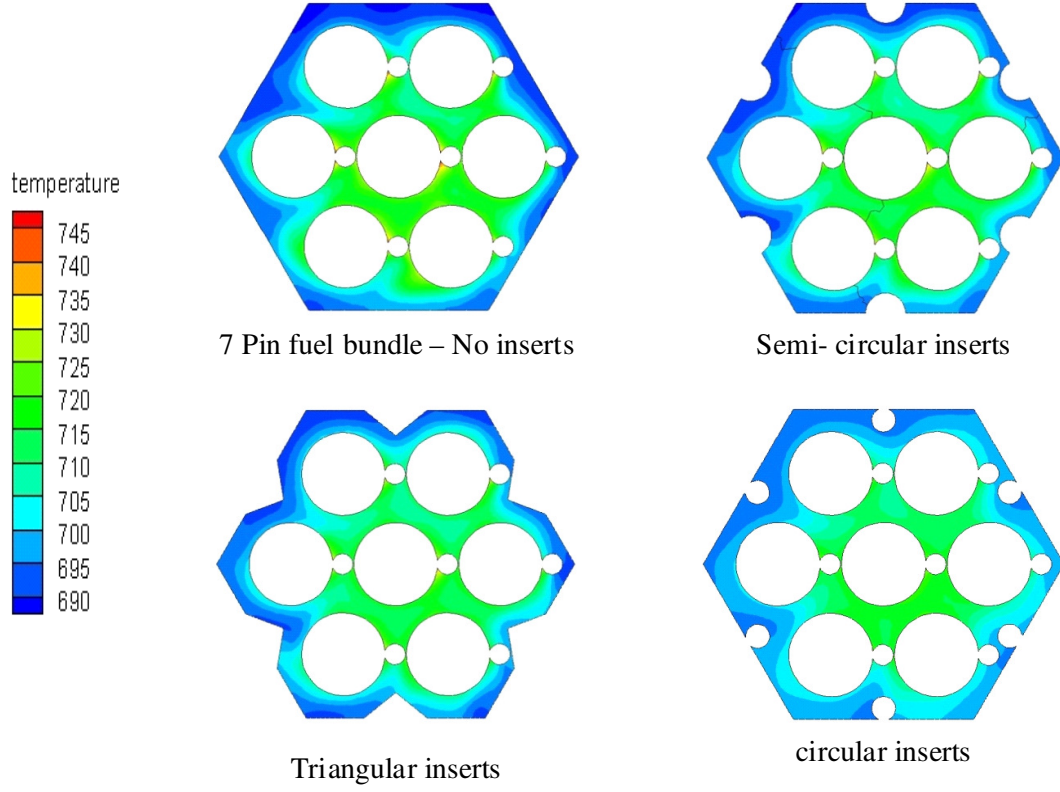
Fig. 5.24: Temperature (K) profile at the outlet of pin bundle for different cases

5.7. NUSSELT NUMBER AT BUNDLE EXIT

The mean heat transfer coefficient at bundle outlet is determined from,

$$\bar{h} = \frac{q^{''}}{(\bar{T}_c - \bar{T}_{Na})}$$

And the Nusselt number is defined as,

$$Nu = \frac{\bar{h}\,D_h}{K}$$

Where,

q'' Heat flux

$\bar{T}_C$ Mean clad temperature of all the pins at the outlet

$\bar{T}_{Na}$ Mean sodium temperature of all sub-channels at the outlet

D_h Hydraulic diameter

K Thermal conductivity of sodium

The values of hydraulic diameter in the cases of reference bundle, bundle with semi-circular inserts, bundle with triangular inserts and bundle with circular inserts, are, 3.990, 3.499, 3.422 and 3.305 mm respectively. It may be indicated that the Nusselt number at the exit is calculated from the averaged clad temperature at the exit of fuel bundle and flow weighted sodium temperature at the exit. The development of Nusselt number with axial distance was also computed based on local sodium bulk temperature and mean clad temperature at every cross-section. The Nusselt number development is depicted in Fig. 5.25 for the reference bundle without any insert. It is clear that the flow is thermally developed at the exit of the pin bundle. This suggests that CFD simulation for one helical pitch length is adequate for the purpose of evaluating the effect of inserts on the Nusselt number and friction factor.
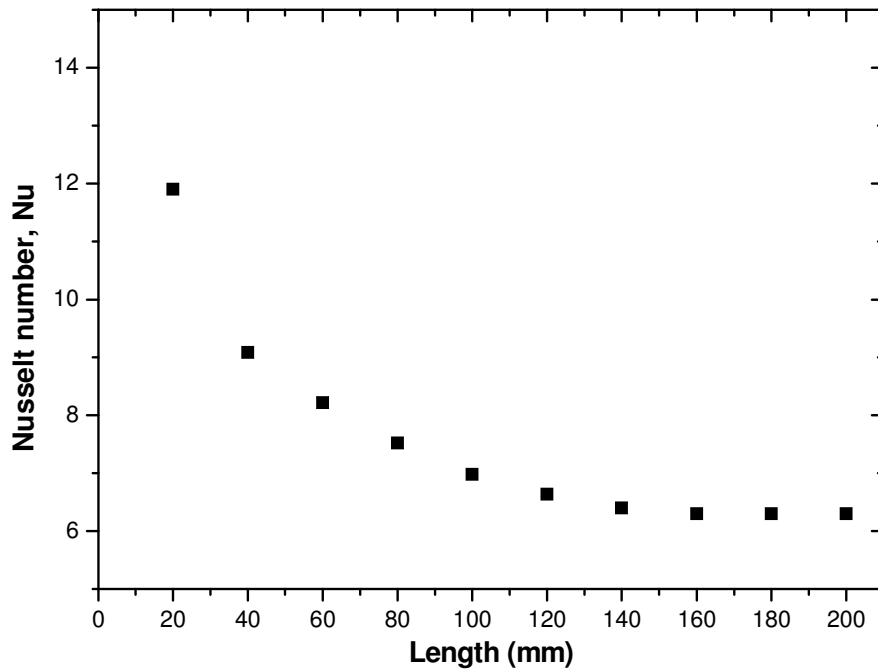
Fig. 5.25: Development of Nusselt number along axial distance for the reference bundle at Re=0.85×10^5

Following these, the Nusselt number at the exit of the pin bundle for all the cases are estimated for various values of Reynolds number ranging from $5{\times}10^4$ to $1.7{\times}10^5$. The variation of Nusselt number with flow has been compared for all the cases of inserts and is shown in Figure 5.26. The increase in heat transfer coefficient due to inserts can be easily observed from the comparison of Nusselt number. The Nu is seen to be proportional to $\mathbf{Pe^{0.8}}$ in the case of reference bundle without any inserts. The Nusselt number for equal sodium flow rate for all the inserts is given in Table 5. 2. Due to the addition of inserts, there is large increase in the Nu for all the cases. The increase is maximum in the case of circular inserts. The Nusselt number is nearly double with circular inserts.

Table 5.2: Effect of inserts on Nusselt number (Equal mass flow rate)

Type of inserts	Pe	Nu	% Change in Nu
No inserts	429	6.37	-
Semi circular	412	7.45	16.95
Triangular	413	8.60	35.00
Circular	378	11.86	86.18
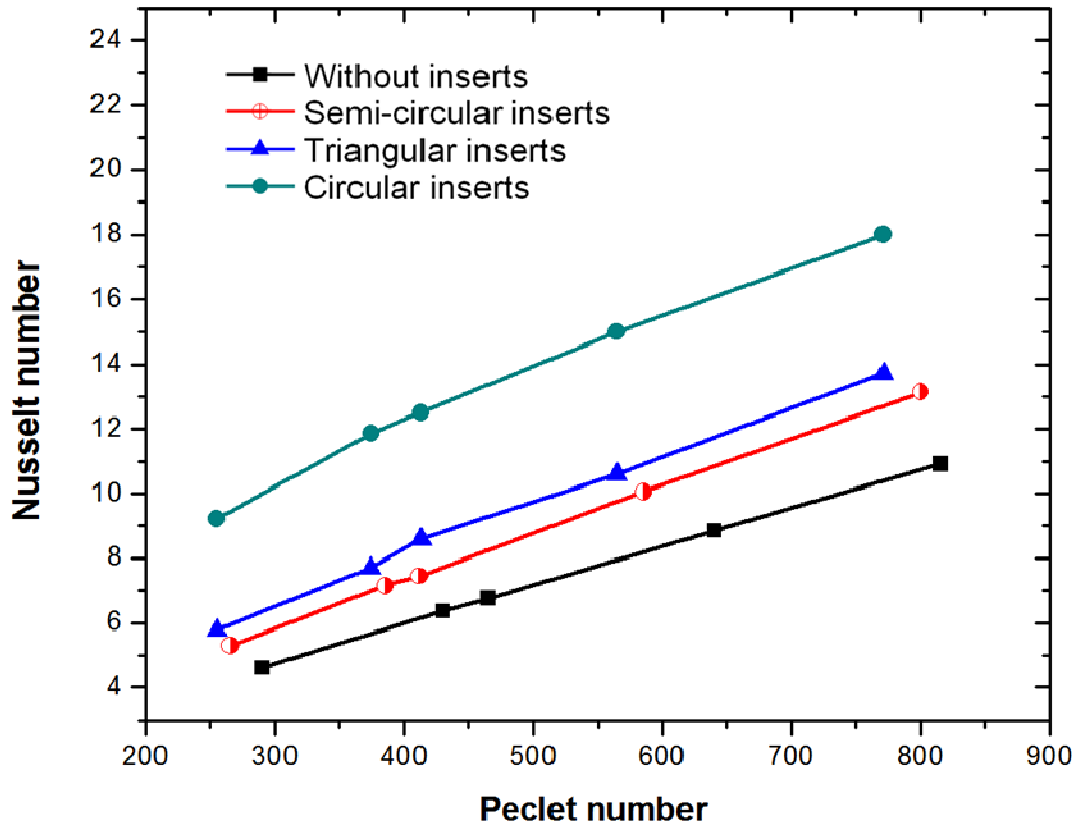
Fig. 5.26: Effect of inserts on Nusselt Number

5.8.   EFFECT ON HOT SPOT FACTOR

The addition of inserts reduces the intensity of hot spot formation in the fuel bundle. The hot spot formation has been quantified using a non-dimensional term hot spot factor, which is defined as

$$\text{Hot spot factor, } \xi = \frac{(T_c - \overline{T_{Na}})}{(\overline{T_c} - \overline{T_{Na}})}$$

Figure 5.27 shows the peak clad temperature along the length for all cases of inserts. The comparison of mean clad temperature along the length has been shown in Figure 5. 28. It is observed that, the circular inserts give the lowest peak clad temperature and lowest mean clad temperature among all the inserts. The hot spot factors for all the cases of inserts for equal mass flow rate of sodium were estimated. The clad hot spot factor is found to be the highest for circular insert due to the following facts. The Nusselt number is high because the temperature difference between clad and coolant is small. As a result, the denominator in above equation is the lowest for the circular insert.
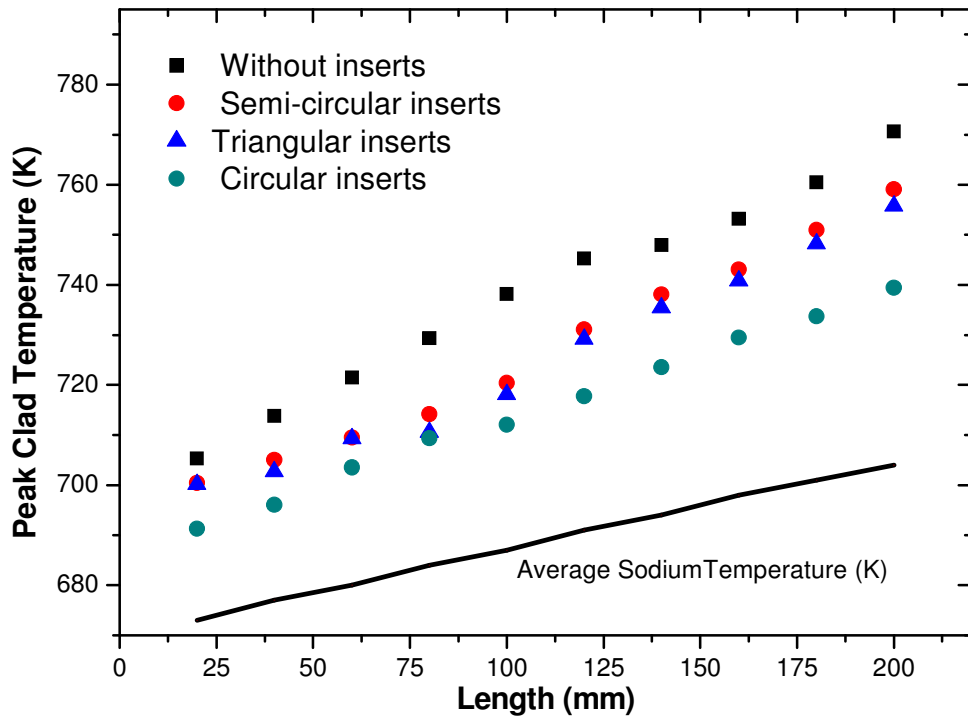
Fig. 5.27: Peak clad temperature of any section along the length for all cases.
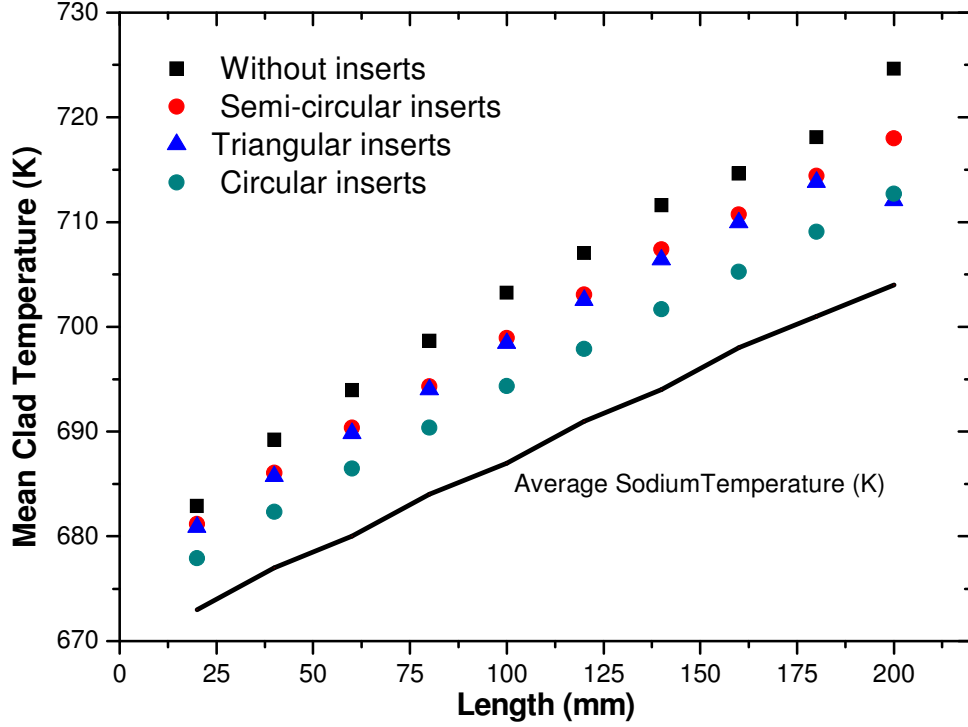
Fig. 5.28: Comparison of mean clad temperature along the length for all cases.

5.9. PERFORMANCE EVALUATION CRITERION (PEC)

The inserts in pin bundle increase the heat transfer coefficient in the subassembly but with an additional pressure drop in the system. The selection criteria for the optimum geometry for the inserts are maximum heat transfer coefficient and minimum pressure drop. Both heat transfer and pressure drop can be quantitatively expressed in terms of Nusselt number and friction factor. The Performance Evaluation Criteria factor compares the relative change in heat transfer coefficient and pressure drop for all the inserts and gives a quantitative measurement of effectiveness of the insert geometry.

PEC is defined as,

$$PEC = \frac{(Nu/Nu_R)}{(f/f_R)^{1/3}}$$

where, the subscript 'R' refers to the values corresponding to reference pin bundle without any inserts. The PEC values for all the inserts have been calculated and presented in Table-5.3. These values are for the case of Re = 0.85×10^5 in the case of reference bundle without any inserts. The sodium flow rates in all the cases presented in Table 3 are the same.

Table 5.3: Performance Evaluation Criteria for inserts

Type of inserts	f	Nu	PEC
Semi circular	0.0217	7.45	1.124
Triangular	0.0213	8.60	1.306
Circular	0.0227	11.86	1.763

It can be seen that, the frictional factor is the highest for the circular inserts and is the minimum in the case of triangular inserts. The circular inserts are very effective in breaking the circumferential flow due to the presence of sharp corner between the inserts and hexcan wall. As a consequence of this resistance for circumferential flow, axial flow uniformity is improved with the associated enhancement in Nusselt number. The maximum value of PEC is 1.763 and it occurs in the case of circular insert indicating circular inserts are the optimum one. The variation of (Nu/Nu_R) as a function of $(f/f_R)^{1/3}$ is depicted in Fig. 5.29.
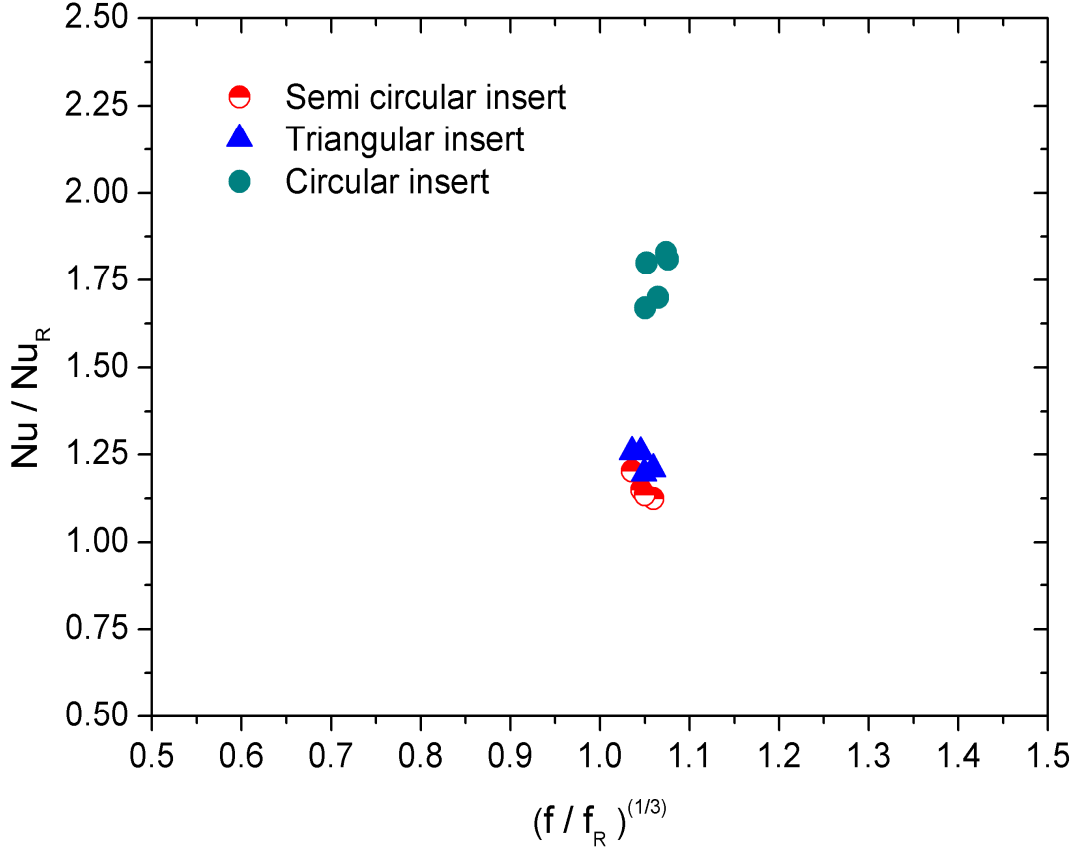
Fig. 5.29: Variation of $(\dfrac{Nu}{Nu_R})$ as a function of $(\dfrac{f}{f_R})^{1/3}$ for various inserts

From the point of view of fabrication also, it is easy to provide circular inserts and tag-weld them to the hexcan walls. It may be further highlighted that the present results / improvements observed are valid only for a 7 pin bundle. As the total number of pins in a subassembly increases, the ratio of number of peripheral sub-channels to number of central sub-channels decreases. Hence, the observed improvements in PEC will be a function of the number of fuel pins and the present results cannot be directly extrapolated to bundles with larger number of fuel pins

5.10. CLOSURE

A combined experimental and numerical study has been carried out to find the effect of addition of inserts on heat transfer coefficient and hot spot temperature. A model with 7 pin SFR fuel assembly has been considered for the computation and the hydraulics has been validated with in-house experiments and the thermal part has been verified against published results. From the analysis it is observed that the addition of inserts have better influence on heat transfer coefficient with additional frictional drop. The increase in the heat transfer coefficient is quantified in terms of Nusselt number. The highest improvement in Nusselt number is with addition of circular inserts and there is an increase of 86 % in Nusselt number due to the addition of circular inserts. When frictional pressure drops are compared, the circular inserts have the highest frictional drop compared to all other insert geometries. There is an increase of 17 % in friction factor for circular inserts. The PEC values for all the inserts have been calculated. The maximum value of PEC is 1.763 and it occurs in the case of circular insert indicating circular inserts are the optimum one.

CHAPTER 6

EXPERIMENTS IN FULL SCALE BUNDLE ASSEMBLY

6.0 INTRODUCTION

Knowledge of pressure drop in various regions of subassembly and across the subassembly is critical for determining the primary pump head, and to quantify the extent of additional pressure drop required using devices such as orifices as well to understand the hydraulic behaviour during various operating scenarios. The pressure drop in the core changes on account of the introduction of inserts in the subassemblies. A quantification of the percentage increase in pressure drop has been made through computational analysis and experimental validation in a 7 pin bundle assembly as brought out in the previous chapters. However to predict the actual pressure drop on account of the inserts in a 1:1 scale assembly, it is required to carry out hydraulic studies in a 1:1 scale assembly. As a first step, the existing PFBR sub-assemblies is tested in water simulating the reactor operating condition to determine the pressure drop characteristics of the sub assembly without any insert. The percentage increase in pressure drop obtained from the 7 pin bundle assembly studies would be used to get a final picture of the pressure drop with inserts in a 1:1 scale assembly. This chapter elucidates the details of the hydraulic studies conducted in the various subassemblies to establish a correlation for determining the pressure drop in 1:1scale subassembly.

6.1 SUBASSEMBLY DETAILS

The geometrical details of the full scale subassembly are listed in Table- 6.1. The subassembly is complex in geometry having radial entry, axial exit and pin bundle with helical spacer wire. It also has a number of varying cross sections along the length. The fuel pins are supported on rails. The subassembly comprises of a diffuser where the cross section

changes from cylindrical to hexagonal, mixing plenum at the bundle exit and a blockage adapter before subassembly exit as shown in Figure 1.4. The pressure drop in the core changes on account of the introduction of inserts in the subassemblies. A quantification of the increase in pressure drop has been made through computational analysis as brought out in the previous chapters. However to predict the actual pressure drop on account of the inserts in a 1:1 scale assembly, it is required to carry out hydraulic studies in a 1:1 scale assembly.

Table 6.1: Geometric details of test subassembly

Parameters	Qty (nos.)
No. of pins	217
Pin Diamater (mm)	6.6
Total Pin length (mm)	2580
Fuel Pin pitch(mm)	8.28
Spacer wire Diameter (mm)	1.65
Spacer wire pitch (mm)	200
Subassembly total length (mm)	4500
Hexcan flat to flat outside dimension (mm)	131.6
Hexcan flat to flat inside dimension (mm)	124.9

1:1 scale assemblies are used to determine the pressure drop of the existing configuration. The percentage increase in pressure drop obtained from the 7 pin bundle assembly studies would be used to get a final picture of the pressure drop with inserts in 1:1 scale assembly. It may be highlighted that the flow from grid plate to the foot of the subassembly is through multiple inlet holes in the grid plate sleeves. The flow enters in the foot of the subassembly through 12 slots provided in the foot of the subassembly. In order to

minimize the effect of blockage from top of the subassembly head, provision of six blockage adaptor holes (one in each face of the hexcan) have been provided at the subassembly top. This provision avoids complete flow from top even in case of fall of some heavy objects at top of the subassembly. But, when the subassembly top is blocked, reduced flow will take place through blockage adaptor holes. Hence, it is essential to determine the flow through the blockage adaptor holes for the purpose of safety analysis.
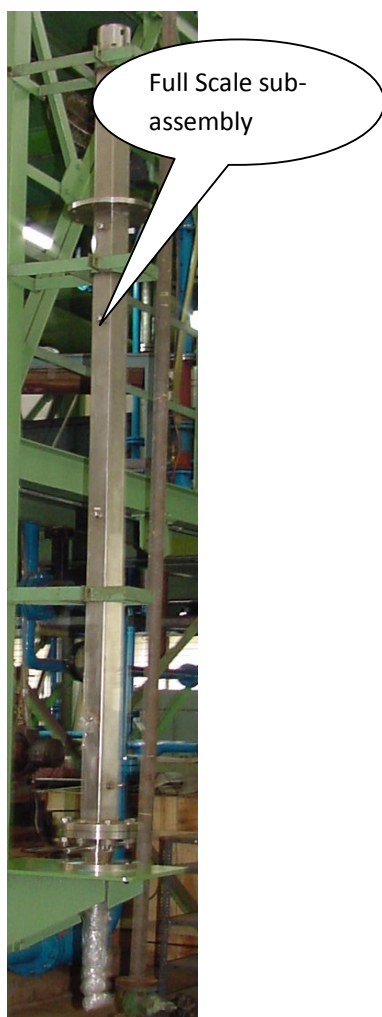
Fig. 6.1 : Various regions of a FBR fuel subassembly   Fig. 6.2 : FBR bundle sub-assembly
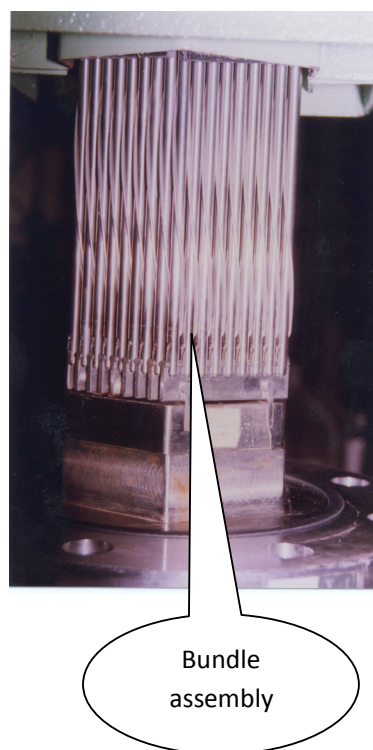
An experimental loop was designed, fabricated and erected for conducting the hydraulic studies using water as the test medium. A 1:1 scale dummy fuel subassembly, was

fabricated and experiments have been conducted for various operating conditions of the reactor and the results were transposed to the reactor condition using appropriate similarity laws. As already indicated, both the normal subassembly and the subassembly with axial exit completely blocked have also been tested. A figure of subassembly and dummy pin internals are shown below in Figure 6.1 and Figure 6.2 respectively.

6.2   SIMILARITY CRITERIA

Sodium is the working fluid in SFR because of its efficient heat removal capability. Considering the fact that important hydraulic properties (density and kinematic viscosity) of water are close to that of sodium, water has been chosen as the simulant in the model studies (Bomelburg, 1968). Testing a subassembly in sodium requires complex instrumentation and stringent handling procedure which becomes costly. Taking advantage of the favorable comparison of the important hydraulic properties of sodium with water, the later was selected as simulant fluid. Pressure drop in the subassembly can be represented as

$$\Delta P = K_t \frac{\rho V^2}{2} \tag{6.1}$$

$$K_t = K_f + K_{en} + K_b + K_{ex} + K_{se} \tag{6.2}$$

Where, K_t is the total loss coefficient for subassembly and is the addition of individual loss coefficients of subcomponents of pressure loss in various parts of the subassembly as given by Eq. (2). Here, K_f, K_{en}, K_b, K_{ex} and K_{se} are the loss coefficient in the foot of the subassembly, entry of the pin bundle, bundle region, bundle exit and subassembly exit respectively. Form loss contributes to most part for all the losses except the bundle region where the skin friction plays a significant contribution as given by Eq. (3).

$$K_b = \frac{f*L}{D_h} \tag{6.3}$$

97

f is the (Darcy) friction factor and is dependent on the geometry of the bundle region, relative roughness ($\frac{\varepsilon}{D_h}$) and the Reynolds number (Re). Hence, all these parameters need to be respected during the simulation of the experimental study. The $\frac{\varepsilon}{D_h}$ ratio is maintained same by carrying out studies on full scale pin bundle made of austenitic stainless steel. The surface roughness is maintained as in prototype by choosing the appropriate manufacturing technique. For maintaining dynamic similarity the non dimensional number to be simulated is Reynolds number (Bomelburg, 1968).

As per the Re similitude,

$$\frac{V_m}{\upsilon_m} = \frac{V_p}{\upsilon_p}$$

(6.4)

Since, the scale factor is 1: 1

Therefore, the model volume flow rate can be estimated as follows:

$$Q_m = V_m \times A_m = V_p \times \left(\frac{\upsilon_m}{\upsilon_p}\right) \times A_p = Q_p \times \left(\frac{\upsilon_m}{\upsilon_p}\right)$$

(6.5)

Euler similarity is used for transposition of the results to reactor condition. Euler number is defined as the ratio of inertial forces to pressure forces.

$$Eu = \frac{\Delta P}{\rho \times V^2}$$

For maintaining Euler number similitude the Eu in model and prototype is equated as,

$$Eu_p = Eu_m$$

$$\left(\frac{\Delta P}{\rho \times V^2}\right)_p = \left(\frac{\Delta P}{\rho \times V^2}\right)_m = K_{exp}$$

Hence as per Euler similitude, the pressure drop in prototype subassembly can be estimated by the following Eq. (6).

$$\Delta P_p = K_{exp} \times \left(\frac{\rho_p \times V_p^2}{2}\right)$$
(6.6)

6.3   EXPERIMENTAL LOOP AND INSTRUMENTATION

The experimental subassembly with dummy fuel pins was installed in the water test loop as depicted in Figure 6. 4(a). A 3.D picture of the subassembly loop is shown in Figure 6.4(b).
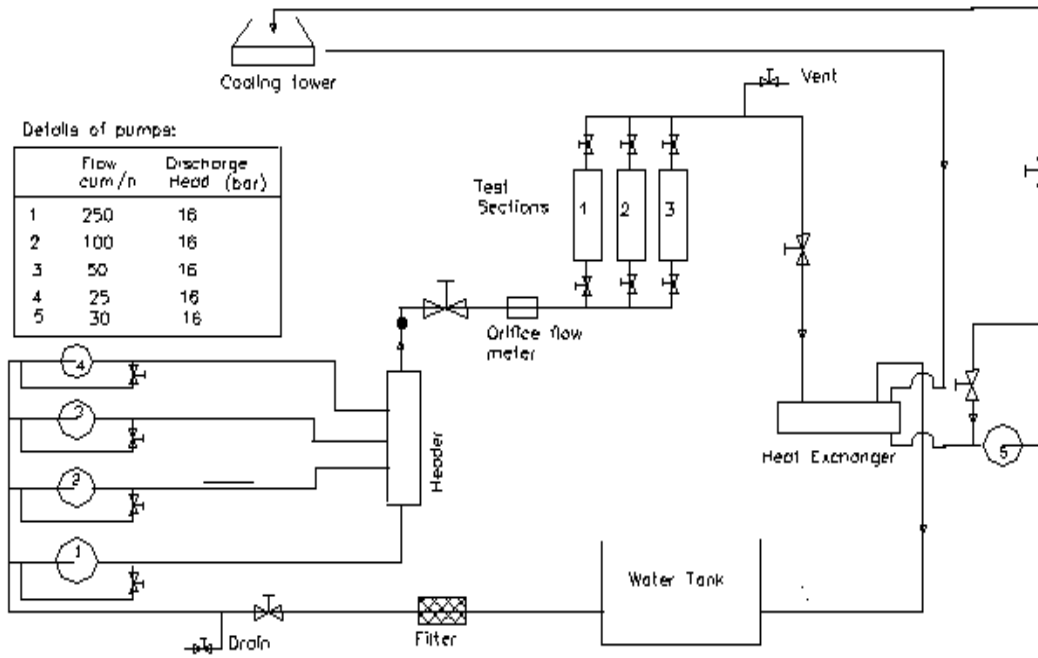
Fig. 6.3: Subassembly Test Rig
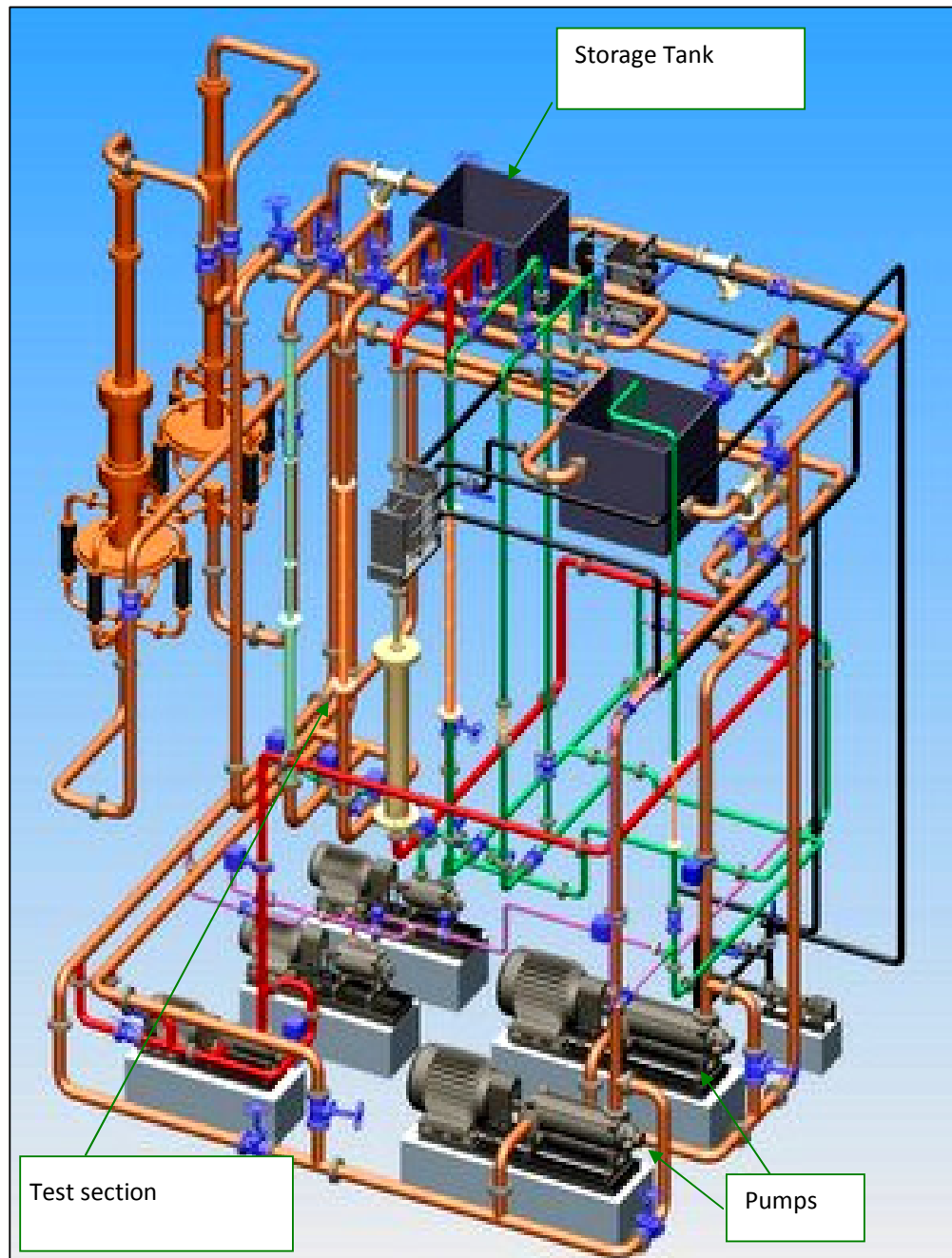
Fig. 6.4(a): Subassembly test loop

The subassembly installed in the test section is shown in Figure 6.5. Water pumps of different capacities ranging from as low as 1m^3/h to 250 m^3/h have been used to cater the flow requirement over a wide range through the test section.
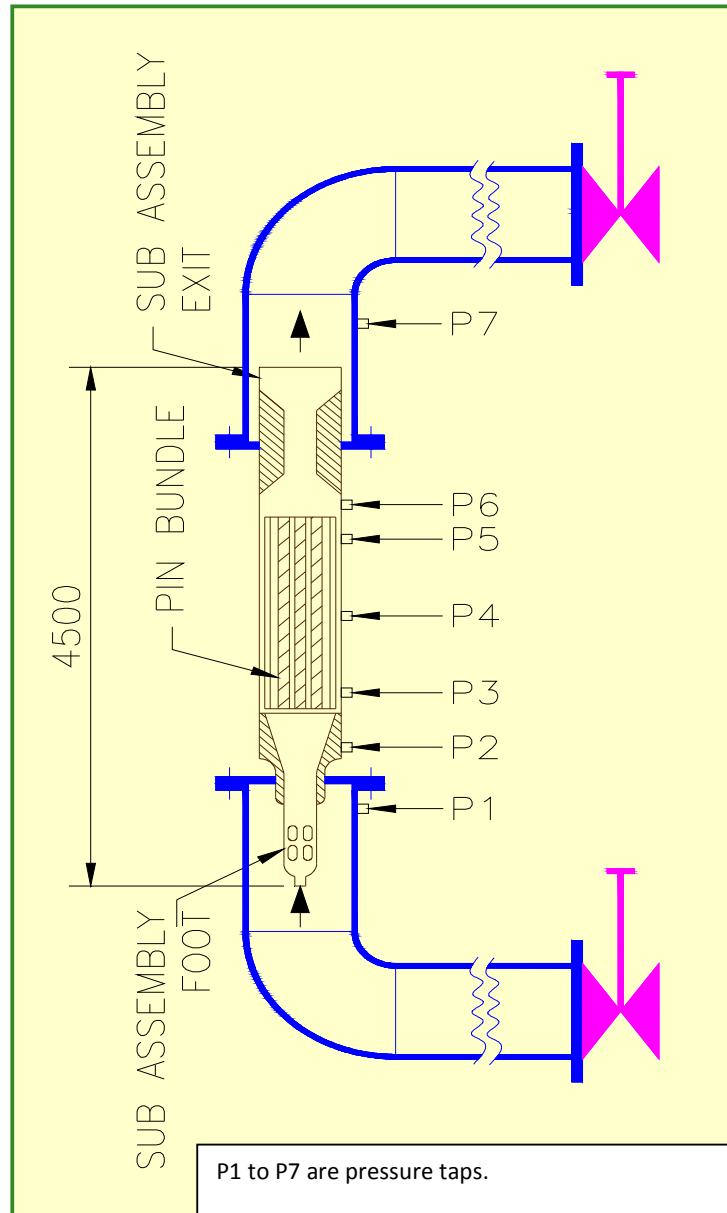
Fig. 6.4(b): Subassembly with test section and pressure tap locations

In order to measure the pressure drop in various sections of the subassembly, many pressure taps have been provided. Differential pressure transmitters of different ranges, have been utilized for this purpose. Static pressure measurement was carried out with the help of pressure transmitters of appropriate ranges. The flow rate is measured using an orifice flow meter for flow rates above 70 m^3/h, while volume collection method was used for low rates

flow measurements. Temperature measurement was carried out by Resistance type Temperature Detector. Various instruments used for the experiments are given in Table- 6.2.

Table 6.2: Instruments utilized for the experiments

S.no	Name of the Instrument	Type	Range	Overall accuracy
1	Flow meter	Orifice with flange tapping	0-275m/h	± 1%
2	Differentia pressure Transmitter	Capacitance	0 – 20 bar 0 – 10 bar 0 – 7 bar 0 –2 bar 0 – 1 bar 0 - 0.3bar	± 0.25%
3	Pressure Transmitter	Capacitance	0-20 bar	± 0.25%
4	Temperature indicator	RTD-PT100	$0 – 100^0C$	± 1.0%
5	Pressure gages (Pump discharge)	Bourden	0 – 40 bar	± 2.0%

6.4   RESULTS AND DISCUSSION

To determine the pressure drop across the subassembly at different operating conditions, pressure drop characteristics were studied at different flow conditions which are detailed in subsequent paragraphs. Subassembly bundle velocity have been considered as reference velocity for calculation of loss coefficient for different experiments discussed in the subsequent paragraphs. Studies were also conducted simulating the blockage of subassembly top and the subassembly flow through the blockage adaptor hole was estimated based on pressure drop measurements.

6.4.1 Pressure drop studies at nominal flow conditions

The pressure drop across the different sections of subassembly and total pressure drop were measured at various flow rates in water at 343K (70 ºC). The model pressure drop characteristics for subassembly as well as the bundle region of the subassembly are shown in Figure 6.5. In Figure 6.5, 'Bundle' refers to pressure drop in the fuel pin bundle and 'Total' refers to pressure drop in the entire subassembly, which includes contribution from foot, diffuser, rail, blockage adapter etc.
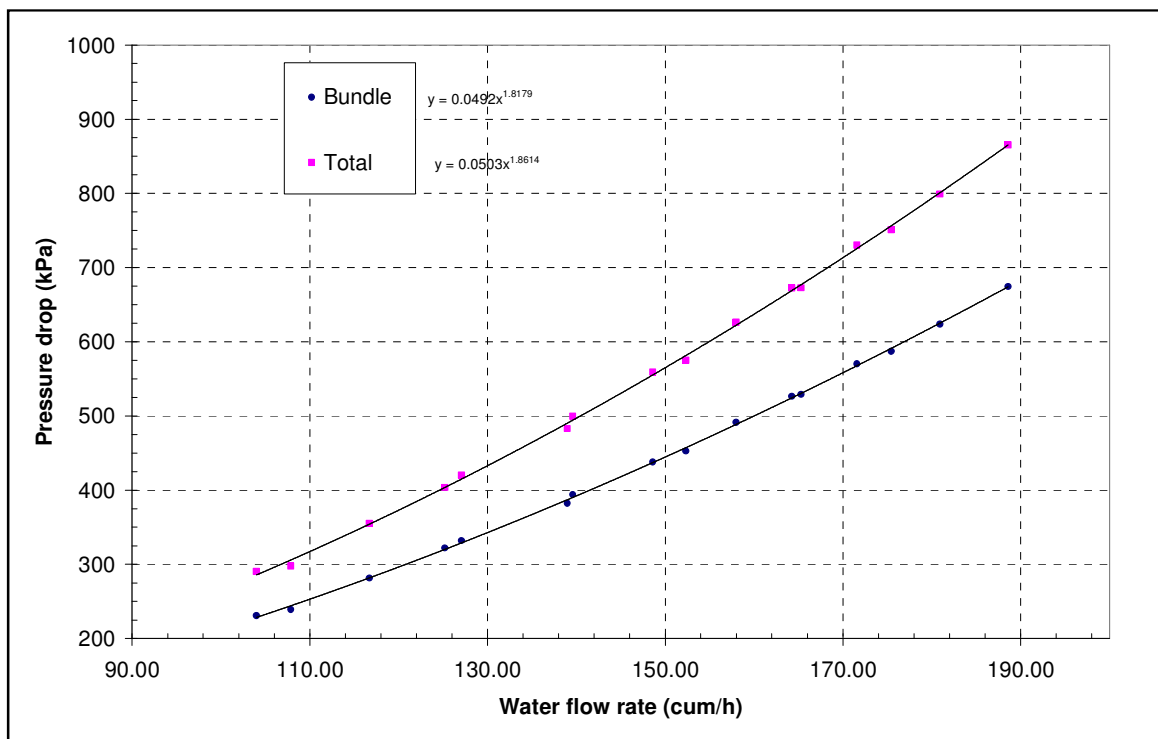
Fig. 6.5: Model Pressure drop through subassembly at nominal flow condition

The data obtained from model were used to calculate the loss coefficient for the subassembly in total as well for bundle region. The loss coefficient is plotted against the Reynolds number in Figure 6.6.
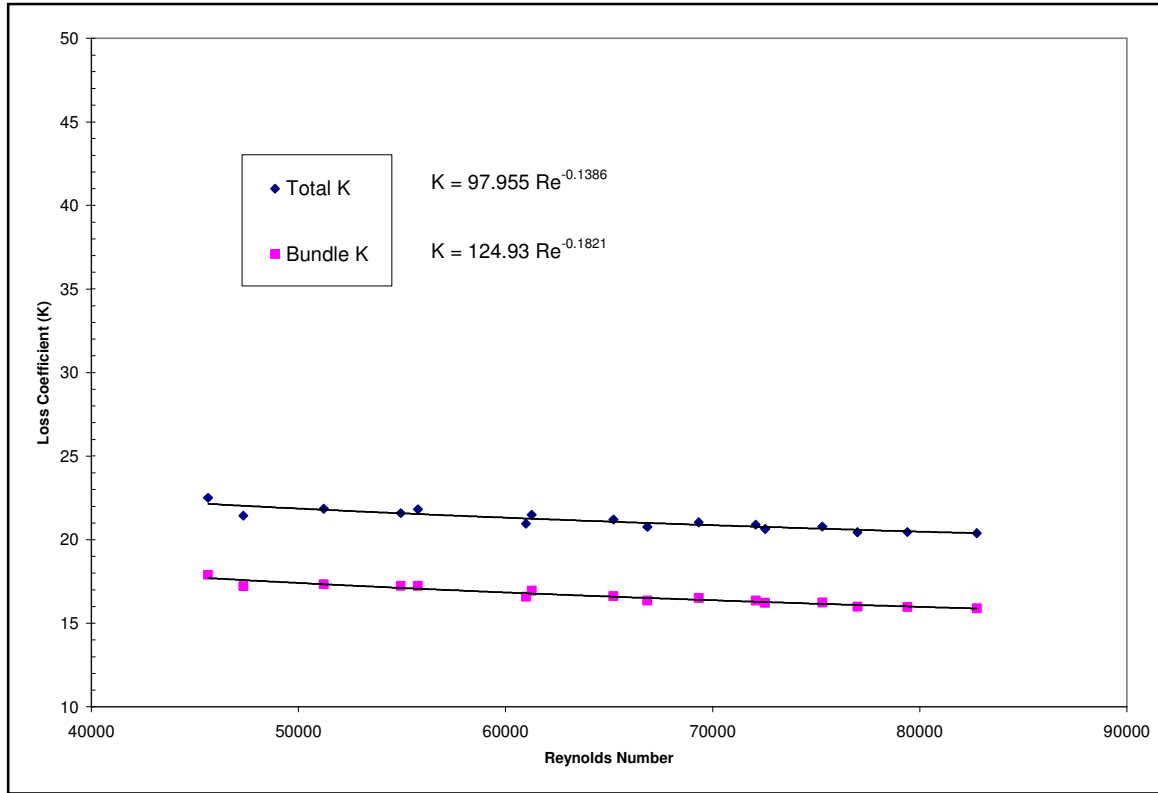
Fig. 6. 6: Loss Coefficient Vs Reynolds Number for Fuel Subassembly

From this figure it can be observed that the Bundle K is proportional to the $Re^{-0.18}$ which is in agreement with the reported correlations for bundle friction factor in turbulent regime. The pressure drop for the reactor condition is calculated using Euler simulation criteria. The total estimated pressure drop across the subassembly is found to be 482 kPa. Based on the measurements across the different sections of the subassembly, pressure drop for different sections were also estimated. Table 6.3 shows these values for different sections at reactor nominal condition.

Table 6.3: Pressure drop contribution of different regions of the subassembly at nominal flow condition

S.No.	Description of SA sections	Pressure drop (kPa)
1	Foot	81.8
2	Bundle entry	29.59
3	Bundle	379
4	Bundle exit	-19.42
5	S/A exit	12.93
6	Total	483.9

Out of this approximately 80% of the pressure drop is offered by bundle region alone. The maximum experimental uncertainty in the measurement of pressure drop across the subassembly and its various parts are estimated to be within ± 1.5%.

6.4.2 Pressure drop studies at low flow conditions

The flow through the subassemblies is different in the reactor under different operating conditions. The estimation of pressure drop during these conditions will be of great importance in understanding its flow behaviour. The pressure drop characteristics for maximum rated dummy fuel subassembly for pressure drop using water in the nominal flow range have been discussed in the earlier paragraph. These studies were carried out at lower flow rates simulating the prototype conditions during   the refueling operation as well as decay heat removal condition. Table 6.4 gives the hydraulic characteristics of the fuel subassembly for different conditions. Major pressure drop in the subassembly is across the pin bundle for all the flow conditions studied.

Table 6.4: Flow rate and Re in model and Prototype

Sl No.	Condition	Flow rate		Pin Bundle Re
		Prototype (kg/s)	Model(m^3/h)	
1	Refuelling	5.4 at 473 K	33.75 at 308 K	7765
2	Decay Heat Removal	0.18 to 0.72 at 823K	2.33 to 9.35 at 303K	540 to 2158

Pin bundle Re at 0.5% nominal flow (Decay heat removal condition) is in laminar regime and it is in transition regime during the refueling condition (15% of nominal flow). The results are discussed individually in the subsequent paragraphs.

6.4.3 Fuel handling condition

Testing was carried out with various flow rates in the range of 26 to 70 m^3/h. Figure 6.7 shows the model pressure drop characteristics for the subassembly. The loss coefficient is plotted against Reynolds number for these conditions in Figure 6.8.
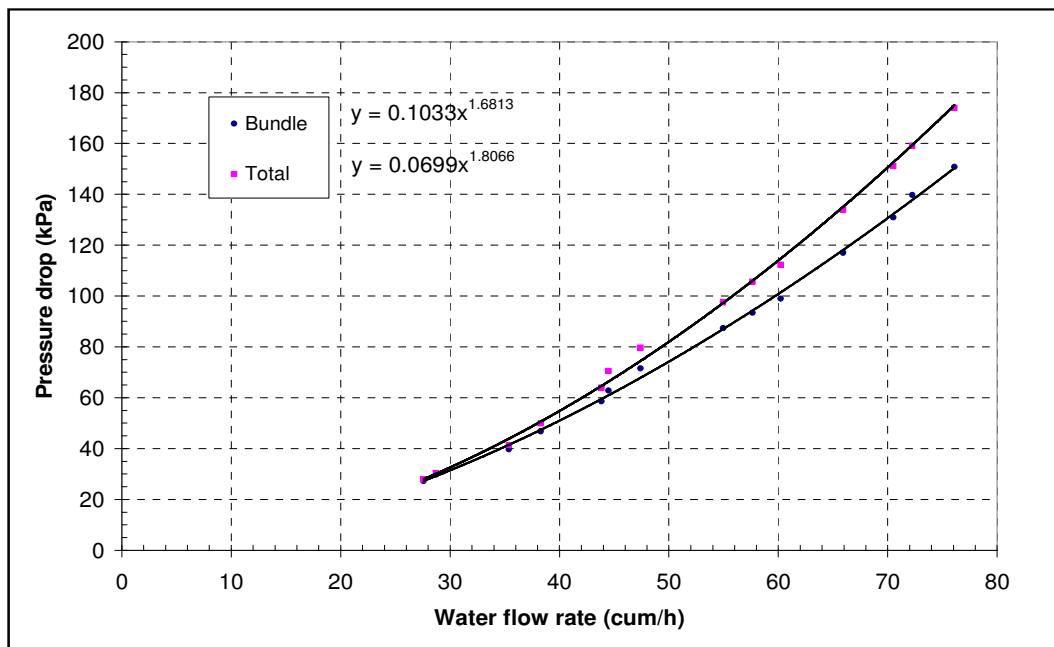
Fig. 6.7: Total and pin bundle pressure drop during refueling condition (water test result)
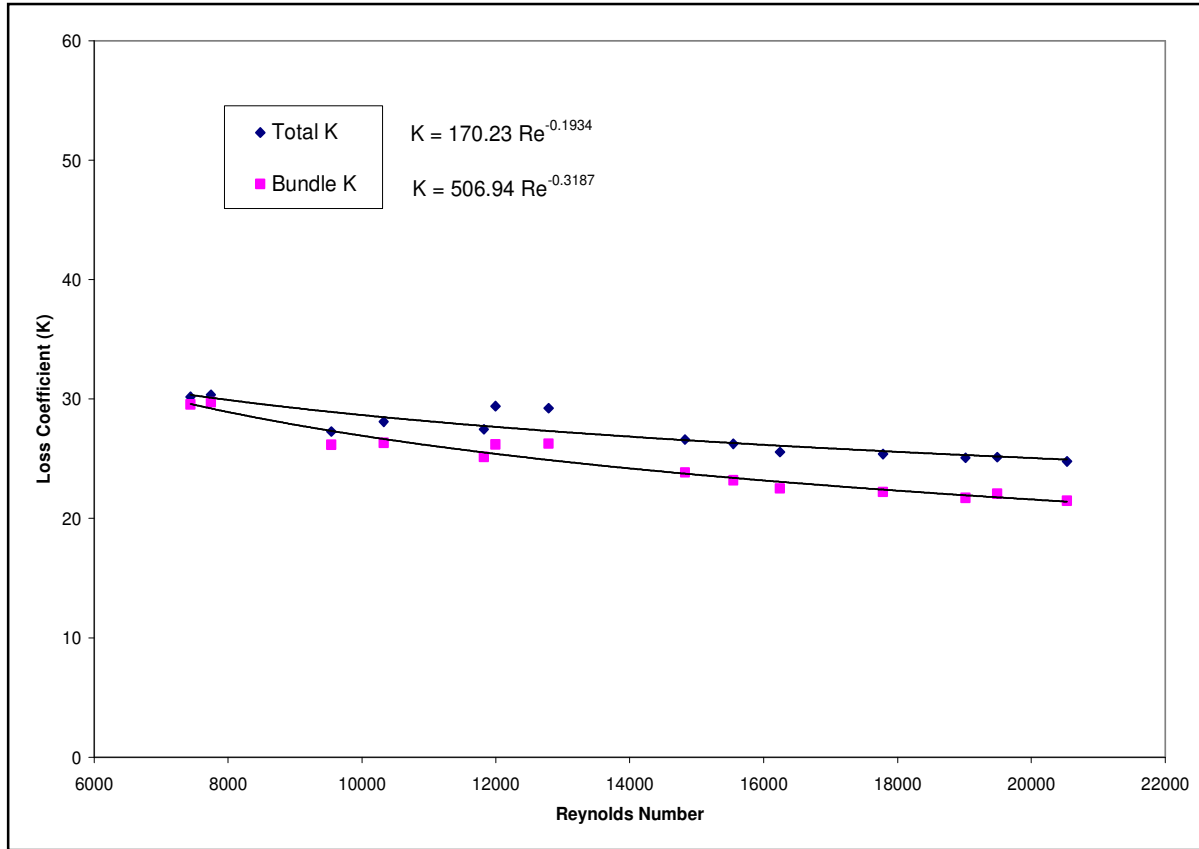
Fig. 6.8: Re Vs K for subassembly at refueling condition

In this case the flow regime covers both transition as well as turbulent flow conditions. It is observed from Figure 6.7 that the loss coefficient for bundle region is proportional to $Re^{-0.318}$. Based on the experimental loss coefficient the total pressure drop across the subassembly at reactor conditions is 16kPa at 5.4 kg/s of sodium flow (15% of the nominal flow condition).

6.4.4 Decay heat removal Conditions

The flow of sodium across the subassembly during decay heat removal condition varies from very low flow up to 2% of the nominal flow. During these range of flow the flow regime varies from laminar to transition. Up to 0.27 kg/s sodium flow, i.e., 0.75% of nominal

flow (3.51 m^3/h in water), flow in the pin bundle is in laminar regime (Reynolds number below 812 is treated as laminar for the geometry being tested). The flow remains in transition regime till the sodium flow rate is 5.01 kg/s. Transition to turbulent regime occurs at Reynolds number above 15,070 based on correlations suggested by Cheng and Todreas, (1986). Since the flow during decay heat removal condition is from 0.18 to 0.72 kg/s, the flow is in laminar regime at lower flow rate and is in transition for the remaining flow rates. Pressure drop characteristics for laminar and transition regimes are quite different and hence tests were carried out with various flow rates in the range of 0.9 to 12.5 m^3/h in water.
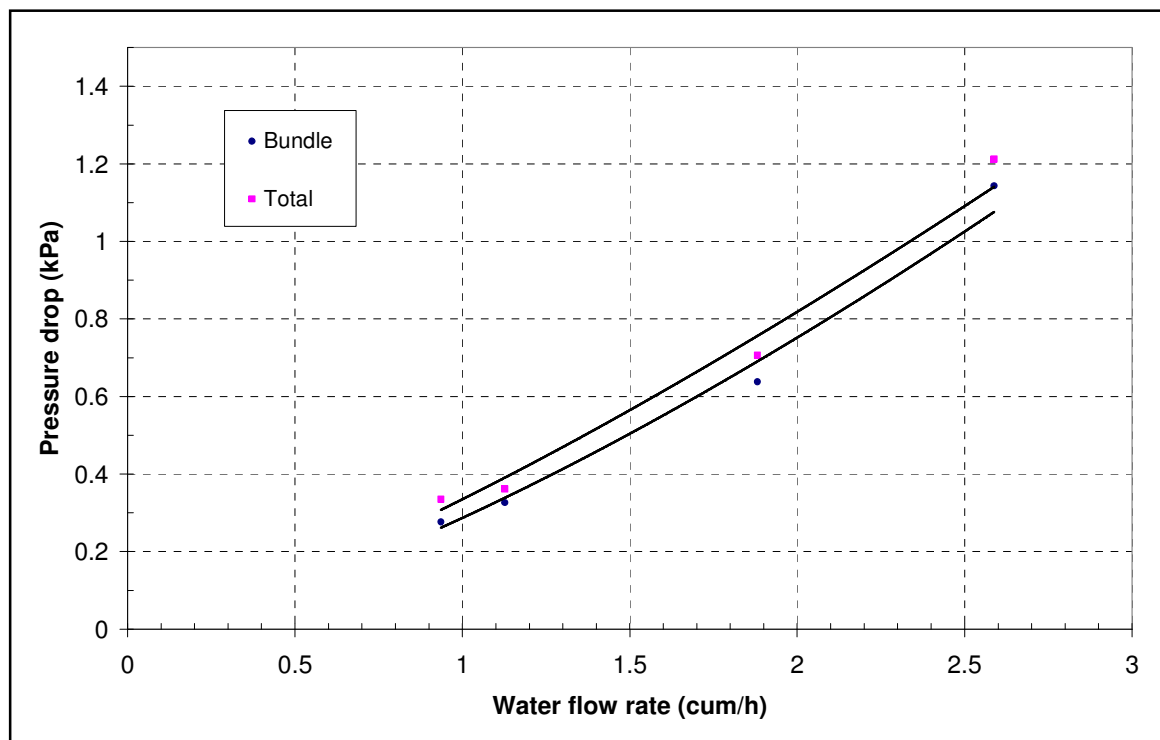
Fig. 6.9: Total and pin bundle Pressure drop during decay heat removal condition-

Laminar regime

Figure 6.9 shows the pressure drop characteristics in water for the subassembly in the laminar regime. The Loss coefficient is also plotted against the Reynolds number in Figure 6.10.
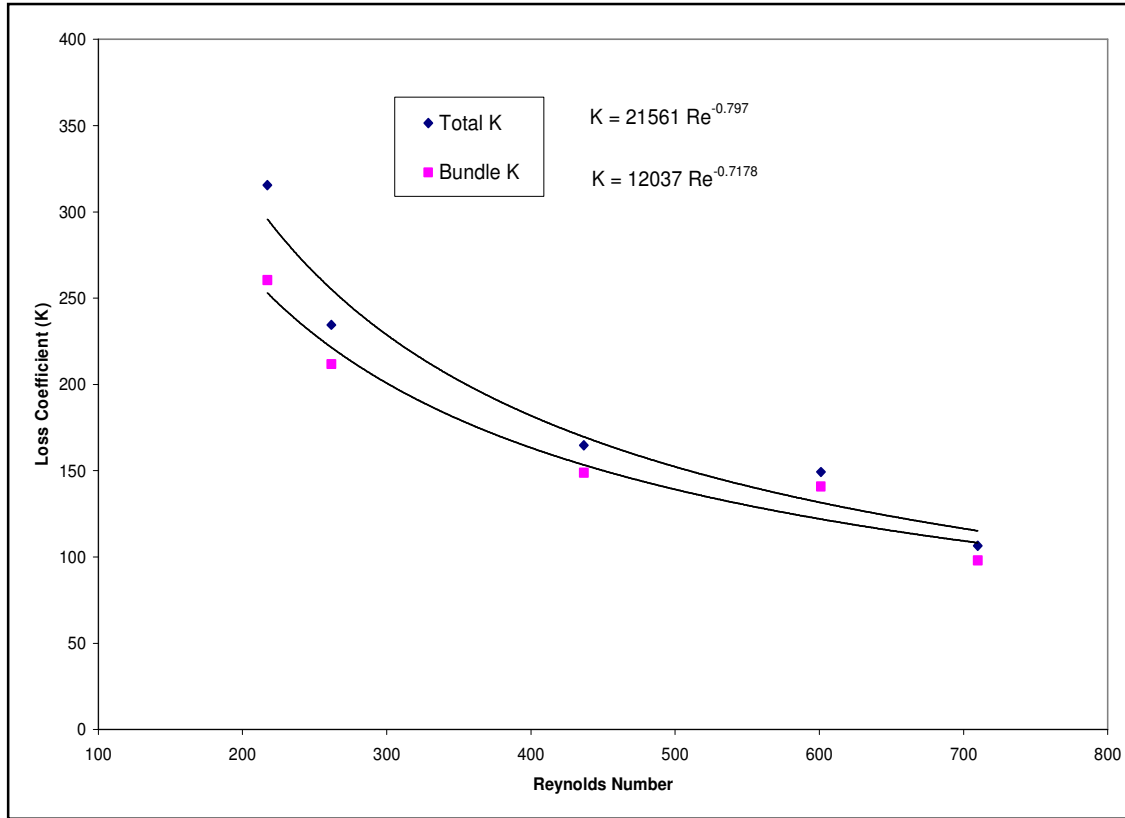
Fig. 6.10: Re Vs K for subassembly at decay heat removal condition -Laminar regime

In this case the bundle loss coefficient is found to be proportional to $Re^{-0.718}$. Total pressure drop across the subassembly at reactor conditions is 103 Pa at 0.18 kg/s of sodium (i.e. 0.5% nominal flow condition). The figures indicate that the pressure drop in the bundle is proportional to linear power of flow rate, demonstrating that the flow is in laminar regime. Figure 6.11 shows the pressure drop characteristics in water for the subassembly for transition regime. The Loss coefficient is also plotted against the Reynolds number in Figure 6.12 where the bundle friction factor is found to be proportional to $Re^{-0.56}$.
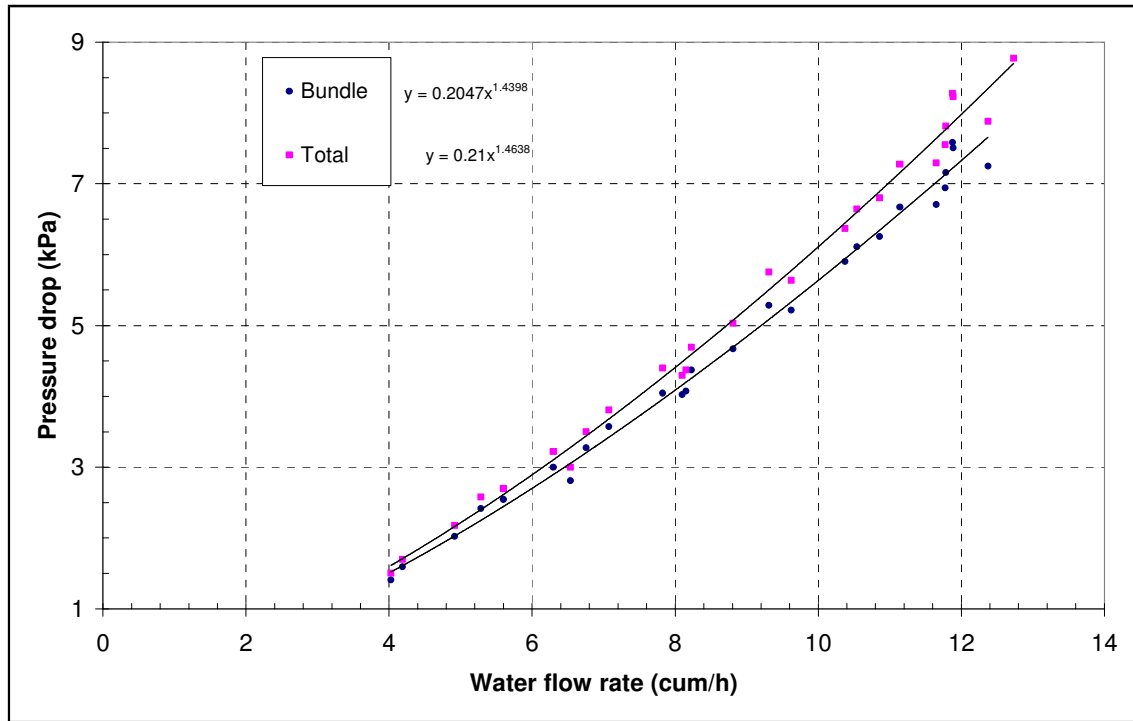
Figure 6. 11: SA and Bundle Pressure drop at DHR Flow condition –Transition Region (model)
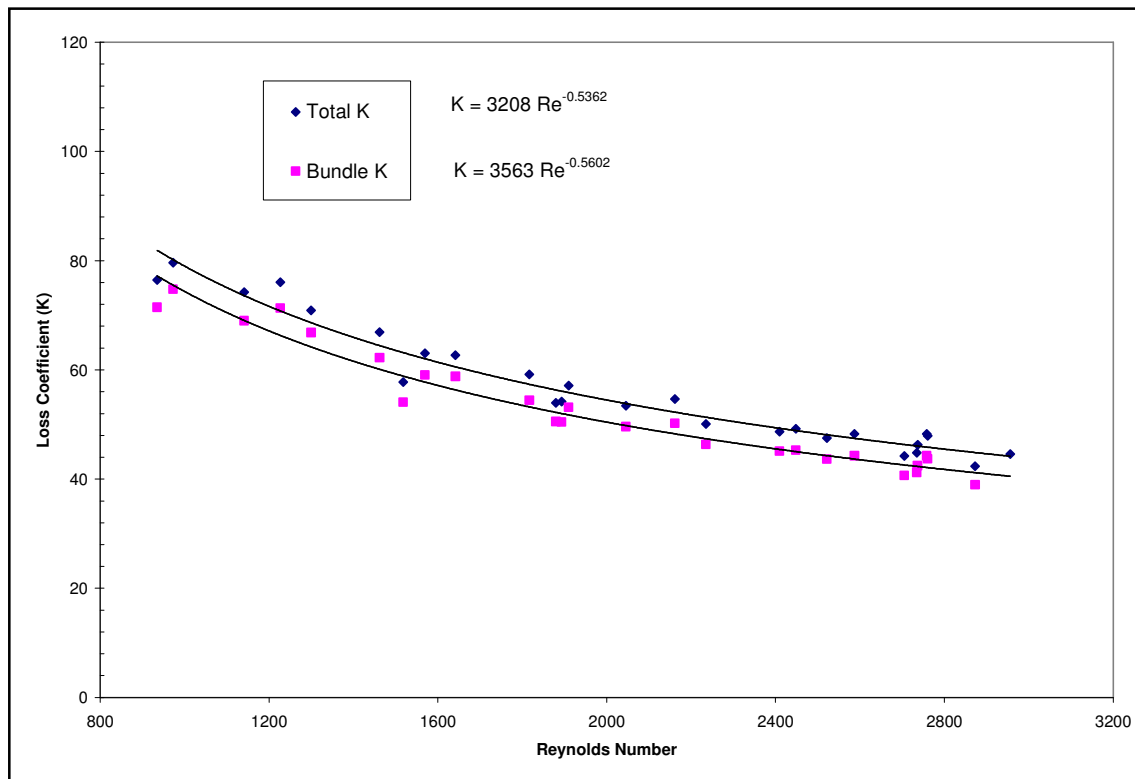
Fig. 6. 12: Re Vs K for subassembly at decay heat removal condition -Transition regime

110

6.5   SUBASSEMBLY BLOCKAGE STUDY

Complete flow blockage in the subassembly is considered as a beyond design basis event in the design of SFR, by having suitable design provisions in the entry and exit regions of the subassembly. There are two paths in subassembly outlet, (i) normal outlet at the top end and (ii) through six adaptor holes in the subassembly wrapper at the head region. Fall of heavy foreign object can block the former; however some sodium flow can take place through the later. Two sets of 21 mm diameter holes (total 6 nos. on six faces of hexagon) are provided circumferentially on the subassembly head near the exit, of the subassembly (as shown in Figure 1.4). Experiments were conducted to determine flow through the subassembly with complete blockage of the normal axial flow exit. For this testing, subassembly top was closed and the pressure drop values were measured as a function of flow rate. Flow rate, whose pressure drop is same as that for nominal conditions, is the flow through the subassembly in the reactor with complete blockage of axial exit. Figure 6. 13 show the model pressure drop characteristic of the subassembly with complete blockage.
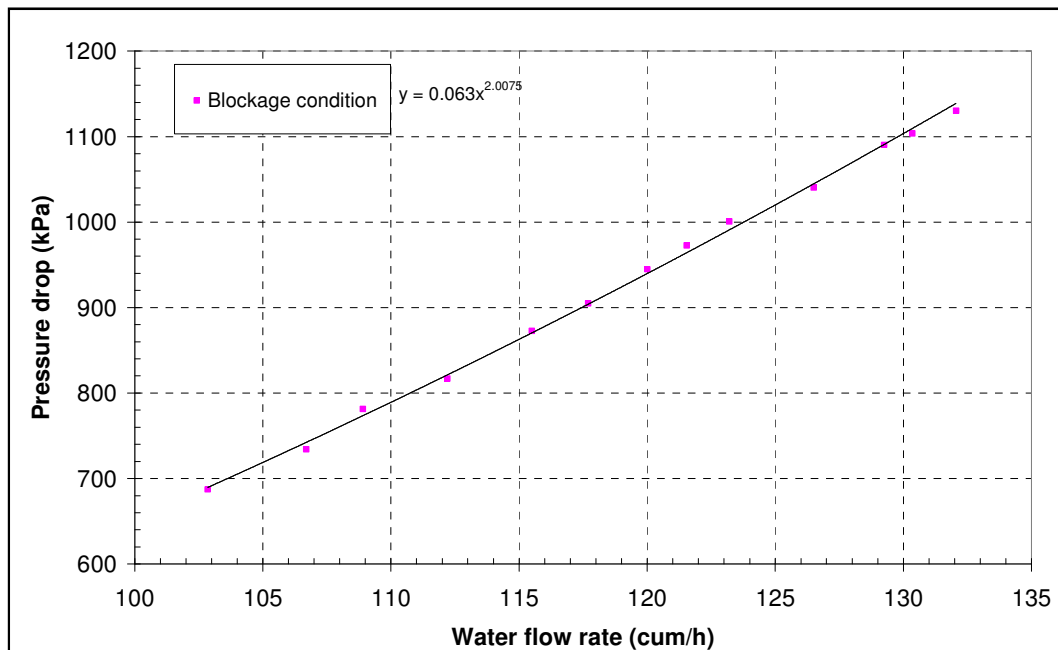
Fig. 6.13: Subassembly pressure drop in blockage condition

In this condition flow passage is only through the blockage adaptor holes provided at the exit. From the experimental result it is estimated that a sodium flow rate of 22.3 kg/s is possible with 483.9 kPa. Hence, the minimum flow rate through the subassembly due to top exit blockage is more than 60% of nominal flow rate. Thermal hydraulic calculation of the subassembly with this flow rate suggests that, there is no risk of sodium boiling in the subassembly due to such blockage demonstrates safety of the plant.

6.6   COMPARISION WITH LITRATURE DATA

There are many correlations reported in the literature to estimate the friction factor for bundle geometry. Since the present study covers a wide spectrum of data and represent all regimes, viz., laminar, transition and turbulent for the subassembly flow, it is worth comparing the present data with reported correlations. Figure 6.14 shows a comparison of the bundle friction factor with the correlations proposed by other authors.
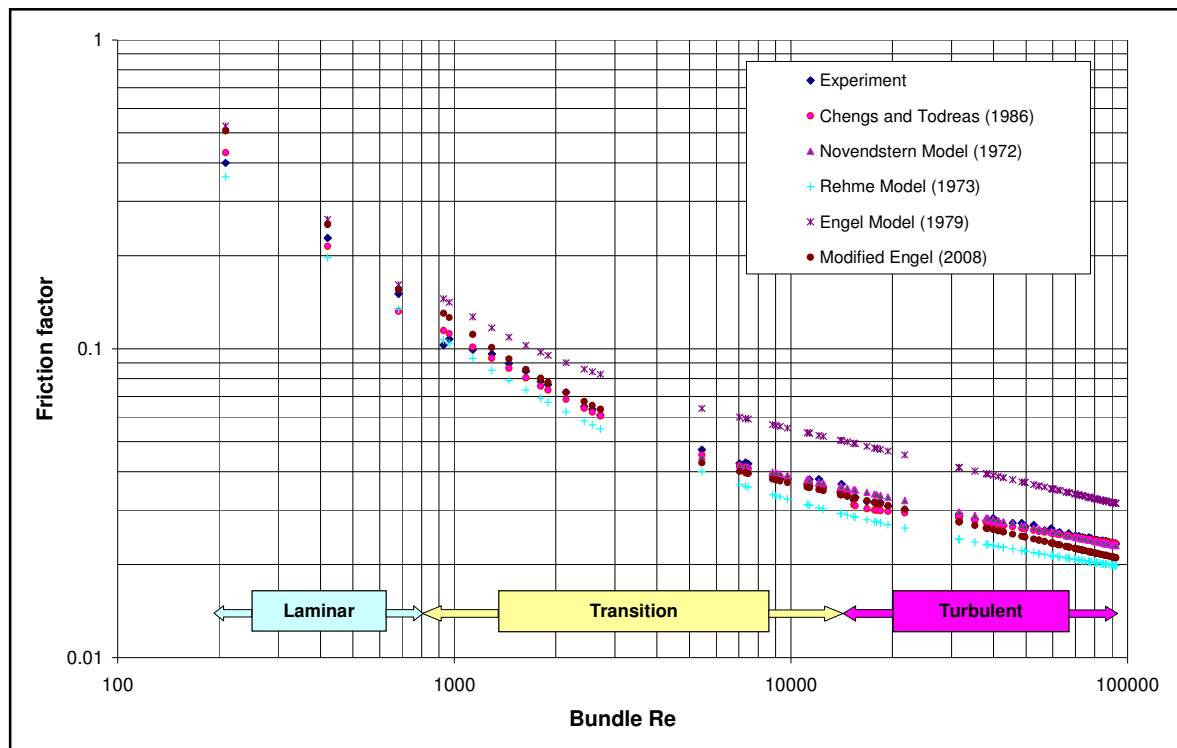
Fig. 6.14: Comparison of results with correlations in literature

The present data of bundle friction factor compares well with the value obtained from correlations suggested by Cheng and Todreas (1986) for all the flow regimes. Present data compares well with Novendstern (1972) correlation also for the turbulent regime. Other correlations also are in close agreement as shown in Figure 6.14.

The present results were also compared with the theoretical results available in the literature. Satisfactory agreement has been observed for all the regimes of flow. The maximum variation in the estimated friction factor based on experimental data when compared with the correlation proposed by Cheng (1986) was found to be 11.4 % with maximum variation in laminar and transition regimes.

6.7 EXTRAPOLATION OF PRESSURE DROP TO FULL SCALE SUBASSEMBLY WITH INSERTS

When frictional pressure drops are compared, the circular inserts have the highest frictional drop compared to all other insert geometries. There is an increase of 17 % in friction factor for circular inserts. Based on these 7 pin bundle results, the pressure drop for full scale subassembly is extrapolated. The increased pressure drop in the bundle and total pressure drop are shown in Figure 6.15. The total pressure drop increase in the case with circular inserts is 13%. The increase in total pressure drop is less due to fact that the pressure drop in foot, diffuser, rails etc does not get affected by the presence of inserts.
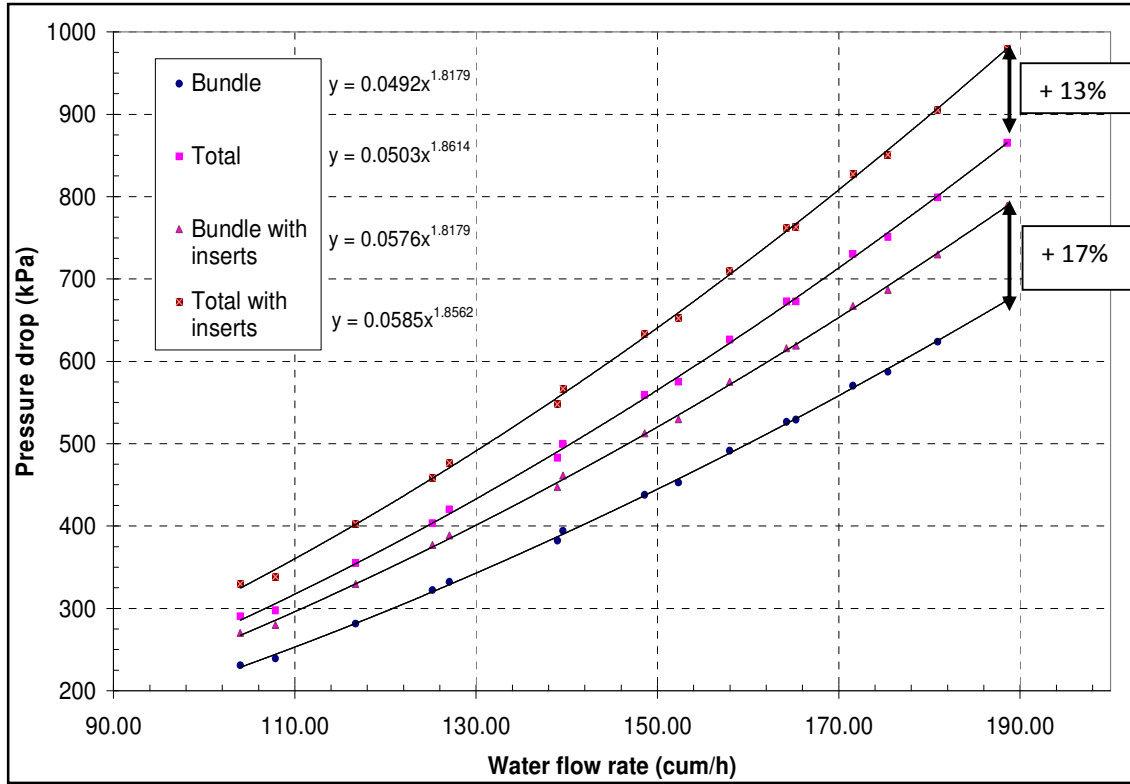
Fig. 6.15: Full scale pressure drop in bundle and total subassembly with circular inserts

6.8   CLOSURE

Experiments were carried out on full scale model of fuel subassembly using water as simulant for a wide range of flow simulating various operating conditions. The data obtained from the experiments were transposed to the reactor condition by Euler number similitude. The total pressure drop across the prototype subassembly is found to be 483.9 kPa at nominal sodium flow of 36 kg/s. Bundle friction factor was calculated from above data and compared with data available in literature. The friction factor matches very well with the data reported in the literature. Studies conducted for subassembly blockage suggests that, there is no risk of sodium boiling in the subassembly due to blockage from the subassembly top. The pressure drop offered by the subassembly was extrapolated to account for the same increase as was in the 7 bundle study. The pressure drop in the subassembly would increase to 537.65

CHAPTER 7

CONCLUSIONS

7.0.   INTRODUCTION

In sodium cooled fast reactors the core is very compact with large heat flux on clad surface. The fuel pins are arranged in a triangular pitch and the gap between the fuel pins forms the sub-channels for the flow of coolant. The mass flow rate of coolant is not uniform in all the sub-channels. Hence, there are significant temperature variations around the fuel pins which give rise to local hot spots. The flow areas of the edge / peripheral sub-channels are more than that of the sub channels around the central fuel pins and hence sodium flow through peripheral subassembly is more. The heat generation being relatively more in the central sub-channels and low in the peripheral sub-channels, a large variation in the sub-channel sodium temperature, characterized by low sodium temperature in the peripheral sub-channels and high sodium temperature in the central sub-channels exist. This study has focused on the attempts to supply more sodium flow to the central sub channel and to reduce the bypass occurring in the edge/peripheral subassemblies to respect the peak clad temperature limits. The scope of the present study therefore was to arrive at suitable hydraulic methods for reducing the sodium bypass in the peripheral channels and diverting it to the central sub channels. Towards this, effectiveness of different types of inserts in the peripheral sub channels has been studied.   The use of inserts was intended to reduce the flow areas and thereby divert more flow towards the central sub channels. The efforts towards reducing the bypass flow occurring in the peripheral sub channels would lead to more uniform subassembly temperatures. This would also result in an optimized subassembly flow and eventually a higher hot pool temperature. The study mainly focuses on uniformity of flow in all the sub-channels and thereby improving the heat transfer coefficient to achieve a lower clad hot spot temperature.

Different types of inserts, viz., circular, semi circular and triangular were studied to understand their relative effectiveness. Studies on a 7 pin fuel bundle have exhibited the beneficial effect of these types of inserts. The investigations based on 3 dimensional Computational Fluid Dynamic (CFD) simulations, has been validated through experiments performed in water models. Also, the pressure drop in a 7 pin bundle with and without inserts has been measured using differential Pressure Transmitter. The CFD predicted results are compared with the pressure drop values in the bundle.

7.1. MAJOR CONCLUSIONS

Detailed numerical studies on grid independence, sensitivity of turbulence models, adequacy of axial length of pin bundle for achieving developed flow etc have been carried out. Hydraulic analysis using a 7 pin bundle geometry was carried out for a range of Re from 4×10^4 to 2×10^5. Computed values of frictional factor were compared with correlations proposed by previous researchers. From the hydraulic analysis it is observed that the addition of inserts in the hexcan enhances the axial velocity fraction of coolant in the central sub-channels with an additional pressure drop. It is observed that with insert, the axial velocity fraction is improved in all central sub-channels. The triangular inserts are found to lower frictional drop compared to all other insert geometries. There is an increase of 9.8 % in friction factor for triangular inserts and 11.9 % rise in semi-circular inserts. Circular inserts have the maximum pressure drop (17%) and hence the highest friction factor.

It is also observed that the addition of inserts has better influence on heat transfer coefficient with additional frictional drop. The increase in the heat transfer coefficient is quantified in terms of Nusselt number. The highest improvement of 86 % in Nusselt number is with addition of circular inserts. When frictional pressure drops are compared, the circular inserts also have the highest frictional drop compared to all other insert geometries. Based on

these results, the pressure drop for full scale subassembly with inserts was extrapolated. The total pressure drop increase due to circular inserts is found to be 13% more than the case without any inserts.

The Performance Evaluation Criterion (PEC) for all the inserts has been calculated and it is found that circular inserts is the best among the all inserts. It was seen that, the friction factor is the highest for the circular inserts and is minimum in the case of triangular inserts. The circular inserts are very effective in breaking the circumferential flow due to the presence of sharp corner between the inserts and hexcan wall. As a consequence of this, resistance for circumferential flow, axial flow uniformity is improved with the associated enhancement in Nusselt number. The maximum value of PEC is 1.76 and it occurs in the case of circular inserts indicating circular inserts are the optimum one among the three inserts investigated.

7.2.   SCOPE FOR FUTURE WORK

The present study aims to bring out the influence of inserts on sub channel flow physics. The prototype sub-assemblies have 217 pins where the number of central sub-channels is too large compared to the number of peripheral sub-channels. Further the friction factor and heat transfer coefficient are a functions of number of pins in the bundle. Hence the effectiveness of inserts observed in 7 pin bundle needs confirmation in terms of extrapolation to prototype pin bundle with large number of pins. This will require experimental and CFD analysis on 217 pins bundle. Effectiveness of other types of inserts can also be studied.

REFERENCES

1.   ANSYS FLUENT 13.0 / User's Guide, November 2010.

2.   Arwikar K, Fenech H., 1979, "Heat Transfer, momentum losses and flow mixing in a 61 tube bundle with wire wrap", Nuclear Engineering and Design, 55, 403-417.

3.   Basehore K.L., Todreas N.E., 1980, "SUPERENERGY-2: A Multiassembly Steady-State Computer Code for LMFBR Core Thermal–Hydraulic Analysis, PNL-3379, Pacific Northwest Laboratory, Richland, WA.

4.   Baxi, Dalle-Donne., 1981, "Heat transfer and fluid flow in Nuclear Systems", In: Pergamon Press, ISBN 0-08-027181-2.

5.   Borishankii V.M., Gotovski M.A., Firsova E.V., 1969, "Heat transfer to liquid metals in longitudinally wetted bundles of rod", Atomnaya Energiya, vol. 27(6), pp. 549-552.

6.   Business Standard, "Now, India is the third largest electricity producer ahead of Russia, Japan". Retrieved 26 March 2018.

7.   Bubelis E., Schikorr M., 2008, "Review and proposal for best fit of wire-wrapped fuel bundle friction factor and pressure drop predictions using various existing correlations", Nuclear Engineering and Design, 238, 3299–3320.

8.   Chandra L., Roelofs F., 2011, "CFD analysis of liquid metal flow in sub channels for gen IV reactors", Nuclear engineering and design, 241, 4391-4403

9.   Chen S.K., Todreas N.E., Nguyen N.T., 2014, "Evaluation of existing correlations for the prediction of pressure drop in wire-wrapped hexagonal array pin bundles", Nuclear Engineering and Design, 267, 109-131.

10. Cheng S.K., Todreas N.E., 1986, "Hydrodynamic models and correlations for bare and wire-wrapped hexagonal rod bundles - bundle friction factors, sub-channel friction factors and mixing parameters", Nuclear Engineering and Design, 92, 227-251.

11. Chen S.K., Petroski R., Todreas N.E., 2013. "Numerical implementation of the Cheng and Todreas correlation for wire-wrapped bundle friction factors-desirable improvements in the transition flow region". Nucl. Eng. Des. 263, 406–410.

12. Chetal. S. C. et al, 2008, "The design of the Prototype Fast Breeder Reactor", Journal of Nuclear Engineering and Design, 236, 852-860.

13. Choi et al., 2003, "Measurement of pressure drop in a full-scale fuel assembly of a liquid metal reactor", Journal of Pressure Vessel Technology, 125, 233-238.

14. Collingham R.E., Yatabe J.M., Hill V.R., 1970. "Development and results of an electrically heated seven-pin bundle assembly for thermal hydraulic testing in liquid metals. Liquid Metal Heat Transfer and Fluid Dynamics", ASME Winter Annual Meeting, CONF-701110-2, New York.

15. Engel F.C., Markley R.A., Bishop A.A., 1979, "Laminar, transition and turbulent parallel flow pressure drop across wire-wrap-spaced rod bundles", Nuclear Science and Engineering, vol. 69, pp. 290-296.

16. Fenech H., 1985. "Local heat transfer and hot-spot factors in wire-wrap tube bundle", Nuclear Engineering and Design, 88, 357-365.

17. Gajapathy R., Velusamy K., Selvaraj P. Chellapandi P., Chetal S.C., 2009, "A comparative CFD investigation of helical wire-wrapped 7, 19 and 37 fuel pin bundles

and its extendibility to 217 pin bundle" , Nuclear Engineering and Design, 239, 2279-2292.

18. Gajapathy R., Velusamy K., Selvaraj P. Chellapandi P., 2015, "CFD investigation of effect of helical wire-wrap parameters on the thermal hydraulic performance of 217 pin bundle", Annals of Nuclear Energy, 77, 498-513.

19. Gajapathy R., Velusamy K., Selvaraj P., Chellapandi P., Chetal S.C., 2007. CFD study of helical wire-wrapped 7-fuel pin bundle and the challenges in modeling full scale 217 fuel pin bundle. Nucl. Eng. Des. 237, 2332–2342.

20. Ginsberg T., Lorenz J.J., 1973. "Experimental mixing studies in simulated wire-wrap fuel assemblies", Proc. Int. Reactor Heat Transfer Conf., Karlsruhe, Germany, Oct. 9-11.

21. Govinda Rasu N., 2013, "Investigations of entrance flow and partial flow blockage in fuel subassemblies of fast breeder reactor", PhD Thesis, Homi Bhabha National Institute, Mumbai.

22. Govindha Rasu N., Velusamy K., Sundararajan T., Chellapandi P., 2013, "Investigations of flow and temperature field development in bare and wire-wrapped reactor fuel pin bundles cooled by sodium", Annals of Nuclear Energy, 55, 29–41.

23. Govindha Rasu N., Velusamy K., Sundararajan T., Chellapandi P., 2014, "Simultaneous development of flow and temperature fields in wire-wrapped fuel pin bundles of sodium cooled fast reactor", Nuclear Engineering and Design, 267, 44– 60.

24.   Govinda Rasu N., 2013. "Investigations of entrance flow and partial flow blockage in fuel subassemblies of fast breeder reactor". PhD Thesis, Homi Bhabha National Institute, Mumbai, Dec.

25.   Jeffery G.S., Bruce R.B., David Pointer W, Paul Fischer, 2008, "Effects of Mesh Density and Flow Conditioning in Simulating 7-Pin Wire Wrapped Fuel Pins" Proceedings of the 16th International Conference on Nuclear Engineering, ICONE16-48306 May 11-15, Florida USA.

26.   Kazimi M.S., Carelli M.D., 1976, "Heat transfer Correlation for Analysis of CRBRP Assemblies", Westinghouse Report, CRBRP-ARD-0034.

27.   Khan E.U, Rohsenhow W.M, Sonin A.A and Todreas N.E., 1975, "A Porous Body Model for Predicting Temperature Distribution in Wire Wrapped Fuel Rod Assemblies" Nuclear Engineering and Design 35, 1-12.

28.   Kim W.S., Kim Y.G., Kim Y.J., 2002, "A sub-channel analysis code MATRA-LMR for wire wrapped LMR subassembly", Annals of Nuclear Energy, 29, 303–321.

29.   Krauss T., Meyeer L., 1998, "Experimental Investigation of turbulent transport of momentum and energy in a heated rod bundle", Nucelar ngineering and Design 180, 185-206.

30.   Lafay J., Menant B. and Barroil J., 1975, "Local pressure measurements and peripheral flow visualization in a water 19-rod bundle compared with FLICA II B calculations: influence of helical wire-wrap spacer system", AIChE/ASME Heat Transfer Conf., Paper 75-HT-22, Cal.

31.   Liu X.J., Scarpelli N., 2015, "Development of a sub-channel code for liquid metal cooled fuel assembly", Annals of Nuclear Energy, 77, 425–435.

32.   Lorenz J.J., Ginsberg T., 1977, "Coolant mixing and sub channel velocities in a LMBR fuel assembly", Nuclear Engineering and Design, 40, 315-326

33.   Moon H., Kyong W.S., 2001, "An experimental study and assessment of friction factor correlations for wire wrapped fuel assemblies" Annals of Nuclear Energy, 28, 1683-1695.

34.   Memmott M., Buongiorno J., Hejzlar P., 2010, "On the use of RELAP5-3D as a subchannel analysis code", Nuclear Engineering and Design, 240, 807–815.

35.   Mikityuk K., 2009, "Heat transfer to liquid metal: review of data and correlations for tube bundles", Nuclear Engineering and Design, 239(4), 680-687.

36.   Natesan K., Sundararajan T., Narasimhan A., Velusamy K., 2010, "Turbulent flow simulation in a wire-wrap rod bundle of an LMFBR" Nuclear Engineering and Design, 240, 1063-1072.

37.   Ninakota H., 1987, "Distributed resistance modeling of wire wrapped rod bundles", Nuclear Engineering and Design, 104, 93-102.

38.   Novendstern E.H., 1972, "Turbulent flow pressure drop model for fuel rod assemblies utilizing a helical wire-wrap spacer system", Nuclear Engineering and Design, 22, 19-27.

39.   Peniguel C., Rupp I., Rolfo S., Guillaud M. 2010, "Thermal-hydraulics and conjugate Heat Transfer Calculation in a Wire-Wrapped SFR Assembly", Proceedings of the ICAPP10, paper 10174, San Diego, USA, June 13-17.

40. Raza W., Kim K.Y., 2008, " Computational Analysis of flow and Convective heat transfer between 7 -pin and 19- pin Wire wrapped Fuel Assemblies", Journal of Nuclear science and Technology 45 97), 653-661.

41. Rehme K., 1987. "Convective heat transfer over rod bundles. Handbook on singlephase convection heat transfer". A wiley inter-science publications.

42. Rehme K., 1973, "Pressure drop correlations for fuel element spacers", Nuclear Technology, vol. 17, pp. 15–22.

43. Roelofs F., Gopala V.R., Chandra L., Viellieber M., Class, A., 2012 "Simulating fuel assemblies with low resolution CFD approaches", Nuclear Engineering and design, 250, 548-559.

44. Rolfoa S., Peniguelb C., Guillaudc M., Laurencea, D., 2012, "Thermal -hydraulic study of a wire spacer fuel assembly", Nuclear Engineering and Design, 243, 251-262.

45. Roychowdhury D. 1998. "Thermal hydraulic design of PFBR core IAEA specialists meeting on LMFR core thermo hydraulics – status and prospects", Obninsk, Russia, IAEA-TECDOC-1157.

46. Sreenivasulu T., Prasad B.V.S.S.S., 2009. "Flow and heat transfer characteristics in an annulus wrapped with a helical wire". Int. J. Thermal Sci. 48, 1377–1391.

47. Subbotin V.I., Ushakov P.A., Kirillov P.L., Ibragimov M.H., Ivanovski M.N., Nomofilov E.M., Ovechkin D.M., Sorokin L.N., Sorokin V.P., 1965, "Heat transfer in elements of reactors with a liquid metal coolant". In: Proceedings of 3rd International Conference on Peaceful uses of Nuclear Energy, New York, vol. 8, pp. 192-200.

48. Syeilendra P., Takahashi M., 2013. "Thermal-hydraulic analysis of wire-wrapped SFR test subassemblies by sub-channel analysis method", Annals of Nuclear Energy, 54, 109-119.

49. "Technology development prospects for the Indian power sector" (PDF). International Energy Agency France; OECD.

50. Wantland J.L., 1974, "Orrible - A computer program for flow and temperature distribution in 19-rod LMFBR fuel subassemblies", Nuclear Technology, 24, 168–175.

51. Wigeland R., and Hamman K.D., 2009. "Fast Reactor Subassembly Design Modifications for Increasing Electricity Generation Efficiency", INL/CON-09-15226, Idaho National Laboratory, Idaho Falls, ID.

52. Wu Y.W., Xin Li, Xiaolei Yu, Qiu S.Z., Su G.H., Tian, W.X., 2013, "Sub-channel thermal-hydraulic analysis of the fuel assembly for liquid sodium cooled fast reactor", Progress in Nuclear Energy, 68, 65-78.